Development of Sensing Platform based on Rare Earth Nanocomposite Films

Thesis

submitted in partial fulfillment for the award of degree

of

Doctor of Philosophy

by

SUMAN DUHAN

(Registration No.: 951401004)

Under the guidance of

Dr. Sudhir K Singh
Associate Professor
Department of Chemical Engineering,
Thapar Institute of Engineering & Technology (Deemed to be University), Patiala

Dr. Manoj Kumar
Associate Professor
Department of Chemical Engineering,
IIT-BHU, Varanasi

Department of Chemical Engineering
Thapar Institute of Engineering & Technology (Deemed to be University)
Patiala – 147004, Punjab, India
www.thapar.edu

Feb'2023

Dedicated

to

My Parents and In-Laws,

My Husband

Mr. Mrinal Jaiswal

and

My Son

Ruhaan

Certificate

This is to certify that the thesis entitled "**Development of sensing platform based on rare earth nanocomposite films"** being submitted by **Ms. Suman Duhan (Roll. No. 951401004)** to Department of Chemical Engineering, Thapar Institute of Engineering & Technology (Deemed to be University), Patiala, for the award of degree of **Doctor of Philosophy,** is a record of bonafide research work carried out by her under our guidance and has fulfilled the requirements for the submission of this thesis, which to our knowledge has reached the requisite standard.

The results embodied in the thesis have not been submitted either partially or wholly to any other university or institute for the award of any other degree or diploma.

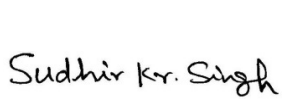

(Dr. Sudhir K Singh)
Associate Professor
Department of Chemical Engineering,
Thapar Institute of Engineering & Technology
(Deemed to be University), Patiala

(Dr. Manoj Kumar)
Associate Professor
Department of Chemical Engineering,
IIT-BHU, Varanasi

Dated: 07-02-2023

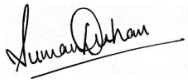

Suman Duhan
(Roll No. 951401004)

Acknowledgements

I devotedly thank the Almighty for providing me the potency to persist on the path to success.

A statement of thanks is not evident to inculcate my deep sense of gratitude and obligation to all who helped me in one way or another in completion of thesis. I would like to take this opportunity to thank many people who helped and encouraged me throughout this research.

I express my deep and sincere gratitude as well as profound regards to **Dr. S.K Singh and Dr. Manoj Kumar** for providing me an opportunity to work under their guidance. Their immense knowledge, expertise and valuable suggestions, patience and motivation provided a great platform for learning and performing research. Their enthusiasm and optimism made this experience both rewarding and enjoyable. Their feedback and editorial comments were also valuable for writing of this thesis. I learned a lot from them over the course of this Ph.D. work. Their goal-oriented style of work, passion towards research, work ethic, has been very inspiring for me. Their daily practice of following up on recent scientific literature is something that I also tried to adopt and greatly benefitted. I really appreciate their unconditional support and encouragement towards doing high-caliber research. It's been a great honor to work under their guidance.

I am extremely thankful to **Dr. Prakash Gopalan**, Director, Thapar Institute of Engineering &Technology (Deemed to be University), **Dr. Rafat Siddique,** Dean of Research & Sponsored Projects, Thapar Institute of Engineering & Technology (Deemed to be University) for extending the opportunity to undertake this doctoral research.

I would like to profoundly thank my doctoral committee members **Dr. Rajeev Mehta and Dr. Haripada Bhunia** of Chemical Engineering and **Dr. Bonamali Pal**, **Professor**, School of Chemistry, Thapar Institute of Engineering & Technology (Deemed to be University) for their immense help and guidance in the right direction. My heartful thanks to the staff members of the Department of Chemical Engineering, Thapar Institute of Engineering & Technology (Deemed to be University) for their valuable contribution and moral support.

I am extremely thankful to **Prof. Md. Imteyaz Ahmad, Department of Ceramic Engineering, IIT-BHU,** for giving their valuable insights. Also, to the **Department of Science and Technology**, New Delhi, (Nano Mission:SR/NM/NS-1320/14-15) and **Center of Energy Resource Development**, IIT (BHU) Varanasi for funding this work. I am also sincerely thankful to the **Central Instrumentation Facility (CIF) IIT (BHU)**for characterizing our samples. I am extremely thankful to **System Design and Fabrication Lab, Department of Chemical Engineering & Technology & School of Biomedical Engineering, IIT-BHU**, for providing all the facility and a friendly working environment for performing all of mine experimental work during my stay in IIT-BHU.

My endless thanks goes to **Mr. Kedar Sahoo, Mr. Sudhir Ranjan, Mr. Shivesh**, PhD. Scholars of IIT-BHU and IIT-Kanpur and my colleague **Dr. Kamaljit Singh,** for their assistance and support at various stages of my research work. I would also like to express my deepest gratitude to my husband **Mr. Mrinal Jaiswal** who always encouraged me and supported me to accomplish this task. Words cannot express how grateful I am to my mother-in-law, my mother, sister, brother and sister-in-law for all the sacrifices they made on my behalf. Special thanks to my beloved son, **Ruhaan** and my niece **Aaira** for enduring with me for not giving them sufficient time and always cheering me up during difficult times.

(Suman Duhan)

Abstract

In the present era, contamination or pollution in water has become one of the global issues because of its serious health consequences and imbalance caused in the ecosystem. There is a continuous rise in the pollution or contamination caused by heavy metals in the atmosphere or in the aquatic ecosystem from the past few decades. Industrial waste plays a great role in polluting the water and is responsible for introducing different pollutants in the form of heavy metals in living beings. Heavy metals like arsenic, mercury, cadmium, cobalt, and many more are highly toxic for human beings. Determination of these heavy metals in the water, soil is a very challenging task. Though, these days a lot of research is going on for removing these heavy metals from the soil, water and atmosphere by adopting different and new methodologies, but those techniques are either expensive, time-consuming or are very complex to use. Current research evaluates the role of different chelating agents and types of substrates on the film evolution, thickness and its characteristics emission when the hydrothermal route is used as a synthesis technique. Moreover, the effect of temperature on the film thickness and surface roughness is also evaluated. Furthermore, a nearly transparent Upconverting (UC) thin-film has been grown entailing capability to ensue fluorescence resonance energy transfer and use it to detect Arsenic in drinking water. The objective of the current thesis is to enhance our understanding of UC film growth over the different glass substrates using the hydrothermal method. This understanding will enable us to use other bio-organic materials such as plant extract to synthesize UC films. Moreover, prepared UC film on glass substrate is proposed to use as a Arsenic sensor, as arsenic contamination in drinking water is very difficult to quantify analytically due to its low detection limit (5 ppb by World Health Organisation (WHO)). Besides, Atomic absorption, Inductively Coupled Plasma (ICP), Inductively Coupled Plasma-Mass Spectrometer (ICP-MS), arsenators and many more are among the few options available for detection.

In the first study, simultaneous crystal growth and deposition of Upconverting Yb^{3+}/Er^{3+} doped $NaYF_4$ Film (UCF) on conducting and non-conducting substrates by one-step hydrothermal method have been developed. The characteristics such as film topography, morphology, crystallographic phase and upconverting luminescence intensity were found to depend both on the chelating agent and nature of the substrate. The characteristics of the prepared films varied interestingly when either the chelating agent or the substrate was

changed. The upconversion emission intensities were found to increase with decreasing film roughness. Further, current investigation demonstrated that the $NaYF_4$ films deposited using ethylenediaminetetraacetic acid (EDTA) or diethylenetriamine pentaacetic acid (DTPA) chelating agents on indium tin oxide (ITO) substrate and ethyleneglycol tetraacetic acid (EGTA) chelating agent on plain glass (PG) substrate were more uniform and resulted in greater upconverted emission intensities. We envision plausible use of current technology in the development of affordable optical platforms for several optoelectronic applications.

In the second study, a sensitive α-$NaYF_4$:Yb^{3+}, Er^{3+} solid-phase upconverting platform (UCP) have been developed and realized using Moringa oleifera leaf extract for selective detection of the trivalent arsenic ion [As(III)] contamination in drinking water. The presence of polyphenols in the leaf extract has showed to induce luminescence resonance transfer (LRET), thereby diminishing the Er^{3+} emission (red and green band) when activated by 980 nm excitation. However, the addition of As(III) species interrupted the LRET process and restored the emissions proportionately. This feature allowed the platform to selectively detect arsenic pollution in water below the safe limit of 10 ppt. The uniqueness of UCP lies in monitoring the As(III) contamination in samples containing heavy ions (Cd^{2+} and Hg^{2+}) also, without an apparent effect on the signal reproducibility. The UCP was also found to be insensitive to other interfering ions including Pb^{2+}, H_2PO^{4-}, F^-, Cl^-, Ca^{2+}, Mg^{2+}, Sn^{2+}, Cr^{6+}, Fe^{2+} and Co^{2+}, if present.

Fig.1 shows the overall outline of the thesis.

Overall, the studies performed shows that we are able to form an optically active thin film for the purpose of sensing which can be formed by using hydrothermal method.

DEVELOPMENT OF SENSING PLATFORM BASED ON RARE EARTH NANOCOMPOSITE FILMS

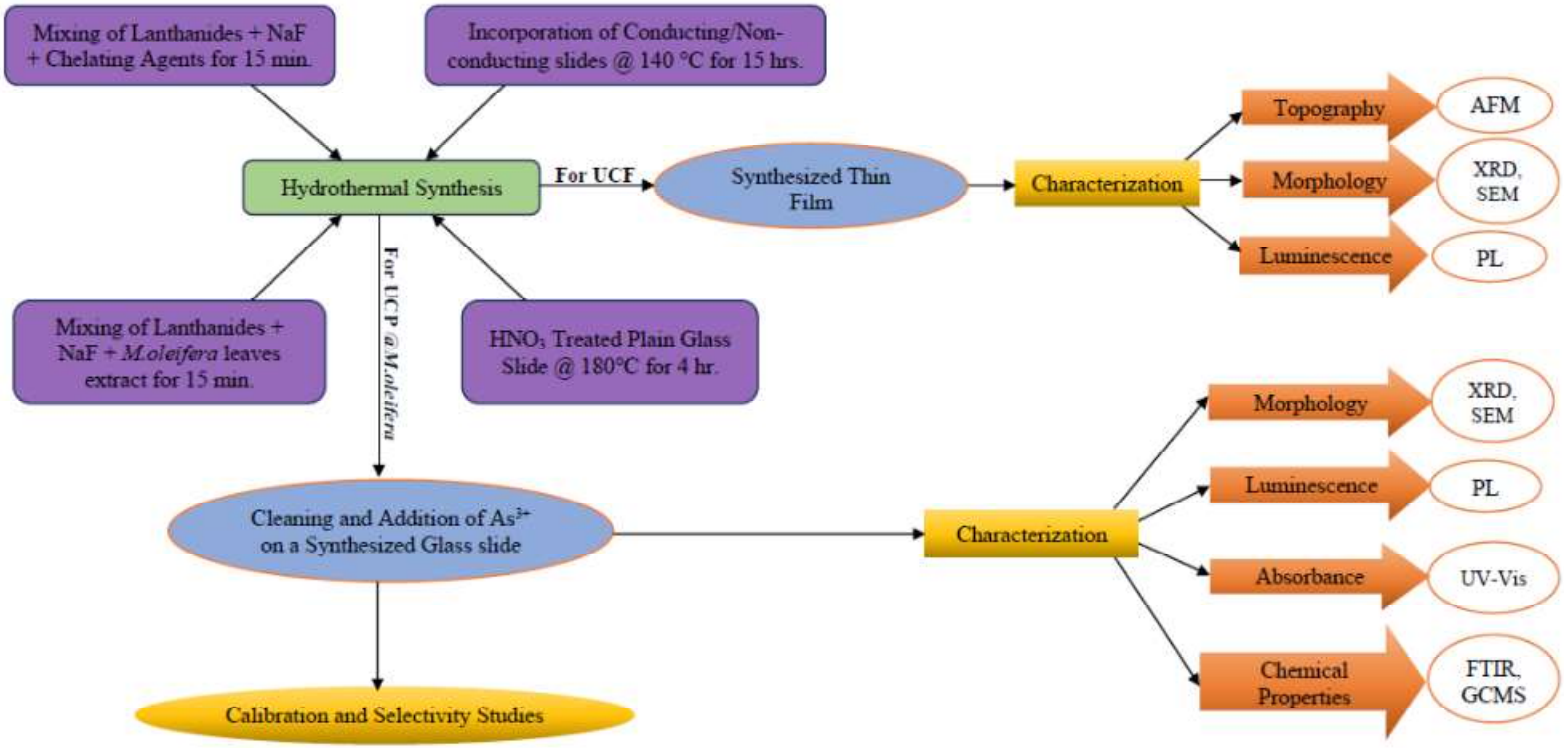

Fig. 1 Schematic of overall thesis work

TABLE OF CONTENTS

LIST OF FIGURES

LIST OF TABLES

LIST OF SYMBOLS

α	Cubic Phase
β	Hexagonal Phase
R_a	Mean Roughness
τ_D	Lifetime of the Donor without an Acceptor
E_{ef}	Flourescence Energy Transfer Tfficiency
τ_{DA}	Lifetime of the Donor in the presence of an acceptor
Rq	Root mean square roughness, nm
3σ	3 times of the standard deviation of the response
L	measured length of a given profile
2θ	angle of detector position from the incident X-ray beam
M	molar
Å	angstrom
λ	wavelength of the incident X-ray beam
mL	millilitre
g	gram scale
mmol	millimole
mW	milliwatt
W/cm	power density
$M\Omega/cm$	megohm-centimeter
μM	micromolar

$\mu g/L$	micrograms per litre volume
ns	nanoseconds
nm	nanometer
nM	nanomolar
μm	micrometer

LIST OF ABBREVIATIONS

A	Adsorbed
AAS	Atomic Absorption Spectrometer
ACL	Arsenic Contamination Level
AFM	Atomic Force Microscopy
ALD	Atomic Layer Deposition
ATR	Attenuated Total Reflectance
CR	Cross Relaxation
CRET	Cross-Relaxation Energy Transfer
CV	Cyclic Voltammetry
CVD	Chemical Vapour Deposition
CW	Continuous Wave
DI	Deionized
DMA	Dimethyl Arsenic Acid
DR	Dynamic Range
DTPA	Diethylene Triamine Pentaacetic Acid
EDTA	Ethylenediaminetetraacetic acid
EGTA	Ethylene Glycol Tetraacetic Acid
EL	Emitting Level
EPA	Environmental Protection Agency
ESA	Excited-State Absorption

ETU	Energy Transfer Upconversion
FRET	Fluoroscence Resonance Energy Transfer
FTIR	Fourier Transform Infrared Spectroscopy
FTO	Fluorine Doped Tin Oxide
G	Ground State
GSA	Ground State Absorption
ICP	Inductively Coupled Plasma
ICP-MS	Inductively Coupled Plasma-Mass Spectrometer
ITO	Tin-Doped Indium Oxide
LBL	Layer by Layer
LED	Light Emitting Diode
LOD	Limit of Detection
LOL	Limit of Linearity
LOQ	Limit of Quantitation
LRET	Luminescence Resonance Energy Transfer
MBE	Molecular Beam Epitaxy
MCL	Maximum Contamination Level
MOCVD	Metal Organic Chemical Vapor Deposition
MOS	Metal-Oxide Semiconductor
MLD	Molecular Layer Deposition
MMA	Mono Methyl Arsonic Acid

NaF	Sodium fluoride
NAPSAL	Naphthalene–Salisaldehyde Conjugate
NP	Nanoparticles
PA	Photon Avalanche
PL	Photo Luminiscence Spectroscopy
PLD	Pulsed Laser Deposition
PMMA	Poly Methyl Methacrylate
PPB	Parts Per Billion
PPM	Parts Per Million
PPT	Parts Per Trillion
PVA	Poly Vinyl Alcohol
PVP	Poly Vinyl Pyrrolidone
PZT	Lead Zirconate Titanate
QD	Quantum Dots
QY	Quantum Yield
R	Reflectivity
Ra	Average
RE	Rare Earth
RET	Resonance Energy Transfer
RhB	Rhodamine
RMS	Root Mean Square

T	Transmission
TEM	Transmission Electron Microscopy
UC	Upconverting
UCF	Upconverting Films
UCNP	Upconverting Nanoparticles
UCP	Upconverting Platform
UPT	Upconverting Phosphor Technology
US-EPA	US Environmental Protection Agency
UV	Ultraviolet
VPE	Vapour Phase Epitaxy
WHO	World Health Organization
XRD	X-ray Diffraction

Chapter 1 – Introduction

1.1. Introduction

Upconverting (UC) materials' ability to upgrade multiple low-energy photons (wavelength in the order of 980 nm) to a high energy photon in visible (400 nm–700 nm) region has propelled its applications in broad areas such as photothermal and photodynamic therapy[1,2], nanothermometers[3], heavy metal detection[4], chemical sensing and multiplex bio-sensing[5]. Additionally, UC materials are being projected as a promising material for the utilization in the areas of multilayer optical storage disks[6], photovoltaic cells[7], diagnostics platform[8], improved cell culture analysis devices[9] and optical security systems[10] requiring design of novel upconverting films (UCF) on the different substrates. In some of the applications, it is desired to grow a thin film of such materials. However, phase crystallinity, surface roughness, film uniformity has an impending effect on the upconverted emission spectrum and its intensity. It is often desired to control precisely some of the parameters that demand highly sophisticated technologies like Phase Vapour Deposition (PVD), Chemical Vapour Deposition (CVD), Layer by Layer (LBL), etc., are often expensive and use multi steps for processing (for instance, for developing a thin film of upconverting nanomaterials from the process of LBL, first it is required to synthesize upconverting nanoparticles then it is allowed to suspend in a solution of desired concentration and then lastly we got the kind of thin film that we wished for) so, in this way the process took long time in developing a thin film. For more details about these technologies, refer to section 2.1 of Chapter 2.

Additionally, film growth of fluorescent materials over the solid substrates results in nanomaterial aggregation followed by fluorescence quenching, ultimately losing its utility. Current research evaluates the role of different chelating agents and types of substrates on the film evolution, thickness and its characteristics emission when the hydrothermal route is used as a synthesis technique. Moreover, the effect of temperature on the film thickness and surface roughness is also evaluated. It is anticipated that the hydrothermal route will allow the single-step formation of the film, scalable to the industrial level.

Among different parameters, temperature and length of reaction time are likely to modulate the film thickness, phase, and crystallinity. At the same time, substrates and chelating agents are also

known to have a strong influence on film coverage, crystallinity, phase purity, film thickness, and roughness[11,12]. It is understood that the surface charge of the substrate of the chelating agent takes a great part in regulating the film microstructures[13]. Furthermore, the phase purity of upconverting materials also affects emission characteristics. For instance, $NaYF_4$, a known efficient upconverter in a pure hexagonal phase, produces highly intense upconverted emission due to low phonon-photon coupling[14]. Besides, doping of Yb^{3+} to the $NaYF_4$ host lattice increases the absorption cross-section for infrared radiation significantly. The Yb^{3+} ions act as a sensitizer (energy donor), and Er^{3+}/Tm^{3+} acts as an acceptor ion, generating emission in the ultra violet (UV)-visible region. Although, this intrinsic energy transfer remains shielded and does not allow environmental changes like solvent or surface polarity, or nearby chemical species to alter upconverted emission intensity or characteristics. Further doping of Er^{3+} ion leads to generation of intense green upconverted emission (540 nm) in addition to weak orange (650 nm) peak[15]. The $NaYF_4$: Yb^{3+}, Er^{3+} is known to exist in two crystallographic phase-α(cubic) and phase-β (hexagonal); among two, the hexagonal phase is known to have superior upconversion efficiency[14].

1.1.1. Upconversion Mechanisms

The upconversion process can be accomplished by applying three distinct methods, i.e., excited-state absorption (ESA), photon avalanche (PA) and energy transfer upconversion (ETU)[16]. All three processes employ subsequent absorption of either two or more photons to hit and occupy the excited state of emitting ions via a transitional metastable level, resulted in the generation of luminescence.

In the ESA process (Fig. 1.1a), absorption of at least two photons by a single emitting ion takes place to hit the excited state, and afterwards emission light happens. ESA is also termed as Ground State Absorption (GSA). This phenomena is considered as the least efficient upconversion mechanism, as it takes place in materials with low lanthanide dopant concentrations and large distance separation[14]. PA is the least popular mechanism among all as it takes place inside the laser cavities. The photon avalanche mechanism emanated from cross-relaxation energy transfer (CRET) (Fig. 1.1b) where two identical ions are in close proximity with each other. These ions are employed to excite from the position of ground state (G) to the intermediate excited state (E1) by excited-state absorption. Subsequently, transfer of energy

takes place during a non-radiative process where one ion returns to the ground state at the same time as another is promoted to the higher emitting level (E2)[14,17]. In the ETU process (Fig. 1.2), the consecutive transfer of energy, out from a donor ion to an acceptor ion takes place. During the ETU process, donor ions are excited to their transitional states through ESA, followed by a non-radiative transfer of energy from donor ions via acceptor ions ending in the backing of the hindmost to its intermediate state. After that, next transfer occurs and rally around the acceptor ions to the emitting state[18].

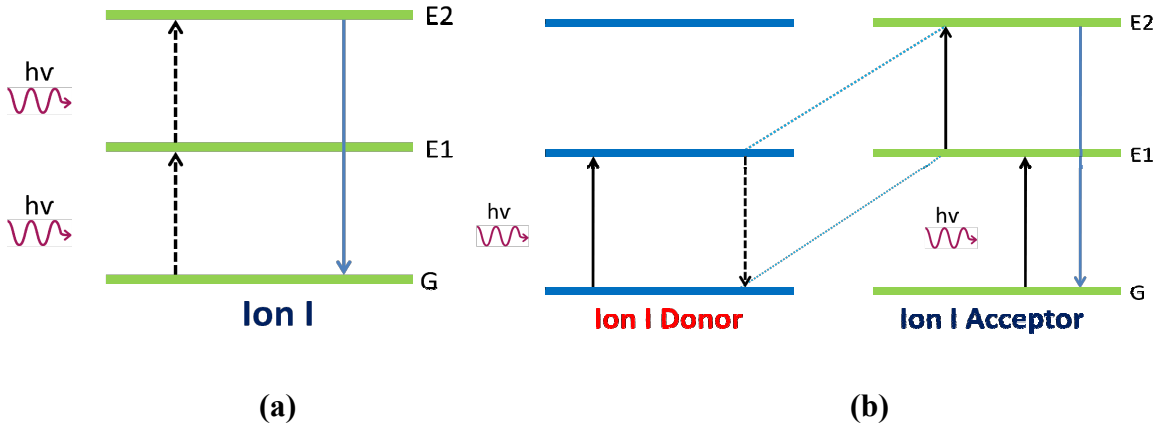

Fig. 1.1 *Schematic shows the Upconversion Process of (a) Excited State Absorption (ESA) and (b) Cross-Relaxation (CR). The dotted arrows, dashed arrows and complete arrows stands for energy transfer, photon excitation and emission process respectively*[19].

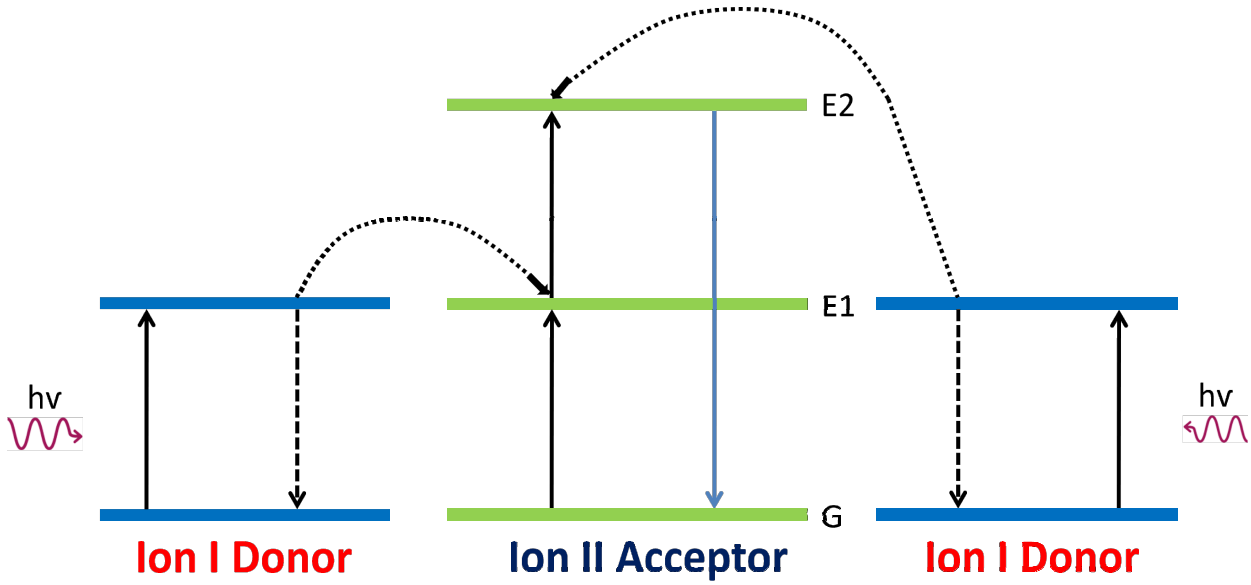

Fig. 1.2 *Schematic diagram showing the Energy Transfer Upconversion (ETU) process* [20].

1.1.2. Deciding Factors for Dopants and Host

The constituent materials of UC are dopants (impurities ~1-2%) and a host material. The doping ions form topical luminescent centers in the host as the host itself doesn't have luminescence. The Lanthanide (Ln) elements starts from an atomic number 57 (Lanthanum) and range to atomic number 71 (Lutetium). For upconverting materials, Lanthanide (Ln) elements act as dopants on account of their exclusive structures of energy level and electronic configurations. The trivalent lanthanide holds an electronic configuration of $[Xe]4f^n$, at which the variation of n ranges from 0 to 14 for the lanthanide series. The energy levels of lanthanide elements is like ladder of 4f states, which let absorption of multiple photons for consecutively appropriate energies to hit till an elevated excited state arrives. During different successive energy levels one ion possess the same distance within, leading to consecutive excitation to a higher excited state (i.e. upconversion) which is made plausible by an exclusive source i.e., monochromatic light. (Fig. 1.3) indicates a segment of the 4f energy levels of two lanthanide ions for instance which is taken from "Dieke diagram"[21].

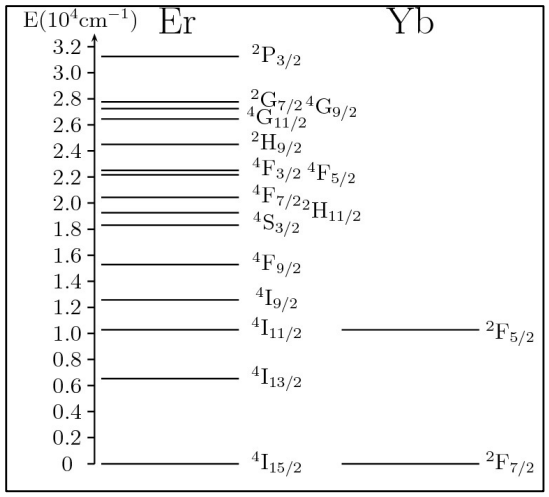

Fig. 1.3 *Diagramatic representation of partial 4f energy levels for two trivalent lanthanides taken from Dieke diagram*[21].

However, the utilization of lanthanide elements as upconversion phosphor cannot be implemented because 4f-4f transitions inside the lanthanides are Laporte-forbidden. During the formation of trivalent ion of lanthanides (Ln^{3+}) which is further doped inside the crystal lattice results in the initiation of a crystal field by the electric field of the surroundings which causes a

loss of symmetry. The Laporte rule can no longer be applied in that case, and the 4f-4f transitions of Ln ions can takes place. The likelihood of 4f-4f transitions can only be altered by the host. On the other hand the 4f energy levels, positions of lanthanide ions can be varied close to a minute amount in distinct hosts (hardly greater than $100cm^{-1}$) since the electrons in the outer 5s and 5p protects the electrons in the 4f orbital from the distress formed in the lattice[22]. This testifies the complete energy structure for a specified lanthanide ion and is independent of the host domain. Hence, the UC emissions' wavelength of lanthanide ions cannot be modified and the host can only affect the UC efficiency of Ln ions.

Principally, in every Ln ion, UC mechanisms takes place. Though, there are few ions which own underneath lying levels of energy right beneath the excited state as a consequence, non-radiative relaxation happens instead of photon emission. Also, for materializing UC processes, the energy gap in all excited as well as its ground level ought to be close enough in order to ease the energy transfer and photon absorption among dopants. Considering the reasons mentioned above, some Ln ions shows an efficacious property of UC luminescence like Er^{3+} and Tm^{3+}. By escalating the concentration levels of Ln ions, which is a key factor for UC processes also, the magnitude of emission can be enhanced in the material. However, quenching of Ln ions takes place because of the cross relaxation process when the critical concentration exceeds[23]. Distance of Ln ions and the saturation point of concentration goes hand in hand in the hosts like in case of Er^{3+} whose highest limit of concentration is 3% inspite of inadequate absorption of Ln.

With a view of establishing a co-doping system, one more Ln ion is doped as well as a sensitizer in order to rise the absorption intensity. The indicated sensitizer needs to have a greater absorption cross-section in order to absorb excitation photons and are obliged to be able to resonant with further Ln ions (activator) for ensuring sufficient transfer of energy. A commonly used sensitizer in the UC process is Yb^{3+}. For example, the gap in the energy distribution of the states $^2F_{7/2}$ and $^2F_{5/2}$ of Yb^{3+} goes well with the shift in energy between the states $^4I_{11/2}$ and $^4I_{15/2}$ and as well as in the states $^4F_{7/2}$ and $^4I_{11/2}$ of Er^{3+} (Fig. 1.3). In spite of that, quenching of Ln ions takes place at 18-20% levels of Yb^{3+} doping concentration[24].

The effect of host material on UC emission is remarkably great and in lieu of that, there is a requirement of cations and doping ions by the host material in order to have a close radius so that lattice strain formed in the host can be lowered. Widely, Na^+, Ca^{2+} and Y^{3+} ions are utilized

concerning UC materials as host cations. In addition, low phonon energy of the host constitutes small lattice and vibrations in the chemical bond. The aforesaid hosts helps in lowering the non-radiative (phonon) loss of lanthanide ions and correspondingly enhance radiation efficiency. The movement of excited electrons of lanthanide ions begins with excited state and ceases to ground state either ways i.e., by non-radiative transition (loss) or by radiative transition (emission). For a given difference in the energies of the host, the efficiency of non-radiative loss and the phonon energy goes vice versa. In addition, there is a little chance of non-radiative transition to occur because it takes greater than 5 phonons to fill the difference in energy levels from the excited state to the energy levels of ground state. In a different situation, where it takes only either 5 phonons or lower than 5 phonons to fill the energy difference, then the likelihood of non-radiative transition to happen is very large[24,25]. So, for a short phonon energy, substantial amount of phonons are needed to ease the electrons in the excited state via non-radiative transitions making the least chances of it to take place. Host of halides like Cl^{-}, Br^{-}, and I^{-} holds short phonon energies i,e., < $300cm^{-1}$ yet are terribly hygroscopic. On the other hand, the Fl^{-} and O_2^{-} hosts carries low phonon energies, i.e., ~ 400 and ~ $600cm^{-1}$, respectively but high chemical stability making them suitable for the host materials[25]. As per the afore mentioned conditions set for Ln ions' dopants and hosts, Er^{3+} and Yb^{3+} co-doped hexagonal-phase $NaYF_4$ (β-$NaYF_4$) come across as the most promising whose UC efficiency is highest also[24] and for that reason $NaYF_4$:Yb, Er are desirable and describable for extensive studies.

UC luminescence efficiency alongwith emission peak ratios get influenced by the type of composition a host matrix possess as these properties describes the (a) coordination numbers (b) crystal fields (c) spatial position (d) and gap inbetween the lanthanide ions in that particular region[27]. One of the most significant features the host matrix holds, is the transparency for the emission and excitation light. Furthermore, to utilize UCNPs in different applications, the host matrix should also enclose features of thermal as well as chemical stabilities[28].

Below described list in the table form are the host matrixes which are used to initiate UC fluorescence alongwith respective synthesis methods[25].

Table 1. Host matrixes for upconversion

Hosts	Synthesis Method	Remarks
LaF_3,$NaYF_4$, $LuPO_4$, $YbPO_4$	Coprecipitation	Fast growth rate without the need for costly equipment and complex procedures. Post-heat treatment typically required.
LaF_3, $NaYF_4$, GdOF	Thermal decomposition	Expensive, air-sensitive metal precursors. High quality, monodisperse $NaYF_4$ nanocrystals. Toxic by-products.
LaF_3, $NaYF_4$, $La_2(MoO_4)_3$, YVO_4	Hydro/solvo-thermal Synthesis	Do not require usage of heat after synthesis. Get controlled particle shape and size. Required particular vessels for carrying out reaction.
ZrO_2,TiO_2, $BaTiO_3$, $Lu_3Ga_5O_{12}$, YVO_4	Sol–gel processing	Cheap raw materials. Calcinations at high temperatures required.
Y_2O_3,Gd_2O_3, La_2O_2S	Combustion synthesis	Time and energy saving. Considerable particle aggregation.
Y_2O_3	Flame synthesis	Time saving and readily scalable.

1.1.3. Sensitizer-Activator Combination

There are two parameters that needs to be balanced that influence the process of UC and those are, the inter-ion distance & the activator ion concentration in a singly doped nanoparticle. However, elevated amount of doping can ease the assimilation of pump energy showing the way to adverse cross-relaxation because of the reduction in the distance between the ions, thereby leading to quenching in UC emission. The selection of the combination of sensitizer-activator relies on systematic transfer of energy between the two of them. Some of the features of good sensitizer-activator pairs are listed as:

- Due to the simple energy level structure of sensitizer ions, cost-effective laser sources are available, which can go with the commercially available one. For example, a simple two-level structure of Yb^{3+}ions matches with laser sources of about 980 nm.
- Comparatively long-lived excited intensity.
- Great absorption cross-section. At 975 nm, Yb^{3+} ion's absorption cross-section is of the order of 10^{-20} cm^2, which is markedly larger in disparity to other RE (Rare Earth) ions of the counterpart wavelength.
- The activator ions follow a hierarchy in order to maintain their energy level structure with enduring transitional states of energy and thus making the energy gaps equivalent to those of the sensitizer ions.
- The activator ions carry a passage of luminescence that accomplishes the needs of particular applications, as, for instance, Tm^{3+} ions exhibit emission at 800nm for deep tissues in the case of biomedical imaging technology.

In the case of co-doped materials, a very low amount of activator is used, usually < 2 mol%, in comparison to the sensitizer, which is normally high, i.e., approximately 20 mol% meant for Yb^{3+} ions in F^- (fluoride) nanoparticles. Tuning of pathways associated with excitation and emission can be done by incorporating a different class of ions. In general, emission bands of several colours may be realized by putting unlike activator ions inside similar nanoparticles for the generation of white light in displays[29] and in optical imaging[30]. Also, the introduction of Ce^{3+} ions into the Yb-Ho arrangement is done to regulate the upconversion emission from green→red[31], in addition to Yb-Tm system in which tri-doping of Nd^{3+} ions is done to increase the blue emission of Tm^{3+} ions in upconversion process[32].

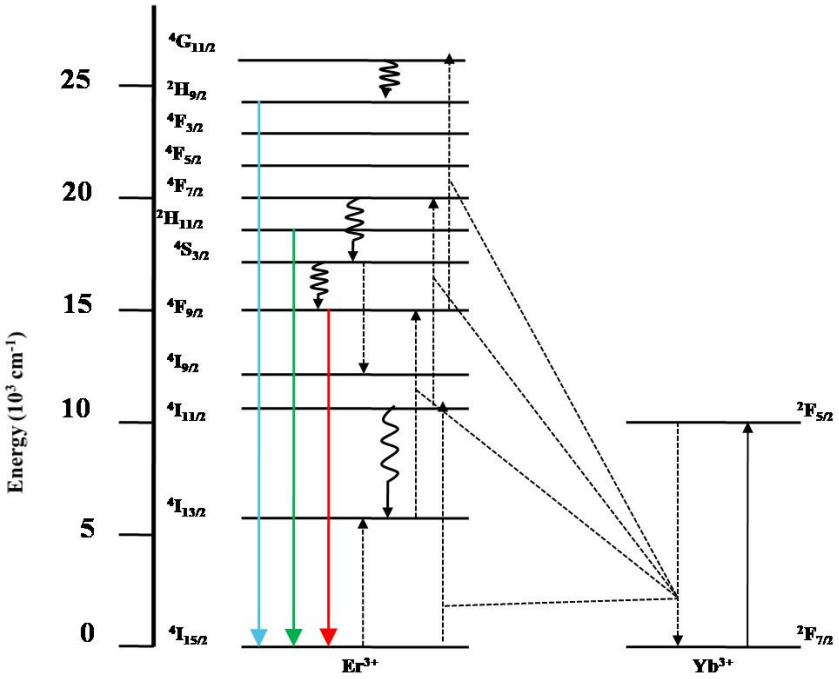

Fig. 1.4 *Schematic showing the UC system of Yb^{3+}/Er^{3+} doped UCNPs. Complete arrows signify radiative processes with coloured arrows signifying the emission wavelength. Dotted arrows signify non-radiative energy transfer and wavy arrows signify multiphonon relaxation processes*[33].

1.2. Basics of Thin Films

A thin film can be formed by any kind of material that can form a coating or layer on a particular substrate, having a thickness in the range of micrometers to nanometers. The layering of material on a substrate serves different functions according to one's requirement, such as protection against corrosion, reduction of wear, and chemical stability of a substrate are some of the main basis of coating. A film is said to be made up of one to many layers, may have a homogeneous depth, or may have an inclination in composition also.

However, coating a surface is not enough for protecting the substrate; rather, surface modification can also be done for that purpose. The surface modification allows the properties of the substrate to alter (near-surface region), which in turn increases its capability to resist corrosion, stress, wear and so on. By modifying the surface region, internal stress, crystal structure as well as chemical composition can be changed. Such alteration splits the surface of the substrate into two regions, namely a modified region and an unaffected region. However, no boundary exists between these two regions except a transition, which can be seen very gradually

on the substrate. The combination of such two regions (modified/unaffected core area) is known as a duplex treatment.

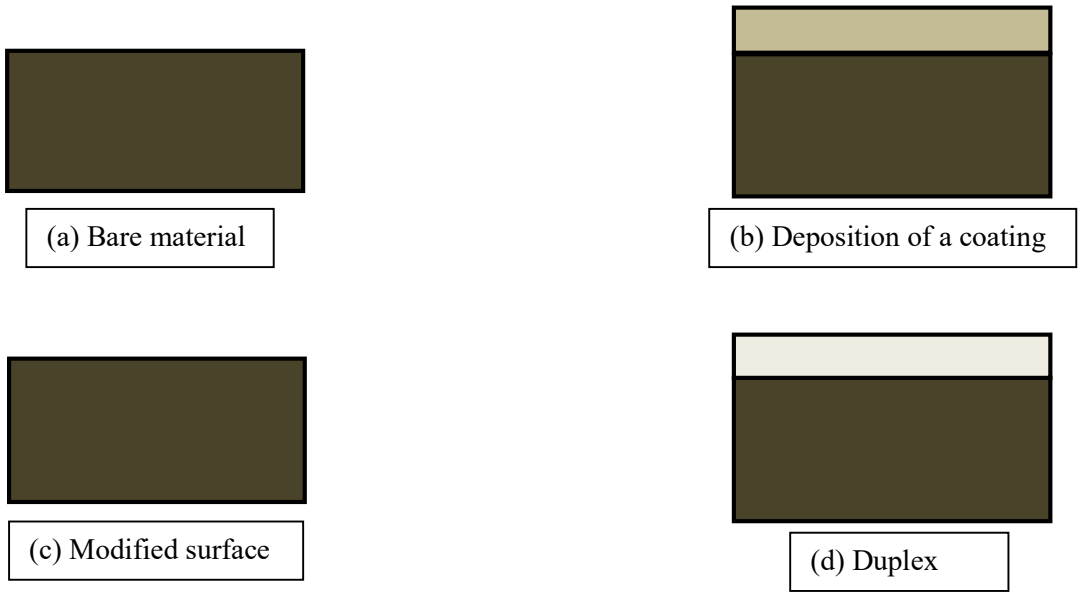

Fig. 1.5 *Types of surface engineering techniques (a) bare material, (b) deposition of a coating, (c) modified surface and (d) duplex (combination of modified surface and deposition of a coating)*[34].

1.2.1. Types of Film

1. **Single layer film:** is formed when its properties do not get disturbed with the change in the depth of the film. Ideally, none of the films achieves the homogeneous nature of the deposition of coating on a film as it is assumed that the deposition conditions do vary a little bit with time.
2. **Double layer film:** is formed when the parameters of the process (deposition) get changed abruptly at least once during the deposition of the film. Being a non-homogenous type of film, it is considered to be the simplest one to form. The composition of both layers can be either the same or different. In case the composition is different, it is very easy to make a distinction between the two layers. On the other hand, if the composition is same then their chemical states, crystal structures and grain sizes must be dissimilar, which can help in differentiating the two layers of the film.
3. **Gradient film:** is formed when the parameters of the deposition process change gradually.

4. **Multilayer film:** is formed when the changes happened during the deposition process take place several times. This change in parameter can be discrete as well as gradual also.
5. **Composite film:** is formed when the grains of the phase of the first film (let us say A) is allowed to be embedded in the matrix of the second film's phase (let us say B)[34].

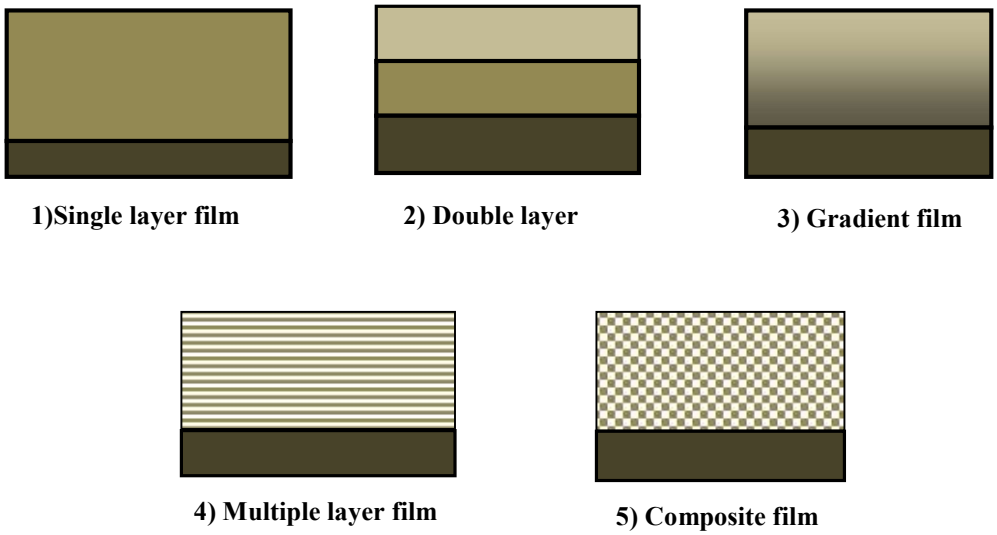

Fig. 1.6 *Basic types of films 1) single layer film 2) double layer film 3) gradient film 4) multiple layer film 5) composite film*[34].

1.2.2 Thin Film Structure

In the course of depositing thin film, many unlikely and complicated chemical reactions occur, depending upon the kind of process & deposition variables utilized, e.g., deposition rate and pressure-temperature of the substrate and the positioning of vapour stream with respect to substrate, which all helps in forming microstructures of diversification. These microstructures establish the properties (chemical as well as physical) of the film, which is further classified structurally as amorphous, polycrystalline & epitaxial.

1.2.2.1. Amorphous Thin Films

These are those films whose structure lies in the order of short-range that is from some micrometers (mm) to hundreds of nanometers (nm)[35]. The structures are extracted from an ideal crystalline lattice when the deflection in the bond length & angle happens. Moreover, during the growth process of the film, the mobility of the adsorbed atoms (adatoms) is limited to the surface of the substrate because of the low temperature of the substrate, due to which these adsorbed atoms proceeds towards a thermal equilibrium along with the substrate by capping the energy for

diffusion via its surface. Alternatively, the incorporation of nearly immobile adsorbed atoms intends to hit almost the surface of the substrate. However, there is one more way of generating amorphous growth on substrate i.e., through a high deposition rate. Due to the high deposition rate, diffusion time gets restricted and hence the migration of adatoms puts a stop to reach higher energetic sites in order to gain equilibrium, following which these adatoms are absorbed in the structure of the film, just going to impact with the surface of the substrate.

A number of researches outlined the initiation of these unsystematic microstructures with the introduction of some specific gases like N_2, O_2 that cause some kind of hindrance in the growth process of crystallites at the time of deposition process[36]. Techniques like phase vapour deposition (PVD) and chemical vapour deposition (CVD) form amorphous structures during the processing of thin films. Such kind of thin films have a vast number of application areas e.g., in dielectric films, solar cells, optoelectronics, transistors and many more.

1.2.2.2. Polycrystalline Thin Films

These films are formed when the rate of deposition temperature is increased above that which was put in order to get amorphous structures. These films are included in a multitude of nano to micro crystallites with distinct orientations, which are segregated with respect to grain boundaries. Deposition parameters like deposition rate and the temperature usually influence or decide the size of the crystallite. Because of the rise in the substrate temperature, adatoms start to move fast, due to which their thermal equilibrium with respect to substrate gets disturbed and starts to diffuse in the surface of the substrate with all of its energy till it gets attached to a prevailing island or forms a new island. In order to attain thermal stability, the sizes of these islands have to hit the nucleation threshold; after that they continue to grow till saturation point comes and afterward a process called coalescence begins between islands that bring on the origination of a layer known as a polycrystalline layer. Also, from the above discussion, we can say that the adatoms diffusion is purely a temperature-dependent procedure in which crystalline size varies in proportion with the substrate temperature. Crystalline size can also be influenced by the thickness of the film. Moreover, the coalescence process limits the growth of the crystallite in the sideways direction, while film thickness limits the growth in the z-direction only. These types of microstructures are used in applications related to thermoelectrics.

1.2.2.3. Epitaxial thin films

These can be described as a solid crystalline film that is deposited on the top surface of the substrate and whose crystallographic and crystal orientation are in the same phase of the substrate's surface. There are two types of epitaxial growth that exist in accordance with the kind of substrate used; a) Homoepitaxial, b) Hetroepitaxial. In the first case, i.e. in homoepitaxial the material of the growth layers and substrate is the same, whereas in the second case, i.e., in hetroepitaxy, the material of the growth layers differs from that of the substrate's material. Commercially the viability of these epitaxy thin films lies in the sector of the semiconductor industry where there is a need to develop quantum wells and wires from fine quality and 13 intricate films. Such films are grown with the help of techniques like molecular beam epitaxy (MBE) and vapour phase epitaxy (VPE). Growth of epitaxial films depends upon several factors, a) Equilibrium thermodynamics of nucleation, b) Formation of vapour from reactants, c) Reactions occurred on the substrate surface, d) Portability of species via the surface of the substrate. The formation of epitaxial films will take place at a particular temperature known as the epitaxial temperature where these tricky interactions takes place and are decided by deposition parameters as well as specific system. Mostly, the growth of epitaxial films happens at an elevated substrate temperature in order to stimulate the mobility of adsorbed atoms in the surface of the substrate that aids in the construction of islands which attains stability after reaching a particular size. The growth of the film will not stop after achieving stability rather, the growth continues and surges the nucleation density, which further shapes a solid film with favorable orientation. One of the factors that greatly make an impact on the quality of the epitaxial thin film is strain. Because of the lattice misfit, the strain is produced during the deposition process of the film. Furthermore, the thermal strain produces an incompatibility between the film and the substrate because of the existence of unlike thermal expansion coefficients. Another influential factor is the contamination of the substrate surface that greatly inhibits the growth by ceasing the development of epitaxial film layers. In order to fend off this factor, reduced pressure or, at times, vacuum are used to precede the deposition process, which further assists in the effusion process in order to eliminate all the current impurities from the substrate's exterior part[37].

In recent years, different types of deposition techniques have been developed and are used by many researchers and industries for making thin films of different sizes, shapes, textures, etc. Thin films have grown from the technologies like PVD, CVD, PLD, ALD, MBE, etc., generally possess internal stress, reduced size of grain; also defect's density is great and holds a columnar microstructure alongwith supersaturated solid solutions, formation of metastable phases and many more. Whereas in some other deposition techniques, the presence of these types of results is quite ambiguous. Thin films grown from these techniques may be an amorphous film, an epitaxial film, a polycrystalline homogeneous film, or a nanocomposite film that may have two or more phases. As is the case, these processes are very costly, which further addstothe cost of thin films when produced commercially. Also, the process setups are large and complex, needs proper technical manpower to operate and handle the apparatus, the temperature requirement for the deposition process is very high, usually between 300° C to 900° C due to which there may be a possibility of getting precursors toxic, low deposition rates, usuage of some toxic gases and many more.

Subsequently, there exist some other processes also which can nullify the cons of above-mentioned techniques, and out of those available processes, one is the hydrothermal method of preparing thin films. It is one of the potential techniques developed in recent times that shows great results while preparing thin films, bioceramics, vanadates, garnets, ceramic oxides and many others[38]. Hydrothermal process is a very simple, inexpensive technique that uses a broad spectrum of temperatures i.e. starting from approximately room temperature to very high temperature, for synthesis. While preparing thin films from this process, we make use of precursors like inorganic salts and solutions of aqueous hydroxide, mainly during a chemical reaction and substrates like glass slides, silicon, metal flakes, plastics and α-Al_2O_3. Preparing film through hydrothermal makes post-crystallization heat treatment step superfluous, keeping away from the defects like cracking, curling, grain coursing, and film's reaction with the atmosphere and substrate throughout the process of heat treatment. The deposited film shows results like a good consistency, high purity, large surface area, high performance of the material, controllable morphology and many more. The parameters which govern the hydrothermal method of depositing thin films include pH of the precursor, growth time and temperature, concentration of the precursor, pressure maintained in the system, annealing and seeding[39]. These parameters help in shaping structural, optical, mechanical as well as electrical properties

of a film which can be further analyzed by using a different kind of optical microscopies like SEM, AFM, TEM, Photoluminescence, XRD and so on. More details about the hydrothermal method and other processes will be discussed further in chapter 3.

1.2.3 Properties of Thin Film

After the deposition process, it is essential to determine the properties of thin films as these properties further decide the applicability sector of these thin films.

1.2.3.1 Structural Properties

1.2.3.1.1 Thickness

One of the most important features of a thin film is the thickness, not the total thickness but also the thickness of each individual layer, as it not only influence but also plays a deciding factor for other properties too. Generally, the as-synthesized or fabricated or deposited thin film is not an ideal film i.e., the smoothness of the film varies at different places, due to which we may get different thicknesses at different positions on the same film. The degree of thickness depends literally on the type of method selected for the measurement of thin film as different methods may employ different results for a similar film. For example, suppose a method is applied for calculating a mass that is grown over a unit area then in that case, the average thickness can be analyzed by utilizing a known value of mass density, and after that, the thickness attained is the mass thickness of that particular area. So, in this way, we can calculate even a small fraction of that layer (monolayer) that may be in the nanometer range. Hence, extremely thin film thickness can be measured by employing a particular method of interest. Measurement of thickness of films not only can be done after finishing the deposition process, but there are methods available that can be utilized for analyzing the thickness even during the formation of the film. Through these monitoring methods, one can prepare a thin film of desired thickness. Deposition rate, a significant factor, manipulates the morphology and other several properties of the film and can be measured by calculating the development of thickness over a unit of time. Methods to keep a check on thickness can be categorized in a number of groups like electrical, balance, optical and some other techniques acquired from chemical analysis, emission and absorption of radiation and so on.

Many characterization techniques (approx 20) are available these days for analyzing the thickness of a thin film. Out of them, atomic force microscopy (AFM) and profilometer are the most commonly used and versatile techniques to work in the laboratory. Both techniques use a sharp tip to scan the surface of the film, which further records the displacement in the z-direction. Though AFM is not used for analyzing very thin films because of the fact that it selects a very small area for scanning and the maximum height is low too.

1.2.3.1.2. Surface Roughness

The establishment of a rough surface of the film begins when the nucleation barrier is increased, and the supersaturation is reduced, then the formation of some little but huge nuclei happens, leading to the development of coarse-grained rough films, which regularizes at fairly large thicknesses. Surface mobility and surface smoothness of a film go hand in hand; if one increase, then the latter also increases by infusing in the concavities. If the influential species are directed at an angle rather than falling straightly on the substrate, it results in the augment of the surface roughness. The occurrence of this incident takes place at frequent intervals because of the shadowing effect of the adjacent columns, which are aligned in the direction of influential species. The surface topography tells the shape of the surface of the film, geometrically, which can be described in three dimensions as x, y and z. Many surface topographical variables exist which can be calculated for different studies. Out of them, mean roughness R_a is the most extensively used variable which can be calculated as

$$R_a = \frac{1}{L}\int_0^L |z(x)|\, dx \qquad (1)$$

where, L is the measured length of a given profile.

For measuring the surface roughness, techniques like optical profilometers, AFM can be used.

1.2.3.1.3. Crystal Structure

Particular geometrical arrangements of atoms constitute a crystal structure in solids, which is one of the prime features of nanotechnology. As we know that the bulk material properties differ in comparison to thin-film properties in the same way the structural properties of bulk material differ from the crystal structure of thin films. In the deposition process, thin films experience

internal stress due to non equilibrium conditions i.e., difference in temperature, which brings in the modification of the film's lattice parameter and hence creates a shift in the diffraction pattern of the film. Also, parameters like grain size, preferential orientation, substrate influence differ from that of bulk polycrystalline film. The deposited film may have a small grain size as the peaks get diffused; there may be effects on the intensity of peaks and substrate peaks too.

The principal characterization techniques available for determining the crystal structure as well as phase of the film are XRD and transmission electron microscopy (TEM). In the case of the XRD technique, the shape of the peak describes the phase-type of the substance, i.e. a broad peak corresponds to the amorphous regions, whereas a sharp peak is constant with the crystalline ones. Crystallite size can be determined by the peak width, revealing broad peaks for small-sized crystallites and narrow peaks for large crystallites.

1.2.4. Optical Properties

In the thin film, optical properties can be analyzed by measuring reflectivity (R) and transmission (T) using optical microscopy techniques. The matter of fact is, the reflectivity of a coated surface in the case of thin films builds on the wavelength of the influential photons and the transmission of light will be subjected to frequency. Thus, the selection of the range of wavelengths must be decided in accordance with the type of information required. In the UV-visible range, if the values of R and T are known, then one can find out the optical absorption too. In reality, if a light goes through a material, then either it will be reflected (R), transmitted (T), or absorbed (A).

There are many characterization techniques that can help in analyzing the optical properties of a thin film. Optical spectroscopy includes UV-vis spectroscopy (UV-vis), fourier transform infrared spectroscopy (FTIR), photoluminescence spectroscopy (PL), electroluminescence spectroscopy (EL), etc. In the case of PL, when a photon is excited from an external source (laser), an optical emission is recorded at a particular wavelength.

1.2.5 Mechanical Properties

Mechanical properties like elasticity, hardness, plasticity, adhesion perform a vital role in deciding the quality of a thin film. Through different characterization techniques, these properties of thin film can be analysed, for example, analysis of freestanding films can be done by tensile testing and by deflection techniques such as micro beam cantilever. Another technique known as nano indentation exists in which tests can be run very fast, accurately and reasonably without preparing any special sample for the technique.

1.2.6 Electrical Properties

During the formation of the thin film, scaling effects start developing, which can further impact the electrical properties of thin-film material. Parameters like the thickness of the film, surface roughness, lattice dimensions, imperfection level of the layer and purity explain the mechanism, type and stability of the electrical transport. Three types of electron materials exist, i.e., metal, semiconductor and dielectric, of which electrical transport behavior is distinguishable in all three of them[40].

1.3. Significance of Arsenic and its Sensing

Current thesis work plans to grow nearly transparent UC thin-film entailing capability to ensue fluorescence resonance energy transfer and use it to detect arsenic in drinking water.

Arsenic is a metalloid (contains properties of both metals and non-metals) that originates in nature and is extensively dispersed in the outermost layer of the earth[41]. The existence of arsenic is divided into three categories, i.e., organic, inorganic and arsine gas[42]. Arsenic is available in four states of oxidation: -3, 0, +3 and +5[43,44,45]. The toxicity of arsenic depends upon the factors like chemical composition, bio availability and oxidation states[43].

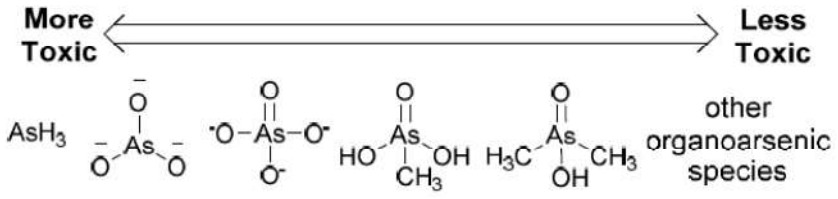

Fig. 1.7 *Showing Arsenic toxicity in declining order (left to right) that can be exited in water as: arsine gas, arseniteoxoanion, arsenateoxoanion, monomethylarsonic acid (MMA), dimethylarsinic acid (DMA), and other organoarsenic species*[46].

Also, the toxicity levels, as shown in Fig. 7, are higher in the case of inorganic arsenic, while according to oxidation states, As^{+3}(arsenite) is more toxic than As^{+5} (arsenate)[47]. Generally, oxyanions (an inorganic form of arsenic) are present in water in the forms of As(III) and As(V). Arsenate (As^{+5}) dominates over other states while using oxidizing conditions, while Arsenite (As^{+3}) is expected to show dominancy in reducing conditions[41]. Arsenic is considered a human carcinogen[48], to which 144 million people have been exposed[49]. Trivalent (+3) oxidations state[50], being the most toxic, causes serious health problems to mankind[51]. Due to this, US Environmental Protection Agency (US-EPA) and WHO lowered the maximum arsenic contamination level (MCL) in drinking water from 50 to 10 parts per billion (ppb)[52]. However, arsenic is reliably detected using an ICP-MS, atomic absorption spectrometer (AAS), stripping cyclic voltammetry (CV), and other sophisticated instruments[52,53]. These facilities are bulky, difficult to transport, incur a high capital cost, and require specialized manpower;besides, its sample preparation is complex and time-consuming[54]. These limitations constrain arsenic detection in resource-crunched areas. Therefore, there is an urgent demand to develop an affordable, lightweight, luminescence-based, arsenic-sensitive and selective sensor amenable to the conventional spectrofluorometer or cell-phone-based systems. For example, the colorimetric sensor developed by Wei et al[55] to detect mercuric ions (LOD =3.5 ppb). This sensor measured changes in the solution absorbance by a cellphone camera attached to a cuvette holder. A number of solution-based LRET upconverting sensors were also developed for the detection of different analytes[56].

1.4. Fluorescence

Fluorescence is a process where a high-energy photon is absorbed and a low energy photon is emitted. The process is spin conserved and occurs in 10^{-9} seconds (Lifetime). When a high-energy photon (proper energy) impinges on the molecule, electrons in ground-state electronic state absorb the energy. This electron is excited to the higher vibrational state of the next higher electronic state. Excited electron relaxes back to the ground's vibrational state of the excited electronic state through internal conversion, releasing the excess energy in the form of heat (radiative transfer). This transition occurs in 10^{-15} seconds, very quick to displace the nucleus from its nuclear coordinate.

Fluorescence takes place during the absorption of light when taken by a fluorophore at a certain wavelength which in turn re-emits photons following the relaxation in a type of heat. The gap

between the energies of the excited as well as the ground state is decided by the wavelength of fluorescence. The pictorial representation of the fluorescence is done with the classical Jablonski diagram as shown in (Fig. 1.8) as proposed by Professor Alexander Jablonski for the very first time in 1935 aiming to report about the absorption as well as emission of light. The molecule rests in the ground state before excitation happens and then only its electronic configuration can be reported. Upon absorption of a photon of excitation light, usually shorter wavelengths electrons may be raised to a higher-energy and vibrational excited state. This procedure barely takes a quadrillionth of a second (oftenly mentioned as a femtosecond i.e., 10^{-15}seconds). The lifetime of fluorescence is typically four orders of magnitude slower than vibrational relaxation so that the molecules take enough time to lose a part of their excitation energy in order to have thermal equilibrium prior to fluorescence emission. The difference between the peak excitation and emission wavelengths of a fluorescent species is defined as Stoke shift.

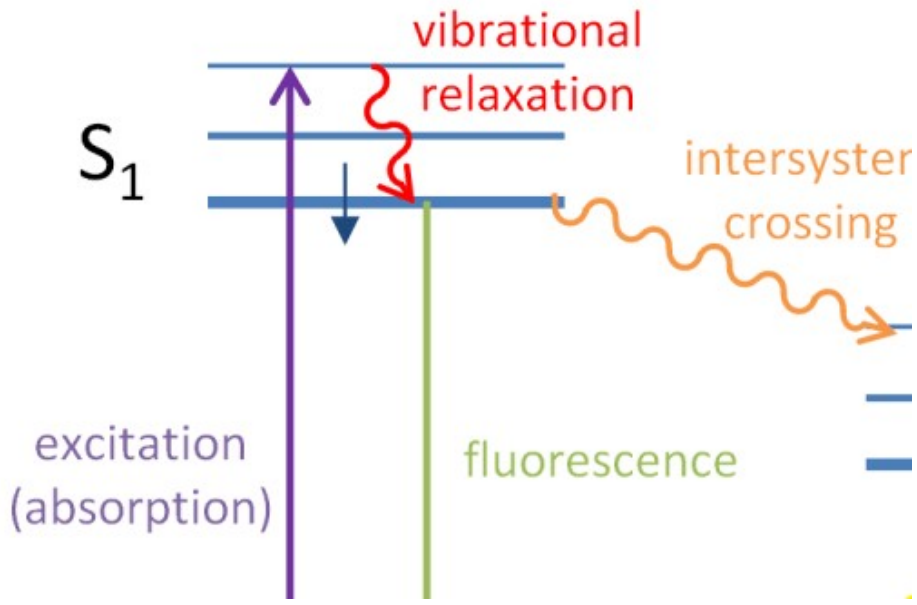

Fig. 1.8 *A pictorial representation of Jablonski diagram*[57].

All the variables of fluorescence and alteration occured may be utilized to encode what is happening in the vicinity of the monitoring molecule and decide the changes in biomolecules. Information on the changes within the targets' molecular environment can thus be derived from their fluorescence signals and their exact locations can be tracked with the use of fluorescence microscopy. Such characteristics makes fluorescent materials potentially high which can further

be widely applied in the biological as well as medical research field. Firstly, the path of biomolecules could be observed over time by labeling with fluorescent labels. Secondly, the interaction between two biomolecules could be observed by labeling both the prey and the bait. Especially, the biomolecular interaction could also be observed from the fluorescence resonance energy transfer (FRET) by labeling with two different types of fluorophore in which one's excitation wavelength matches the other's emission. Thirdly, the activities of light-sensitive biomolecules could be observed by observing the fluorescence change of the fluorophores linked to them. Last, environmentally sensitive fluorophores may be used as molecular reporters and the change of environment around the molecule could be monitored by observing the fluorescence labels.

1.4.1.Tuning Upconversion Emission using FRET

In recent years, the influence of fluorescence-based detection has increased in biomedical, biological and related sciences. It has also become one of the foremost sensing technology due to its dominant characteristics, which makes it a pandemic. Its sensitivity, an important characteristic, makes it likely to sense even a single biomolecule through labeling it with an appropriate fluorophore. Properties like brightness and photostability are the two principally and fundamentally important properties in order to achieve a high level of sensitivity in many conventional fluorophores. Fluorescence-based sensors and biosensors have been valuable analytical tools since fluorescence is a highly sensitive and selective phenomenon[57,57]. Recent developments in the field of biosensors enabled their employment in new applications primarily focusing on real-time monitoring of biomolecular interactions. For example, biosensors were used to monitor processes like ligand fishing[58], signal transduction in cells[59,60], cell adhesion[61], enzymatic reactions[62], and protein conformation changes and aggregation[63,64]. Fluorescence-based biosensors have also been used in drug discovery in studies involving primary screening of drug candidates as well as clinical trials[65–68]. Fluorescence biosensors demonstrate significant advantages over commonly used electrochemical sensing techniques since they do not consume their targeted analyte.

Applications of upconverting nanoparticles in sensing and detection promise the most important research fields now a days. The luminescent behaviour of rare-earth ions depends upon the host lattice and the quenching centers of the nanocrystal, which usually resides in or on the surface of

it. UCNPs usually retort slightly to variations in the environs except temperature[69], resulting in the usage of UCNPs difficult as direct sensors for detection-based applications. Propitiously, energy transfer processes make it possible to familiarise an analyte responsive chromophore as the optical detection component, and the wavelength conversion ability of UCNPs can extend the working wavelength of this chromophore from the original short-wavelength region to the NIR range.

Various concepts and principles of energy transfer had been proposed and it was observed that the energy transfer from a donor (refers as D) to the acceptor (refers as A) takes place usually in two dissimilar ways i.e., radiatively and non-radiatively. In the radiative form of energy transfer, the emission of a photon takes place from the donor, and then that photon is subsequentially absorbed by the acceptor[70]. Oppositely, in the non-radiative energy transfer, no emission or re-absorption of photons occurs; rather, the deactivation of the donor and the excitation of the acceptor occurs simultaneously, and the energy transfers through coulombic interactions. Due to this phenomenon, non-radiative energy transfer is also termed as "resonance energy transfer" (RET), or more specifically, foster resonance energy transfer (FRET) or luminescence resonance energy transfer (LRET), specifying the energy is transferred due to the "resonance" between the donor and the acceptor. Although it is required that the emission spectrum of the donor overlaps the absorption spectrum of the acceptor in both cases, the resonance energy transfer process possibly occurs only when the distance **r** between donor and acceptor is relatively small (typically < 10 nm) (Fig 1.9). Granting, energy transfer takes place simply on condition of the spectral overlap of the D–A pair, yet in related studies, it is also necessary that the excitation wavelength of the donor resides out of the absorption band of the acceptor so as to eliminate the possibility of direct excitation of the acceptor, ensuring that the acceptor is only activated by the energy transferred from the donor[71]. However, this prerequisite is generally not easy to meet for conventional D–A pairs, as classic donors are usually excited in the UV and visible range, despite the fact that the acceptors (e.g., dye molecules, semiconductors, noble metal nanoparticles) show broad absorption bands in the same range.

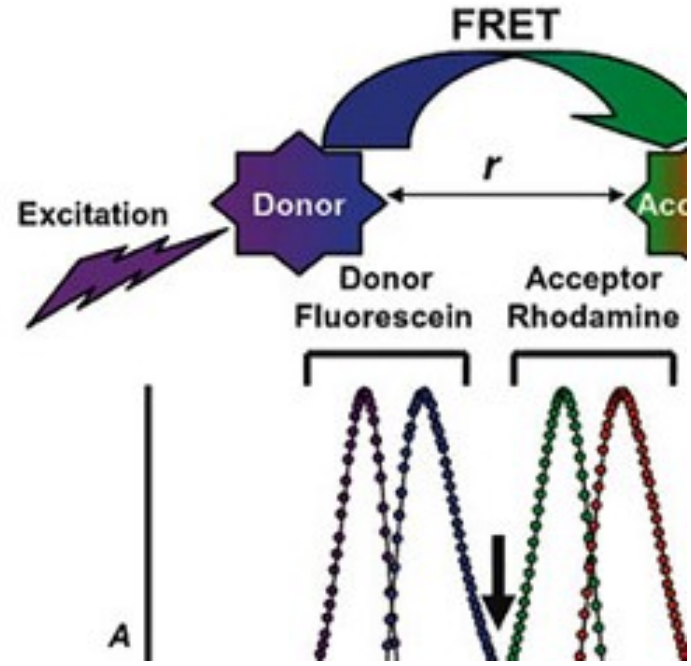

Fig. 1.9. *Schematic of the FRET process*[72].

However, during the event when UCNPs serves as the donor, they are excited in the NIR region, where the acceptors are barely absorptive. Therefore, UCNPs can be employed as ideal donors for different acceptors in the studies of energy transfer. Two foremost approaches have been utilized in order to manipulate the LRET efficiency[73] :

1. By tuning the spectral overlap and
2. By tuning the distance among UCNPs and the acceptors.

1.4.2. Tuning Spectral Overlap

The LRET efficiency can be controlled by modulating the absorption of acceptors affected by the physiological change (intensity/wavelength) in the environment when the analyte approaches the sensing surface. In a sequence, the analyte will act in response with the recognition groups to chunk the LRET process, leading to the recuperation of the emission of UCNPs. It has been perceived that triggering as well as blocking the LRET processes are effective detection strategies that works in either way too. Since an array of fluorescence probes have been taken into account to sense ions and tiny molecules through the modification in absorption/

fluorescence, it's an incredibly suitable way to create a LRET based probe by putting together correct sensing groups in contact with the surface of UCNPs.

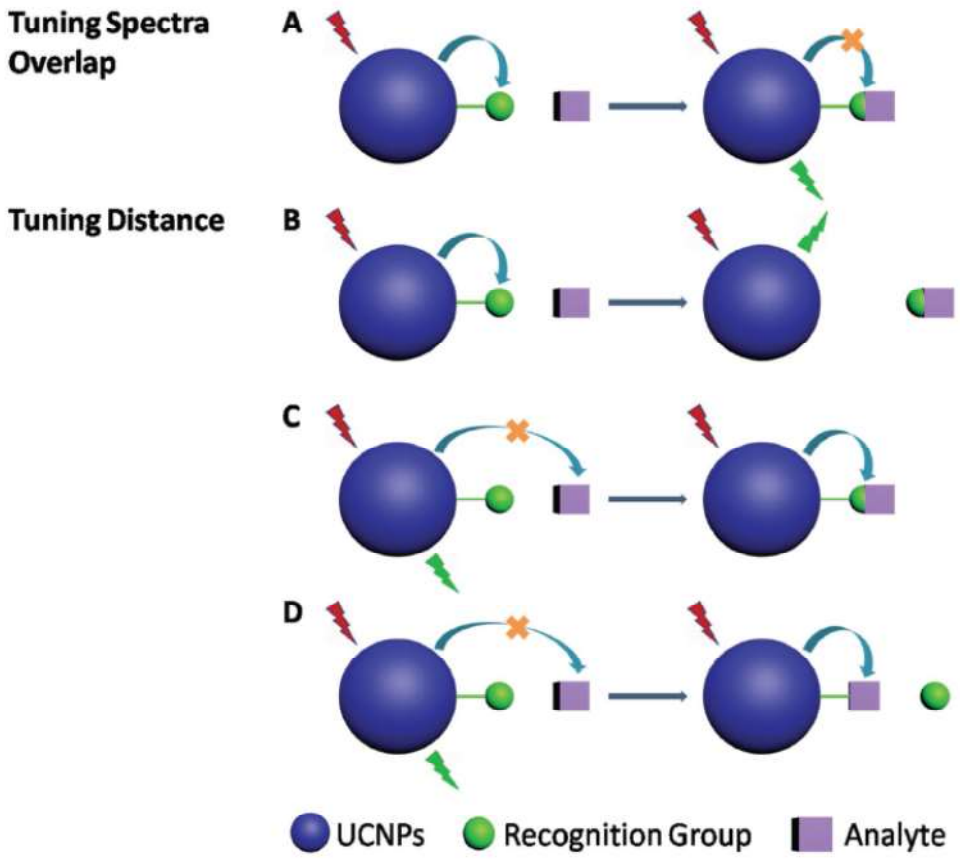

Fig. 1.10 *Shows the two main detection schemes of LRET* [73]

1.5. Synthesis Methodology of Upconverting Nanophosphors

Generally, the synthesis of phosphors relies upon the type of applications one wishes for and accordingly, the synthesis of phosphors by using different categories is carried out. These are listed in Fig. 8.

1.5.1. Synthesis of Bulk Phosphors

Traditionally, for synthesizing phosphors (bulk), a method called solid-state reaction is used. The bulk phosphors are processed at high temperatures keeping environmental conditions in check. The selection of solid compounds is made on the basis of their chemical equations (precise stoichiometry), which should be balanced well and that could provide the product output which is wanted. The process involves homogeneous mixing as well as grinding of the sample taken, which is further set up for heating. Afterward, the sample is flattened gently and washed several times thoroughly so that all the impurities (flux) attached with the sample can be removed away and hence, a final product is obtained in the last. There are two major steps for synthesizing bulk phosphors in order to attain utmost energy efficiency, i.e., (a) optimal fire cycle(b) doping concentration.

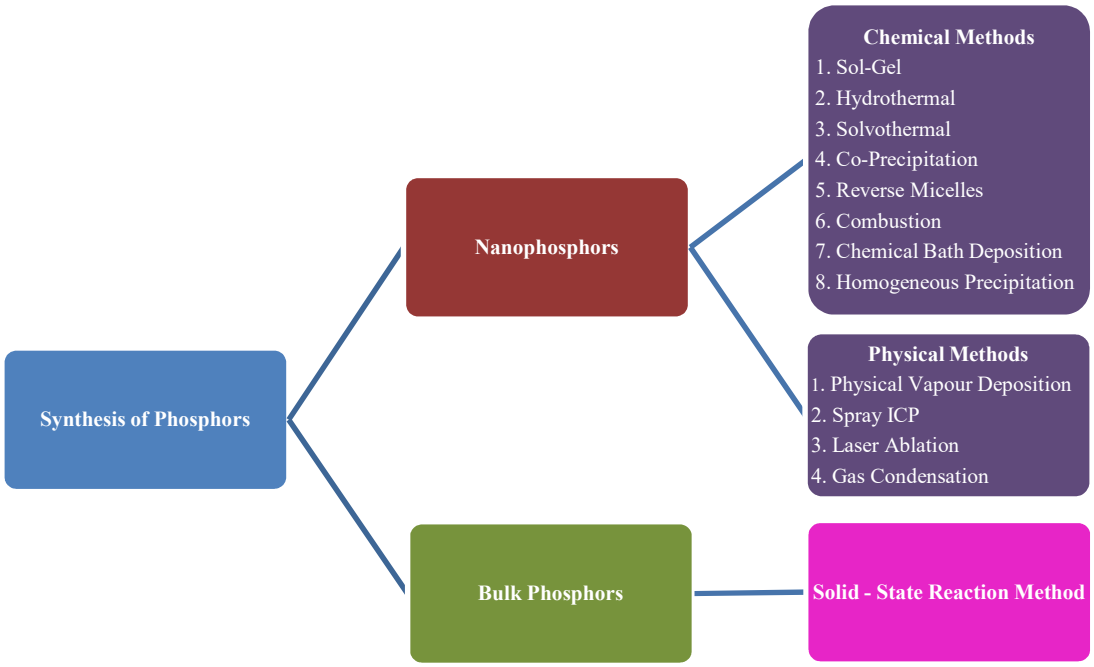

Fig. 1. 11 *List of synthesis procedures employed for bulk and nanophosphors.*

1.5.2. Synthesis of Nanophosphors Films

Synthesis of phosphors at the nanoscale in the form of nano-thin films/nanoparticles/nanocrystals can be produced by using two types of methods which can be classified broadly as (a) Chemical Methods (b) Physical Methods (Fig. 8). Chemical methods of synthesis are usually carried out in solution form and are imperative for the development of nanoparticles/nanocrystals at fairly low temperatures. The chemical methods are cheap, easily available and can be prepared in great quantities using different elements and compounds. Precipitation of precursors is a typical step laid down in solution during the wet chemical process in which it is totally optional of the final product to treat it with heat or not. Out of all methods (chemical), it has been investigated that the hydrothermal method is the most promising technique because of its advantageous features like economically viable, can be operated at low temperatures, environment friendly, etc.

Through physical methods of synthesis, we can develop thin films of nanophosphors from micro to nanoscale, either via evaporation or ejection in a highly sophisticated vacuum atmosphere. These films are synthesized from bulk (phosphors), and in order to produce a high grade of pure and stable thin films, one needs to check on experimental conditions. As shown in Fig. 5, there are a number of physical methods, but among the entire techniques, pulsed laser deposition (PLD) holds great attention from researchers. PLD embraces some great advantages over others like it is conceptually simple, versatile in nature, easy to use, cost-effective, fast, etc. This technique has gained enormous success while depositing materials which are having complexities in their stoichiometry. Through the PLD technique, researchers were able to deposit a superconducting thin film also.

1.6. Thesis Motivation and Objectives

From the past few decades, there is a continuous rise in the pollution or contamination caused by heavy metals in the atmosphere or in the aquatic ecosystem. Industrial waste plays a great role in polluting the water and is responsible for introducing different pollutants in the form of heavy metals in living beings. Heavy metals like arsenic, mercury, cadmium, cobalt, and many more are highly toxic for human beings. Determination of these heavy metals in the water, soil is a very challenging task. Though, these days a lot of research is going on for removing these heavy metals from the soil, water and atmosphere by adopting different methodologies, but those

techniques are either expensive, time-consuming or are very complex to use. So, this Ph.D. thesis highlights an imperative call for developing an affordable, lightweight, handy, luminescence-based arsenic sensitive and selective sensor, acquiescent to the conventional spectrofluorometer or cell-phone supported systems.

The main objectives of the thesis are:

- Preparation of rare earth ($NaYF_4$: Yb^{3+}, Er^{3+}) nanocomposite material and its characterization.
- Controlling the thin film deposition of rare earth material ($NaYF_4$: Yb^{3+}, Er^{3+}) on the different substrates (e.g., simple glass/conducting glass, etc.)
- Its application as a sensitive and selective As(III) sensing platform.

1.7. Outline of the Thesis

The total thesis has been divided into six chapters.

Chapter 1 is the introduction which highlights the recent advancement in UC-film deposition, upconversion mechanisms that decide the type of phenomena taking place, how the suitable dopants and hosts are selected, optical properties of upconversion, concerns related to shape, size and efficacy of upconversion phenomena. Further, this chapter entails the significance of arsenic and why there is a need to sense it. Next to it, a prologue about the LRET, its basic principle, detection strategy based on it is done. A brief discussion about the synthesis methodology of upconverting nanophosphors is also done.

Chapter 2 covers a detailed literature review describing different methods to grow rare-earth-doped UC platforms by several investigators.This chapter also describes the UC-films over the substrates using difficult and costly methods and also a long and tiresome chemical procedure for the modification of the platform. Furthermore, a literature survey on different types of fluorescent platforms that may or may not use upconverting materials deposited over some substrate as a sensing platform for the detection of arsenic or some other heavy metals has been discussed.

Chapter 3 covers the experimental section of the thesis. In the beginning of the chapter, a brief introduction about the different synthesis methods was done. The chapter is further divided into

four sections: the first section includes all the chemicals and materials used for research work, the next section shows how the substrate (conducting glass/simple glass) was processed. The third section deals with $NaYF_4:Yb^{3+}$, Er^{3+} film grown using different chelating agents on different substrates. Next, $NaYF_4:Yb^{3+}$, Er^{3+} film grown using M. oleifera leaf extract and its experimental details will be presented. The fourth and the last section cover the characterization of the film, calibration curve generation, LOD, selectivity experiments, and spike recovery experiments.

Chapter 4 covers the controlling of the thin film deposition of rare earth material ($NaYF_4:Yb^{3+}$, Er^{3+}) on the different substrates (e.g., simple glass/conducting glass). The result section of the as-prepared thin film shows the X-ray diffraction patterns of UCF (upconverting film) over various substrates, SEM images of isolated particles (upconverting) and cross-section of the fractured surface of the prepared UCF, followed by the size distribution analysis of particles (upconverting), surface topography study was evaluated with the help of AFM and in the last luminescence properties of the UCF prepared was done. Statistical parameters based on AFM images, the effect of chelating as well as the substrate on the luminescence intensity was also studied and was presented in a table format.

Chapter 5 covers the development of an ultrasensitive platform for detecting the As(III) selectively in different water samples. It includes the design of the As(III) sensitive upconverting platform that further shows the optical absorption and emission of the UCP. A study of the spectral response of UCP was also done accordingly. XRD pattern of UCP and SEM micrograph of the $NaYF_4:Yb^{3+}$, Er^{3+} crystallites on the platform was performed. Next, detection by UCP at M.oleifera (plant extract) and its selectivity was performed by plotting a calibration curve between I_{signal} vs As(III) and checking the response of UCP in a solution containing various species. A study of UCP related to the ability to distinguish As(III) even in the presence of other heavy metal ions was done. Spike recovery using UCP in tap water having a pre-determined concentration of As(III) ions was also studied.

Finally, chapter 6 summarizes the major outcomes drawn from the current study and also gives some recommendations about the future research work.

The last part of the thesis contains a list of cited references used in the thesis, followed by the reprints of the published articles.

Chapter 2 – Literature Review

2.1. Introduction to different Film Deposition Techniques

In the chapter 1, we talked about the basic principle of upconverting nanomaterials that they absorb multiple low energy photons (wavelength in the order of 980 nm) to emit a high energy photon (400–700 nm)[74]. and there are several processing methods for growing rare-earth doped upconverting nanophosphors. Though many upconverting platforms have been reported using thin-film deposition techniques, such as layer by layer deposition (LBL)[75], dip-coating[76], pulsed laser deposition (PLD)[77], spin coating[33], thermal evaporation[78], electron-beam vaporization[79], etc. however, these technologies start with an already synthesized upconverting base material, which are subsequently processed to make films. The methods mentioned above uses pre-synthesized upconverting nanomaterial processed further to make films, adding additional optimization and synthesis step. Besides, low-temperature phase pure hexagonal upconverting thin films are difficult to obtain. Further, these techniques are very costly, labor-intensive, and require highly trained workforce. On the contrary hydrothermal provides a unique opportunity to grow a hexagonal phase pure film at large-scale and low temperatures. Further, it allows one-step synthesis in reaction vessels without step-wise intervention from growth to material deposition. However, one downside/advantage to such a process, that there are only a few degrees of freedom available to tune the film properties. Nevertheless, an additional degree of freedom to the process can be introduced by adding solid substrates of different surface charges along with the chelating agent. Further, the hydrothermal method of synthesis is a trendy yet simple technique to use. Its advantages include (a) feasibility to develop crystals of compounds through elevated melting points at lesser temperatures, (b) possibility of growing those materials whose melting point and vapour pressure are close (c) possibility to grow large-sized good quality crystals by controlling material composition.

The hydrothermal technique has been regarded as one of the most popular process/method for the synthesis of nanoparticles, gathering interest from scientists and technologists of different disciplines, particularly in the last fifteen years. The word "*hydrothermal"* is said to have its geological origin. As explaining itself, word "hydro" means water and "thermal" is related to heat. Sir Roderick Murchison (1792–1871), was a British Geologist who used this word for the

very first time for describing the behaviour of water at high temperature and pressure. The first publication was published in 1845 by K. F. E. Schafthaul on hydrothermal research that reports about the efficiently synthesized quartz crystals (tiny) which were transformed from the precipitation of silicic acid. Hydrothermal as a term submits to a heterogeneous reaction which can take place in the presence of aqueous mineralizers/solvents under conditions of elevated temperature and pressure.

Different researchers proposed different definitions for hydrothermal process in literature. For example, Morey and Niggli in 1913, defined the hydrothermal process of synthesis as "in the hydrothermal method the components are subjected to the action of water, at temperatures generally near though often considerably above the critical temperature of water (~370°C) in closed bombs, and therefore, under the corresponding high pressures developed by such solutions". Similarly, Laudise defined the process as "hydrothermal growth means growth from aqueous solution at ambient or near ambient conditions". In the same manner, scientists like Rabenau, Lobachev, Roy and Yoshimura explained hydrothermal process with their own definitions. Recently, in 2001 K. Byrappa, defined hydrothermal reaction as "any heterogenous chemical reaction in the presence of a solvent (whether aqueous or nonaqueous) above room temperature and at pressure greater than 1 atm in a closed system"[80].

Current work plans to develop nearly transparent UC thin-film entailing capability to ensue fluorescence resonance energy transfer and use it to detect Arsenic in drinking water. The objective of the current thesis is to enhance our understanding of UC film growth over the different glass substrates using the hydrothermal method. This understanding will enable us to use other bio-organic materials such as plant extract to synthesize UC films. Since plant extracts have different cyclic ligands which can serve as an energy acceptor in the FRET process. Further use of plant extract is likely to incorporate those cyclic ligands in the UC film forming an intrinsic donor-acceptor pair. In the current work, prepared UC film on glass substrate is proposed to use as a Arsenic sensor, as arsenic contamination in drinking water is very difficult to quantify analytically due to its low detection limit (5 ppb by WHO). Besides, Atomic absorption, ICP, ICP-MS, arsenators, strip cyclic voltammetry[54] are among the few options available for detection. These instruments are too costly to manage, run, and maintain and require elaborate methods for exact analysis. UC having a high signal-to-noise ratio, large antistoke shift, and near-infrared excitability provide an opportunity for sensitive and selective

detection of Arsenic in drinking water. Besides, the other commercial methods such as LOVIBOND dip and read sticks involve mixing several toxic components, resulting in the formation of arsine gas more toxic than arsenite ions. Due to the high cost and difficulty in maintaining the instruments mentioned above, the water in the different wells could not be analyzed for Arsenic as low as 10 ppb in resource-limited places. Due to which several hundred people get exposed to Arsenic poisoning unknowingly.

Development of UC-film based arsenic sensor though will have to show selectivity towards arsenite ions and signal mechanism indicating arsenite-UC film interactions. One way to design such UC films would be to design a LRET based system capable of modulating UC-emission on arsenite ions interaction with the film. On the other hand, the seamless integration of the $NaYF_4$:Yb^{3+}, Er^{3+} system on glass substrates is well known and it possesses following advantages: (i) easy to use, (ii) simple to functionalize, and (iii) low signal transmission loss. Moreover, early studies have demonstrated that polyphenolic groups present in the leaf extracts chelate very well the arsenic ions. Therefore, development of UC film based on glass substrate for arsenic sensing would require the following: (i) Development of a UC film using low-temperature technique, (ii) integration of polyphenols to the UC film, (iii) Signal mechanism that relates arsenic interaction with the polyphenols and UC film and (iv) selectivity of the film towards arsenic only. All these steps require thorough evaluation of each step. Therefore, current research proposes evaluating the above four points in detail and developing a UC-film-based arsenic sensor.

2.2. Synthesis methods of UC thin films

2.2.1. Pulsed laser deposition (PLD)

Qin et. al in 2002[81] and 2003[82] prepared an amorphous fluoride film codoped with Yb^{3+} & Er^{3+} and Yb^{3+} & Tm^{3+} respectively by using PLD technique. These films were developed in order to convert IR radiation to UV emission. It was observed that during PLD technique there is a drop in the value of Judd–Ofelt parameter (Ω2), which is responsible for enhancing the energy transfer process. In an another approach, Bubb et al[83] deposited a single phase thin film of $LaEr(MoO_4)_3$ using PLD technique. The developed thin film when excited using laser at 980 nm shows visible emission spectra. Though the quality of the thin film processed from the PLD technique is good and shows great results too however, it was also observed that the rate of deposition (average) is slow during the process. Also, the laser technique is not suitable for large

deposition area. It has been observed that PLD process is viable to only certain technology fields such as sensor and optical technology, microelectronics and films processed from advanced materials.

2.2.2. Thermal deposition technique

Chwalek and Paz-Pujalt[79] jointly deposited an upconverted thin film of Ba–Y–Yb–F, doped with Tm^{3+} on semiconductor, GaAs and silica fused substrates using thermal and e-beam deposition technique. Although these films displays wide luminescent peaks in the UV-Vis range but includes some losses which arrived due to the thermal stress on the surface of the substrate. In another study done by Jia et al.[78] thermal evaporation method was used to deposit thin film on Al_2O_3 ceramic substrate, co-doped with Yb^{3+} and Tm^{3+}, under a high vacuum. The deposited thin-film displayed excellent UC emission, particularly in UV region in comparison to fluoride thin films. Liu et al.[84] successfully synthesized a thick inorganic upconverted nanofilm which is exceptionally transparent, strong, well oriented and possess a controlled morphology. The film was developed by using a self assembly one step procedure. Upconverting nanoparticles were also synthesized via thermal decomposition method and hydrothermal process. The investigator compared the Quantum Yields (QYs) of the film in the UV range which were approximately 4.7 and 16.1 times greater than the upconverted nps. However, it is perceived that the film growth rate is poor and varied as a function of vacuum applied. Also, thermal evaporation techniques are not suitable in multi-component thin films due to the difference in melting point and the vapor pressure of participating compounds.

2.2.3. Atomic layer deposition (ALD)

Xu et al.[85] used ALD technique to fabricate nanolaminates. The fabricated polycrystalline YAG ($Y_3AL_5O_{12}$) garnet nanofilms annealed to 1150^0C. The MOS (Metal-Oxide Semiconductor) made light emitting devices (LED) used on YAG:Yb nano-laminates to demonstrate the external quantum efficiency films of 0.65% and the fluorescence life-time of 80-200 μs. Giedraityte et al.[86] prepared an inorganic-organic hybrid kind of thin film via atomic/molecular layer deposition (ALD/MLD) thin-film fabrication technique. The luminescent emission of the amorphous film arises from the 3- and 2- photon NIR-Vis range. Also, the intensity emissions of these films are greatly angle-dependent. Despite of good results, complex and expensive

techniques leads to non-reproducible results. Further, the reactor and reaction kinetics was too complicated to follow or control the reaction. Besides, poor deposition rates, low reaction yield, and poor economic viability are significant drawbacks of the process.

2.2.4. Electro-Deposition Technique

Jia et al. in 2014[87] used electro-deposition technique alongwith annealing for the preparation of transparent upconverted thin film. It was noted that emission intensity of the film is directly proportional to the annealing temperature with strongest at 560°C for 2.5 h. In 2018[88], the investigator again used the electrodeposition technique at common temperatures to fabricate the upconverted hexagonal phased thin film. With the addition of polyvinylpyrrolidone (PVP) in the electrolyte, the phase of the film was controlled from cubic to hexagonal and that resulted in the enhacement of the UC luminescence. However, this process is very costly, consumes more time and may or may not deposit a uniform layer on the substrate.

2.2.5. Sol-Gel Technology

Further, Park et al.[89] used sol-gel and soft lithography process for the fabrication of upconverted thin film and nanopatterns. It has been found by the investigator that the fabricated thin films are comparatively more uniform and smooth than the films processed from thermal evaporation and electrodeposition. The emission intensity of the green and red transitions in case of nanopatterns increased by 2.1 and 2.7 times respectively in comparision to the thin films. Additionally, Pellegrino et al.[90] too used the sol-gel process, a synthetic process of synthesizing an upconverted thin film. The investigator studied many upconversion properties such as ageing time, annealing temperature, precursor's molar ratios etc., for the synthesized UC thin film. Though the process is simple and cheap but it may take long time to process and also the cost of the raw materials/chemicals is a matter of concern.

2.2.6. Chemical vapour deposition (CVD)

Pallegrino et al. in 2017[91] used metal organic chemical vapor deposition (MOCVD) process for the production of thin films. The investigator utilizes the process for the formation of upconverted Yb/Er or Yb/Tm codoped CaF_2 films on substrates like Si, quartz and glass. Further, study of different properties like structure, composition, morphology and photoluminescent were studied for all the three substrates. Again in 2020[92], the investigator used MOCVD technique

combined with sol-gel/spin coating process in order to compare both procedures for the undoped and lanthanide doped CaF_2 thin films. It was concluded that both chemical routes are reliable and can reproduce the thin film with a faster rate. Also the developed films exhibit an elevated degree of uniformity over vast areas. However, MOCVD is considered to be a hazardous for humans because of the toxic and corrosive gases that one has to handle during the process. Also, contamination of carbon and incorporation of hydrogen is a tedious task to perform to which may often creates a problem while executing the procedure. High temperatures and complex processes also make this process less popular.

2.2.7 Layer-by-Layer/Spin Coating

Bao et al.[75] reported a simple yet highly-controlled process of developing the multilayered upconverted thin films which is finely distributed with Ln doped nanocrystals. These nanocrystals were coated with citrate and were synthesized via single phased high boiling point solvent method and subsequently by ligand exchange. The as synthesized nanocrystals were found to be hydrophilic in nature and were deposited on a sacrificial layer via layer-by-layer (LBL) assembly method. These nanocomposites multilayered thin film shows a marvelous mechanical stability as well as NIR-to-visible upconversion luminescence. In another approach, Lin et al.[33] described a method through which a highly luminescent upconverted thin film can be produced. First, the hexagonal phased upconverted nanocrystals were synthesized through a single phase high boiling point solvent method. Then a matrix consists of nanocrystals and polymethyl methacrylate (PMMA) was formed which was further spin coated on a glass substrate producing a thin film. These films vary in thickness but shows great luminescence property. However, this method offers certain limitations such as the efficiency of the material to be coated while spinning, size of the substrate is also a matter of concern because if the size of the substrate increases then it becomes very difficult to coat a layer with such great speed and hence film thinning will be a nightmare to develop.

2.2.8. Microfluidic Method

In another work, Liu et al.[93] applied the microfluidic method to deposit transparent inorganic UC-film on a silica glass substrate with 31-227 μm spatial height variation. However, spatial height variation beyond 150 μm resulted in high transmission losses due to large thickness (~67 nm). On the contrary spatial variation from 110-150 μm enabled better distribution of

upconverted emission and low transmission losses. Despite above advantages, trapped defects in the film lead to failure of the film microstructure.

2.2.9. Dip Coating/Casting

Huang et al. in 2012[76], used dip coating method for developing a nanocomposite thin film which was highly transparent in nature. The upconverted nanoparticles were synthesized successfully by tuning the temperature of the initial reaction. The prepared nps were found to be monodispersed and were then stabilized with oleic acid. The transparent nanocomposite thin film shows high intensity emission in green and blue region when excited with 980 nm. The dip coated thin film showed higher transparency in contrast with blank substrate. However, the thickness of the film is not uniform resulting in the formation of the "wedge effect".

2.2.10. Hydrothermal Synthesis

UC-film was assembled on a silicon substrate by Wang and Cheng in 2015[77] via self assembly method. Primarily, pre-synthesized (hydrothermal route) $NaYF_4$:Yb^{3+}, Er^{3+} nanoparticles were integrated over the silicon substrate via a covalent bond between the two. Further, UC-film displayed a long life-time (1350 ns), indicating strong interfacial bonding between Si and UC nanoparticles. However, incorporating upconverting nanomaterial within the Si-matrix decreased the exposure of upconverting nanomaterial to the sensing atmosphere. Further, such film growth required multistep processing such as synthesizing upconverting nanomaterial followed by its encapsulation to form a film over a substrate. Besides, the encapsulation method used toxic chemicals as well.

Deposition of thin film (β-LaS_2 nanostructured) was effectively performed by Ghogare et al.[94] on a stainless-steel substrate (acidic medium) using hydrothermal method. The hydrophilic orthorhombic nanostructured film were formed with a flower-like morphology and this resulted in high surface area and low charge transfer resistance material to apply on the capacitor electrode. However, films over stainless steel substrate often have altered properties due to hardness, corrosivity, abrasiveness, and cohesion. So, choosing a good grade of a substrate (in this case: stainless steel) is the most critical factor for growing thin films on a substrate. Also, due to phase stoichiometry, stainless steel as a substrate may form defects during the film growth.

Recently, Zhang et al.[95] used hydrothermal method of synthesis for the preparation of nitrogen doped graphene quantum dots (N-GQDs) alongwith $NaYF_4$:Yb,Er. The $NaYF_4$:Yb,Er/N-GQDs displays green color when an external excitation was given at 980 nm, and shows blue color when excitated at 365 nm. The luminescence property of $NaYF_4$:Yb,Er/N-GQDs are independent of each other. For obtaining a transparent film, polyvinyl alcohol (PVA) matrix was incorporated directly to the synthesized mixture. Though such films exhibit good luminescent properties but the process of forming thin films involves multiple steps and is a time consuming process too.

Zhang et al.[96] prepared a nanocrystalline thin film of antimony sulfide (Sb_2S_3) on a ITO substrate via hydrothermal method which is further assisted by polyvinylpyrrolidone (PVP). These films formed a honeycomb-like structure having thickness of around 360 nm and a band gap of 2.0 eV on the ITO substrate without any heat treatment. It was observed that PVP plays a crucial role in the formation of honeycomb like films as its absence forms large aggregates on the surface of the ITO substrate. The Sb_2S_3 film was also found stable in neutral as well as in acidic solutions. However, the PVP is said to have a great water sorption capacity which may affect the thickness of prepared films.

Li et al.[97] synthesized nanoparticles of cubic sesquioxide materials i.e Sc_2O_3: Er^{3+}, Yb^{3+} using hydrothermal process. These nps shows a strong and effective upconversion luminescence property especially in the red region which got a hike by a factor of 4, when a comparison was done with the samples prepared via solvothermal method while keeping the value of ion concentration same. Longer lifetimes and scaling down the surface groups might be credited in the enhancement of UCL. The investigator further plots a graph for the red and green emissions i.e plots of log(I) vs log(P), the values for which came out larger than 2 that proves that there exists 3-photon processes. Though sesquioxide materials show great properties but they are less soluble even in a moderately acidic medium which can limit down its application area.

Mathew et al. in 2018[98], deposited a high grade nanocrystalline ternary film on a glass substrate via hydrothermal process alongwith an aid of chemical bath deposition. The ternary film displays lattice defects in form of vacancies and interstitials, ohmic behavior when illumination was done and fast rise and decay in photo response. Besides all, in the chemical deposition process, after every deposition, one has to change the solution which shows a great wastage in form of solution.

Hydrothermal process was used by Ishikawa et al[99], Shimomura et al.[100] and Morita et al.[101] for depositing a film (thick/thin) of lead zirconate titanate (PZT) on a titanium substrate. All the three investigators developed different kind of hydrothermally deposited PZT films and studied different properties and parameters of it. Similarly, Dongale et al.[102] fabricated a memristor device using (Ag/TiO_2/Al) TiO_2 as an active layer via hydrothermal process. Further, it was concluded by the investigator that the hydrothermal process of synthesis will soon come up as a breakthrough elucidation in the area of electronic memory device fabrication.

2.3. Different Materials used as Arsenic Sensors/Probes

Solution-based fluorescent As(III)/As(V) sensors were developed and reported by several investigators which are either organic for e.g. APSAL [(4E)-4-(2-Hydroxybenzylideneamino)-1,2-dihydro-2,3-dimethyl-1-phenylpyrazol-5-one], acriflavine and oxime based or inorganic such as gold nanoclusters, quantum dots and ZnO/curcumin in nature.

2.3.1. Organic Sensor/Probe

An organic sensor (APSAL) for living cell imaging was developed by Lohar et al.[103] for which the limit of detection (LOD) calculated is ~ 225 ppb while that of binding constant for arsenate is 8.9×103 M^{-1}, using the Benesi−Hildebrand equations. It was inferred by the investigator that fluorescence quantum yield (QY) of the probe increases more than 12 times when arsenate ion was binded with it. Similarly Dolai et al. in 2016[104] designed an oxime based called as DHAO (2,4-dihydroxy acetophenone-oxime) sensor to detect As(V) selectively. The sensor illustrated a limit of detection (LOD) of 29μM. Likewise, in another organic sensor which worked on the principle of FRET (Flourescence Resonance Energy Transfer) developed by Saha et al. the limit of detection (LOD) was calculated to be 10μg/L against natural lake water. In 2013, Sahana et al.[105] established a "turn-on" fluorescence sensor i.e Naphthalene–salisaldehyde conjugate (NAPSAL) for the detection of arsenate (H_2AsO_4) in contaminated drinking water as well as living cell. The LOD value of arsenate selective probe was calculated as 0.37ppb which is below the allowed limit issued by the WHO.

These sensors do holds several benefits such as low standard deviation, multicolor emission, high quantum yield (~ 0.9) and large dynamic range. However, they are affected by numerous

factors like, poor colloidal stability, quenching, solvent dependent emission, pH sensitivity and overlapping broad excitation and emission spectra. Due to the spectral overlap, inherent noise is carried out in the signal which results in a poor signal to noise ratio and hence low sensitivity.

2.3.2. Inorganic Sensor/Probe

Taghdisi et al.[106] designed a flourescent aptasensor, for the recognition of As(III) in tap water and blood serum of human beings. The sensor was formed by coating the silica nanoparticles with streptavidin and was targeted in a way, so that information can be collected, if any alteration in the complementary strand of aptamer alongwith silica was induced. The limit of detection (LOD) and limit of linearity (LOL) were calculated as 33.7 ppt and 0.15-37.4 respectively. Again an aptamer based flourescent sensor for the detection of As (III) was designed by Ravikumar et al.[107] in 2017 for which MoS_2 nanosheets were synthesized by co-precipitation procedure. The LOD and LOL for the developed biosensor were calculated as 1.34 ppb and 0-0.6 ppb respectively. Liao et al.[47] developed a bacterial biosensor which was based on green flourescent protein in order to detect species like As(III), As(V) in groundwater samples. This E.coli based biosensor showed the LOD of 30 ppb for As(III) and 75 ppb for As(V). In some other work, inorganic flourescent sensors such as ZnO/curcumin were developed by Moussawi and coworkers[108] using wet chemical approach. The synthesized nanostructures were found to have a grain like and hexagonal crystal shaped structure with great crystalline quality. The investigator further inferred that the photoluminescence of bare ZnO is quite insensitive towards arsenic concentration in water, however when nanostructured zinc oxide surface modified with curcumin was excited at a wavelength of 425 nm, it sensed the arsenic very sensitively in the concentration dynamic range of 1-3000 ppb.

Gold based nanosystem was established successfully by Roy et al. in 2012[109], with the help of wet chemistry procedure. These hydrophilic fluorescent gold clusters display large Stoke's shift , photochemical stability and QY of 41.3%. The gold clusters were selective and ultra sensitive towards As^{3+} ions and the calculated LOD is 4.02 ppb which is in the allowed limits issued by WHO and USEPA.

Several types of quantum dots (QDs) were used as a probe for detecting arsenic. Quantum dots such as CdTe QDs by Vaishanav et al.[110], CdTe/ZnS QDs by Ensafi et al.[111], DNA QDs by

Zhang et al.[112], CQDs by Pooja et al.[113], GSH-CdTe Qds by Wang et al.[114], GSH-CdSe/ZnS QDs by De Villiers et al.[115], CdS-MAA QDs by Butwong et al.[116], $CuInS_2$ at Fe_3O_4 QDs by Liu et al.[117], ZnO QDs by Pal et al.[53], and MPA: CdTe QD-R6G by Tang et al.[118], were established by different investigators for sensing As^{3+} and As^{5+}. These probes display different values of limit of detection (LOD) and limit of linearity (LOL) in a particular dynamic range (DR) shown in table 2.1. These sensors shows poor reliability due to their OFF-type signaling, employ expensive nucleotides, complex chemistry, show heavy metal toxicity and false positive signals. The false positive signals occur due to inability of the sensor in differentiating between the analyte and the interfering ions present in the vicinity of the sensor.

Table 2. *List of fluorescence sensors developed for arsenic [(As (III)/As (V)] detection along with limit of detection (LOD), dynamic range (DR) and limit of linearity (LOL).*

Sensor used	**Species detected**					
	As (III)			**As (V)**		
	LOD	**DR**	**LOL**	**LOD**	**DR**	**LOL**
Acriflavine-RhB (FRET)[48]	--	--	--	10 ppb	--	0.04-0.09 ppm
APSAL[103]	--	--	--	~225 ppb	--	--
DHAO[104]	--	--	--	2.2 ppm	--	--
NAPSAL[105]	--	--	--	0.37 ppb	--	--
Silica NPs Aptasensor[106]	33.7 ppt	--	0.15-37.4 ppb	--	--	--
MoS_2 nanosheet[107]	1.34 ppb	--	0-0.6 ppb	--	--	--
E-coli-GFP sensor[47]	30 ppb	--	--	75 ppb	--	--
ZnO-Curcumin NPs[108]	--	1-3000 ppb	--	--	--	--
Gold clusters[109]	4.02 ppb	--	--	--	--	--
CdTe QDs[110]	0.15 ppb	--	0.15-37.4 ppb	--	--	--
CdTe/ZnS QDs[111]	0.09 ppt	0.74 ppt-74.9 ppb	--	--	--	--
DNA-QDs[112]	0.2 ppb	--	1-150 ppb	--	--	--

CQDs[113]	0.086 ppb	5-100 ppb	10-50 ppb	--	--	--
GSH-CdTe QDs[114]	1.5 ppb	--	375-18.75 ppm	--	--	--
GSH-CdSe/ZnS QDs[115]	750 ppb	--	--	--	--	--
CdS-MAA QDs[116]	0.07 ppm	6-240 ppm	--	--	--	--
$CuInS_2@Fe_3O_4$[117]	--	--	--	9.7 ppt	0.01-15 ppm	--
ZnO QDs[53]	27 ppb	10-100 ppb	--	7 ppb	10-100 ppb	--
MPA: CdTe QD-R6G (FRET)[118]	0.5 ppb	--	1.5-150 ppb	--	--	--

***DR:** Dynamic Range, ***LOD:** Limit of detection, ***LOL:** Limit of Linearity, ***RhB:** Rhodamine B ***QDs:** Quantum Dots, ***NPs:** Nanoparticles, ***APSAL**: Aminoantipyrene-Salicylaldehyde, ***NAPSAL**: Napthalene-Salisaldehyde, ***DHAO:** 2-Hydroxyacetophenone-Oxime, ***ppm:** parts per million, ***ppb:** parts per billion, ***ppt:** parts per trillion.

2.3.3. LRET based UPCN Sensing Devices

The upconverting material ($NaYF_4$:Yb^{3+},Er^{3+}) exhibits excitation near-infrared, narrow bands in the wavelength range of 300–800 nm, and strong emission due to its f–f electronic transitions with s-orbital and p-orbital shielding[73]. The orbital shielding does not allow the solid substrate to interfere in the process of emission, enabling the deposition of $NaYF_4$:Yb^{3+},Er^{3+} upconverting nanoparticles (UCNPs) on a solid substrate for use as a sensor. The solid $NaYF_4$:Yb^{3+},Er^{3+} upconverting-platform (UCP) involves the luminescence resonance energy transfer (LRET) mechanism for the detection of arsenic selectively.

Several solution-based LRET upconverting sensors have been developed for the detection of different analytes. Liu et al.[56] formed a chromophoric ruthenium complex-assembled nanophosphor (N719-UCNPs) for the detection of mercury ions in the water as well as in the living cells with the help of bioimaging. The as developed nanoprobe is highly selective and sensitive with a 1.95 ppb limit of detection (LOD), which is said to be in lower limits as the maximum level of Hg^{2+} in drinking water is set to 2 ppb by the USEPA. Further, Deng et al.[119] designed a novel method for the detection of glutathione in aqueous solutions alongwith in living cells. This method is an amalgamation of Ln doped UPCN and MnO_2 nanosheets which can selectively and rapidly detect glutathione. Next, Yao et al.[120] fabricated a hybrid material which consists of iridium complex and UCNPs in order to sense selectively cyanide (CN^-) ions in pure water. The detection of cyanide ions was performed by luminescent resonance energy transfer (LRET) process. It was concluded by the investigator that the probe wasn't able to produce great sensitivity and limit of detection as reported in actual use. Liu et al.[121] designed a water soluble, highly sensitive nanophospher system for sensing and bioimaging of methylmercury ions in water and living cells. The limit of detection was found to be 0.18 ppb in aqueous solution. Recently, Liu et al.[122] designed an upconverted probe on the principle of FRET for the detection of copper ions.

These solution based sensors have limitations as follows: (i) irreproducible response, (ii) weak emission due to interaction of UCNP with solution[122], thereby compromising the detection limit and sensitivity, (iii) poor colloidal stability under ambient conditions, and (iv) integration difficulty with point-of-care devices. In contrast, solid-substrate based LRET sensors have simple conjugation chemistry, low cost, improved stability, and good repeatability of results,

long shelf-life, and easier handling. Moreover, they can be integrated easily with cell-phone or handheld devices for real-time applications.

2.3.4. Different Substrates used for Sensing

Numerous substrates have been used with the $NaYF_4:Yb^{3+},Er^{3+}$ upconversion system. Zhou et al.[123] developed a cellulose based nucleic acid hybridization assay based on LRET in association with UCP. The limit of detection was calculated as 34 fmol. The as developed assay is highly sensitive, selective and provides fast response. In a similar fashion, Niedbala et al.[124] used glass substrate for developing a upconverting phosphor link utilizing upconverting phosphor technology (UPT). Yliharsila et al.[125] used polymer as a substrate for developing array-in-well method that utilizes upconverting phosphor technology.

These substrates are known to have low cost, easy disposal, and straightforward use. However, despite these advantages, the substrate-assisted synthesis requires multi-step processing, and complex conjugation and purification steps. Additionally, these platforms have never been used in arsenic [As(III)/As(V)] sensing applications. On the other hand, the seamless integration of the $NaYF_4:Yb^{3+},Er^{3+}$ system on glass substrates is well known[126]. Furthermore, it possesses advantages as follows: (i) easy to use, (ii) simple to functionalize, and (iii) low signal transmission loss.

2.4. Summary of Literature Review

The comprehensive literature review indicates that different deposition techniques like PLD, ALD, thermal deposition, electrodeposition, sol-gel, CVD, layer-by-layer, microfluidic, dip coating and hydrothermal are used for the formation of thin films. Among these, hydrothermal method is the most viable choice for the synthesis of thin film, owing to its advantages like cost-effectiveness, simple and easy to use, 1-step synthesis process, formation of crystalline phases at low melting points, can use different raw materials at the same time, flexibility to obtain nanostructures of wide range of morphology such as thin films, nanorods, nanowires, nanodiscs, nanotubes etc. and many more. These thin films can be grown on different substrates like glass slides (conducting/non conducting), silicon, metal flakes, polymer, cellulose etc,. The developed thin films can be used for the purpose of heavy metal sensing for example, arsenic which has gained a lot of interest by the researchers these days as it helps in solving major issues like contamination of water due to soil, air and water pollution alongwith the presence of heavy

metals in industrial waste water. Studies reveal that many researchers developed different types of probes/sensors based on different materials for detecting arsenic in contaminated drinking water. But these designed probes suffers from many drawbacks such as low sensitivity, poor colloidal stability, complex chemistry, false-positive signals, poor signal to noise ratio, quenching, pH sensitivity, display poor reliability due to their OFF-type signaling, introduction of expensive nucleotides, solvent-dependent emission and overlapping broad excitation and emission spectra.

Chapter 3 – Materials, Experimental Methods and Characterizations

This section deals with the fabrication of Yb^{3+} /Er^{3+} doped $NaYF_4$ film using the hydrothermal method on various substrates (conducting and non-conducting) in the presence of various chelating agents together with different characterization techniques pursued to analyze its characteristics.

3.1. Chelating Agent and Substrate Effect on Hydrothermal Growth of Yb^{3+}/Er^{3+} Doped $NaYF_4$ Film

3.1.1. Chemicals and Materials

Yttrium chloride hexahydrate($YCl_3.6H_2O$), Ytterbium chloride hexahydrate($YbCl_3.6H_2O$) and Erbium chloride hexahydrate ($ErCl_3.6H_2O$) were purchased from Sigma Aldrich India.Sodium fluoride (NaF), Ethyleneglycoltetraaceticacid (EGTA), Ethylenediaminetetraacetic acid (EDTA)and diethylenetriaminepentaacetic acid (DTPA), all 99.99 % pure were procured from SRL Chemicals India. All the reagents were of analytical grade and used without further purification. Conducting (Indium doped tin oxide (ITO), Fluorine doped tin oxide (FTO) and non-conducting glass slides were purchased from Techinstro Pvt. Ltd (India).

3.1.2. Fabrication of Yb^{3+}/Er^{3+} Doped $NaYF_4$ Film by Hydrothermal Method

All glass substrates were cut into 1.5cm x1.5cm sizes and cleaned in warm (50°C) concentrated nitric acid for ~15 min followed by washing 2-3 times in deionized water (DI =18 MΩ cm^{-1}) and acetone. Subsequently, the substrates were dried at room temperature in a desiccator. Finally, cleaned substrates were etched using dilute hydrofluoric acid (HF) solution for 5 sec followed by DI water washing and drying.

Upconverting films were deposited using a well-established hydrothermal protocol with some modifications. Briefly, stock solution of 0.2M $YbCl_3$, YCl_3, $ErCl_3$, CA (= EDTA, EGTA, DTPA), and 0.83M of NaF were prepared. From the stock solutions, 0.17mmol of $YbCl_3$, 0.80mmol of YCl_3, 0.03mmol of $ErCl_3$ and 1.0mmol of the chelating agent (CA) were mixed for 30 min in a glass vial. After 30 min of mixing, 12.45mmol of NaF was added to the solution and transferred to Teflon lined stainless steel autoclave.The cleaned and etched substrates were fully

submerged in the solution present inside the autoclave. The autoclave was sealed and placed in a preheated oven at 140℃ for 15h. After completion of the reaction, the autoclave was cooled to room temperature, and the substrate was washed with DI water under sonication.

The different UCFs prepared using a combination of various chelating agents and substrate are designated according to the nomenclature adopted in Table 3.1 and the same nomenclature has followed throughout the manuscript.

Table 3.1. *Nomenclature adopted for several described UCFs in the current experiment*

Chelating agent	Substrate	Nomenclature
EDTA	ITO/FTO/PG	UCF at ITO_EDTA/UCF at FTO_EDTA/UCF at PG_EDTA
EGTA	ITO/FTO/PG	UCF at ITO_EGTA/UCF at FTO_EGTA/UCF at PG_EGTA
DTPA	ITO/FTO/PG	UCF at ITO_DTPA/UCF at FTO_DTPA/UCF at PG_DTPA

3.2. Development of Ultrasensitive As(III) Selective Upconverting ($NaYF_4$:Yb^{3+},Er^{3+}) Platform

This section deals with the development of ultrasensitive and As (III) selective upconverting ($NaYF_4$: Yb^{3+}, Er^{3+}) platform and different characterization techniques performed.

Present work schemes to grow nearly transparent UC thin-film entailing capability to ensue fluorescence resonance energy transfer and use it to detect Arsenic in drinking water. The objective of the current thesis is to enhance our understanding of UC film growth over the glass substrate using the hydrothermal method. This understanding will enable us to use other bio-

organic materials such as plant extract to synthesize UC films. Since plant extracts have different cyclic ligands, which can serve as an energy acceptor in the FRET process. Further use of plant extract is likely to incorporate those cyclic ligands in the UC film forming an intrinsic donor-acceptor pair. In the present work, prepared UC film on the glass substrate is proposed to use as an Arsenic sensor, as arsenic contamination in drinking water is very difficult to quantify analytically due to its low detection limit (5 ppb by WHO). Besides, Atomic absorption, ICP, ICP-MS, arsenators, strip cyclic voltammetry[54] are among the few options available for detection. These instruments are too costly to manage, run, and maintain and require elaborate methods for exact analysis. UC having a high signal-to-noise ratio, large antistoke shift, and near-infrared excitability provide an opportunity for sensitive and selective detection of Arsenic in drinking water. Besides, the other commercial methods such as LOVIBOND dip and read sticks involve mixing several toxic components, resulting in the formation of arsine gas more toxic than arsenite ions.

3.2.1. Chemicals and Materials

All chemicals procured from Sigma Aldrich [Hydrated Yttrium chloride ($YCl_3.6H_2O$), Ytterbium chloride ($YbCl_3.6H_2O$), Erbium chloride hexahydrate ($ErCl_3.6H_2O$), Catechol] SRL Chemicals [Sodium fluoride, Tin chloride, Cobalt Sulphate, Ferrous Sulphate], SDF Chemicals [Sodium arsenite, sodium arsenate, nitric acid], Alfa Aesar [hydrofluoric acid, sodium fluoride, and sodium chloride], Merck [Mercury chloride, Lead chloride], Fischer Scientific [Cadmium chloride, Phosphoric acid], and Rankem [Calcium chloride, Magnesium chloride, potassium dichromate] were used as such without any further purification. Importantly, for the preparation of hexavalent chromium solution, protocols outlined in the American Public Health Association, American Water Works Association, and Water Pollution Control Federation have been employed.

3.2.2. Glass-Slide Processing and Extract Preparation

Initially, plain glass slides were cut into 1.5x1.5cm^2 size, cleaned in nitric acid at 50 ºC for ~ 20 min, rinsed with deionized water (DI) (18 MΩ cm), and acetone in succession and dried. Finally, they were etched in hydrofluoric acid (HCF) and washed with deionized (DI) water and acetone again before depositing $NaYF_4$: Yb^{3+}, Er^{3+} layer on them via a hydrothermal process. M. oleifera

leaves (matured) were collected from the botanical garden of the Banaras Hindu University, Varanasi. Their extract was prepared by boiling 10 g of washed leaves in 100 mL of DI water at 90 °C for four hours and subsequent filtration through the Whatman #1 filter paper.

3.2.3. Fabrication of Upconverting Platform

For experimentation, a set of three upconverting platforms termed as UCP at M.oleifera, UCP at Catechol and UCP at DW were made using a well-established protocol with minor variation[4]. For UCP at M. oleifera, 4ml of YCl_3 (0.2M), 0.85 ml of $YbCl_3$ (0.2M), 0.15 ml of $ErCl_3$ (0.2M) solutions prepared in M.oleifera extract were added to 15 ml of NaF (0.83M) solution and stirred for ~30 min. Glass substrates were immersed in this mixture and hydrothermal reaction was carried out at 180°C for 4h in a Teflon lined stainless steel autoclave. This process led to the deposition of a $NaYF_4$: Yb^{3+}, Er^{3+} film on the glass substrate. After cooling down to room temperature, the platform was washed with DI water with mild sonication before drying. The $NaYF_4$:Yb^{3+}, Er^{3+} coated glass slide served as the upconverting platform (UCP) for As (III) detection. Fig. 3.1 shows the schematic diagram of the synthesis process. The other UCPs (labeled as UCP at DW or UCP at Catechol) were produced similarly using either DI water or catechol solution (instead of M.oleifera extract) as the solvent and rare earth precursors as before. The catechol solution was prepared in deionized water with a concentration of 22.4 mg/ml.

3.2.4. Calibration and Selectivity Studies

The strong emission of doped Er^{3+} at 655 nm was chosen for As (III) detection. The 5 ml standard As(III) solution of each 2, 4, 6, 8, 10, 20, 30, 40, and 50 nM was prepared by repeated dilution of 0.1M sodium arsenite ($NaAsO_2$) aqueous solution. Initially, bare UCP at M.oleifera was excited with 980 nm radiation and intensity (I_{blank}) corresponding to 655nm emission measured, taking the five-point average in the wavelength range 653-657 nm. UCP at M.oleifera was thereafter drop casted with (2-50 nM) standard solutions for 5s and dried before measuring 655 nm emission (I_{655i}) again. The signal (I_{signal}) was obtained from the normalized intensity (I_{655i}/I_{blank}) using the relation $I_{signal} = [(I_{655i} - I_{blank})/I_{blank}]$. Every time before repeating the process with another standard solution, UCP at M.oleifera was washed with DI water for 5s and dried. The I_{signal} versus As(III) concentration (i.e., solution nM) plot was then made to serve as the

calibration chart. Similar calibration curves were prepared for other heavy metals (such as Hg^{2+}, Pb^{2+}, Cd^{2+}, $H_2PO_4^-$, F^-, Cl^-, Ca^{2+}, Mg^{2+}, Sn^{2+}, Cr^{6+}, $Fe^{2+}$and Co^{2+}) following the above-mentioned protocols and using respective standard solutions in the concentration of 10, 20, and 50 nM. For comparison, signals appearing from UCP at DW and UCP at Catechol were also recorded using the same procedure.

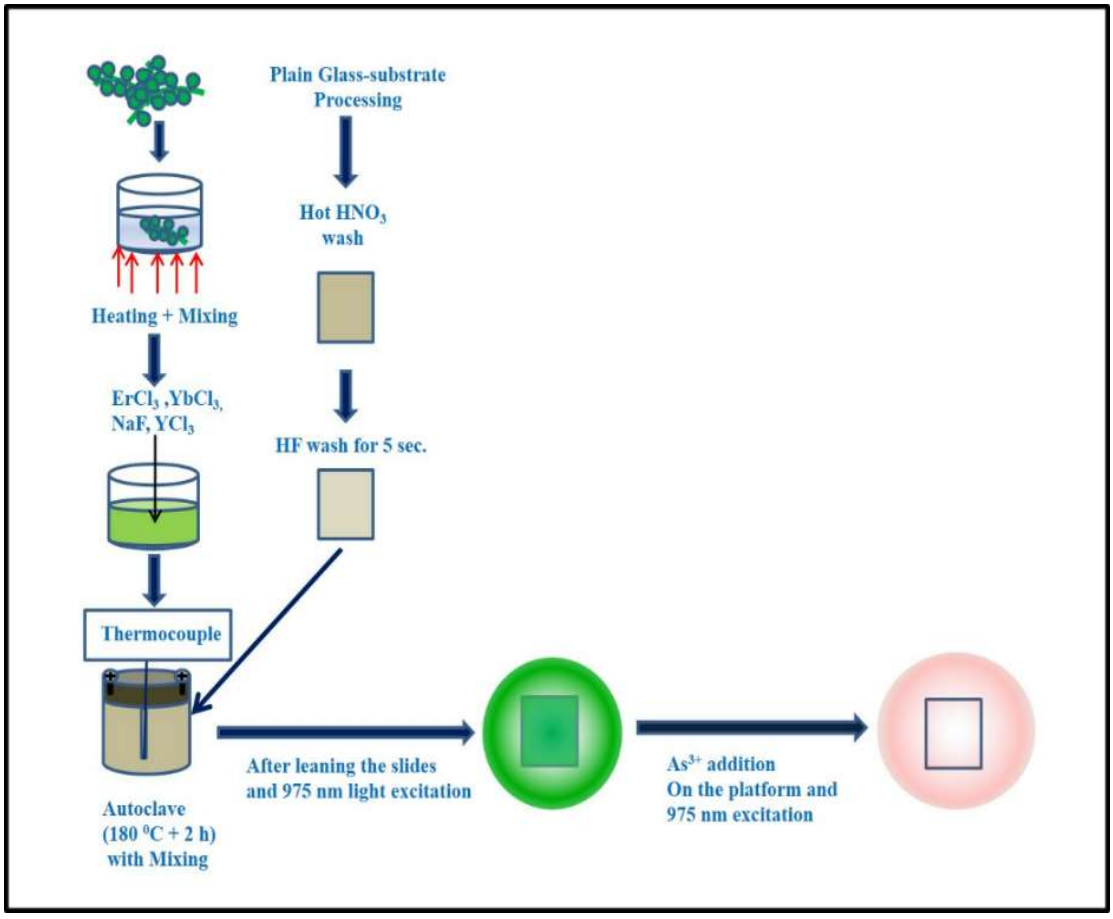

Fig 3.1.*Schematic showing synthesis process of UCP with M.oleifera leaf extract.*

3.3. Characterization Techniques

Upconverting films fabricated on various substrates using different chelating agents were characterized for its morphological, structural and optical properties using various characterization techniques. Also, upconverting platform fabricated for sensing As(III) was characterized for its morphological, structural, phytochemical and optical properties using various characterization techniques, which have been elaborated in the subsequent sections given below:

3.3.1. X-Ray diffraction (XRD)

This characterization technique is nondestructive in nature which evaluates a material's chemical composition, physical properties and crystallographic phase of the films. The technique not only helps in identifying a material's diffraction pattern but also its phase and how the internal stress and defects influence the real structure of a material from an ideal one. In XRD, the unfolding of a material's atomic crystal structure has been done by x-rays which is based on Bragg's law.

$$2d\sin\theta = n\lambda \quad (2)$$

where, d = space between diffracting planes,
θ(theta) = angle of incident,
n = any integer and
λ = beam wavelength.

Here, we analysed the phase structure and crystallinity of the synthesized UCP on XRD (Rigaku Smart Lab diffractometer, Miniflex), using CuKα radiation source (λ=1.54 Å), 2θ ranging from 10^o to 80^o at a scanning rate of 5^o min^{-1} and 0.02^o min^{-1} step size.

3.3.2. Scanning Electron Microscopy (SEM)

This characterization technique uses high beam of electrons for scanning the surface of a sample in a raster scan mode. Through SEM, surface morphology such as particle size and shape, size distribution, formation of particles on the deposited films can be analysed. Here, the morphological information was analyzed by SEM (FEI NOVA NANOSEM 450). Images were

taken and further analysis was performed and presented in the form of histogram which tells the size distribution of nanoparticles on the UCP.

3.3.3. Atomic Force Microscopy (AFM)

This microscopy technique is a high-resolution method of scanning both conductive and non-conductive surfaces. Properties like surface texture, height, roughness, magnetism, size etc can be inferred from this scanning method. AFM is considered as a very powerful microscopic technique which produces a sample's image at atomic level with a resolution of 10^{-10}m without any sample preparation. The forces that govern the technique is the van der Waals forces between the sample and the tip of the AFM. It is viable in both type of mediums i.e in air as well as in liquid. The sampling can be done in two different modes i.e in contact mode and tapping mode as per need. Here, the surface topography of the deposited films was studied using AFM (Veeco, USA) in the tapping mode.

3.3.4. Spectrofluorometer

The luminescence spectra of the films recorded on a spectrofluorometer (Horiba, Quanta master 400-PTI, Canada) using 980 nm continuous wave (CW) diode laser (PSU-III-LED, 500 mW) as an excitation source.The luminescence spectrum was acquired with an emission slit opening of 0.4mm and an integration time of 0.1 seconds.

In the case of Upconverting Platform, the luminescence measurements under taken were slightly different than the above one. The spectrofluorometer (QM-400), equipped with a continuous wave (CW) 980 nm diode laser (MD-III-980-2W; power density used ~ 250 Wcm^{-2}), at a step size of 1nm, slit size of 0.5 nm and integration time of 0.1s. Absorbance was measured in the spectral range of 280-700 nm with a UV-VIS Spectrophotometer (Elico SL-159, India).

3.3.5. Gas Chromatography-Mass Spectrometry (GC-MS)

This instrument is used to distinguish the chemical components present in a mixture of specimen (done by GC component) and then detects the presence of components at molecular level (done by MS component). It is considered as the most precisely operated technique for the detection of green (environmental) samples. Here, in this study we found out the phytochemical constituents

of M.oleifera leaf extract by gas chromatography-mass spectrometry (GC-MS) analysis with a Shimadzu GC-MS-QP2010 plus ultra-system.

3.3.6. Fourier transmission infrared spectroscopy (FTIR)

This technique is particularly used for identifying the organic, inorganic and polymer components present in a specified sample. When a specimen is analysed through FTIR technique, an infrared spectrum is obtained through absorption or transmission. Here, the surface functional groups were identified from a FTIR spectrometer (Thermo Scientific Nicolet iS5) in attenuated total reflectance (ATR) mode that ranges from 500-4000 cm^{-1}.

Chapter 4− Chelating Agent and Substrate Effect on Hydrothermal Growth of Yb^{3+} /Er^{3+}Doped $NaYF_4$Film

4.1.Chelating Agent and Substrate Effect

The effect of chelating agents on rare earth thin film deposition when different substrates (e.g., simple glass/conducting glass etc.) are used, have been investigated. Different characterization techniques were pursued to analyze the characteristics of as-synthesized rare earth ($NaYF_4$: Yb^{3+}, Er^{3+}) nanocomposite material by controlling the thin film.

4.1.1.X-Ray Diffraction (XRD) Analysis

X-ray diffraction patterns (Fig. 4.1) of the deposited films matched with standard hexagonal (JCPDS Card No. 98-007-6718) $NaYF_4$ phase. It can be observed that the majority of XRD peaks belong to hexagonal (β)-$NaYF_4$ phase. However, the presence of NaF (JCPDF Card No. 98-004-8929) and the traces of cubic (α)-$NaYF_4$ (JCPDS Card No. 98-001-9092) are also confirmed. Formation of hexagonal (β)-$NaYF_4$ phase is in line with the proposed hypothesis of phase pure upconverting system prepared by hydrothermal reaction. Moreover, the long reaction time and high-pressure conditions inside the autoclave is likely to favor the formation of hexagonal phase of the upconverting system at a low temperature (140 ^oC). It has been reported earlier that thermal decomposition reaction at lower temperature produced cubic phase $NaYF_4$, which underwent transition through mixed phase (cubic and hexagonal) and ultimately converted to hexagonal phase at a temperature above 300^oC[127,128]. Interestingly, no cubic phase was observed in the case of UCF, prepared by the combination of various substrates and chelating ligands possibly due to the absence of stabilization of small-sized α-$NaYF_4$ nuclei, formed during dissolution recrystallization process of hexagonal phase, assisted by surface-attached ligand[129]. Since the $NaYF_4$:Yb^{3+}, Er^{3+} in the hexagonal phase is known to have better upconversion efficiency, hence the hydrothermal process of film deposition is found to be more economical and less labor-intensive. In addition to β-$NaYF_4$ peaks, two more peaks at 2θ ~ 38.88, 56.14 and 70.39° appeared in all UCFs samples, which matched with the standard pattern of NaF (JCPDF Card No. 98-004-8929). It is to be noted that YF_3 peak is absent in all UCFs samples excluding NaF as decomposition product. It is important to note that NaF is a major constituent of the $NaYF_4$ host lattice and is responsible for the photon-phonon interaction.

Hence, NaF quantity was added ~ 4 times in excess of YCl_3 to compensate for losses incurred during a longer period of solution processing. Further, the addition of excess NaF in the solution is known to play an important role in controlling the phase and morphology of resulting upconverting particles through the acceleration of the crystallization process[130–132].

During synthesis, NaF was taken in high amount, which resulted in its precipitation due to long reaction duration and therefore visible in X-ray diffraction peaks. At the same time, Yb^{3+} and Er^{3+} are dopants and present in small amounts and not visible in the XRD peaks. The peaks corresponding to NaF varied in intensity with substrate and chelating agent depending upon ligands coordinating affinity towards rare-earth ions and subsequent precipitation of extra NaF dissolved in solution. Octadentate DTPA ligand having high formation constant as compared to EDTA and EGTA, chelates better with Re^{3+} ions. During synthesis, improved chelation of Re^{3+} ions and subsequent bond weakening results in primary nucleation followed by crystal growth and stabilization. In addition, to bulkier size of DTPA facilitates faster aggregation of unstable smaller nuclei during the crystal growth process. Thus, rapid nucleation and subsequent stabilization of resulting crystals during UCF synthesis may have resulted in more unconsumed NaF precursor which is reflected in the X-ray diffraction pattern. Apart from this, the lesser solubility of DTPA in aqueous medium as compared to EDTA and EGTA, makes the former ligand a limiting reactant; thus amount of NaF used during synthesis is not utilized completely for crystal formation and thus reflected XRD pattern.

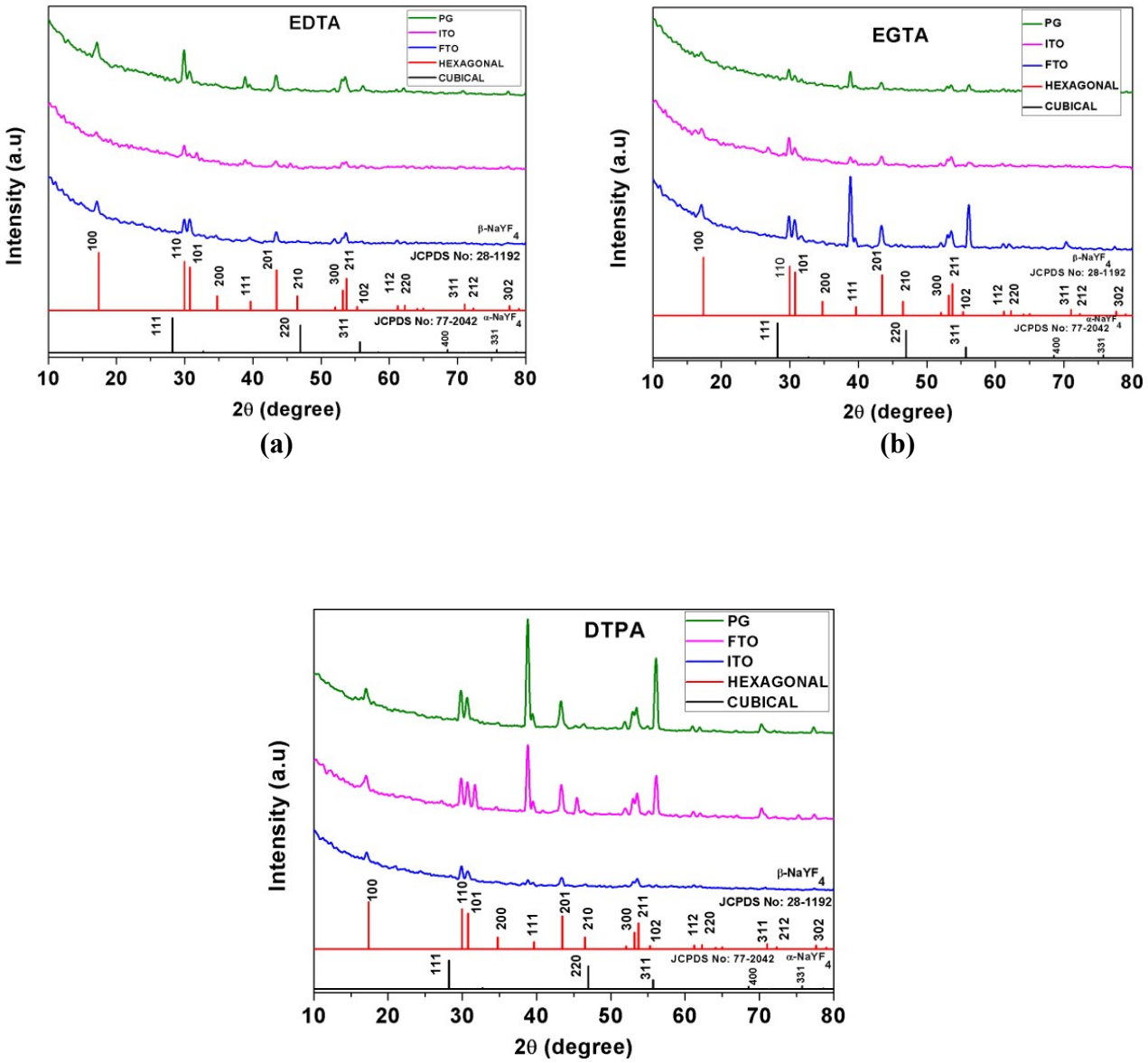

Fig 4.1. *X-ray diffraction pattern of UCF on various substrates using (a) EDTA (b) EGTA and (c)DTPA as the chelating agent.*

4.1.2. Scanning Electron Microscopy (SEM) Analysis

The SEM micrographs of UCFs on three types of substrates, PG, ITO and FTO employing three different chelating agents (CA= DTPA, EDTA and EGTA) are depicted in Fig. 4.2. In general $NaYF_4$:Yb^{3+}, Er^{3+} film coating on various substrates seems to consist of two parts: a compact thin layer in contact with the substrate and a second layer of isolated well faceted hexagonal or equiaxed morphology (sizes ~1 μm in the lateral direction). The SEM images of the fractured substrate with UCF grown over it (Fig. 4.2) may indicate the formation of a compact layer of nanostructure attached to the substrate followed by growth of bigger sized upconverting particles upon it. The magnified SEM image provided in Fig. 4.5 clearly represents this texture. This could be an indication of the probable growth mechanism of the films where the island of upconverting particles clusters may form initially, which merge to give a dense uniform film or vice-versa during the continuous growth process (Fig. 4.3). It is important to note that since there was no unusual phase, crystallinity and luminescence behavior observed in the case of prepared UCFs, it is expected that no compositional difference exists between two layers.

In the case of EDTA as a chelating agent, films deposited on FTO and PG substrate appeared similar, with uniform background coverage layer and identical hexagonal faceted grains (Fig. 4.2 b and c), while the coverage of the films was not good when deposited on the ITO substrate and isolated chunks were observed (Fig. 4.2a). The films deposited on all the substrates, using EGTA as a cheating agent, exhibited good surface coverage with varying morphology. The grains were equiaxed for the films deposited on the FTO substrate (Fig. 4.2e), while on the other hand, ITO and PG substrates displayed elongated hexagonal morphology (Fig.4.2 d and f), with much finer crystals in the case of ITO when compared to PG substrates. A glassy matrix around the particles could be observed in the case of films deposited on all substrates using DTPA as a chelating agent, while the films deposited using EDTA and EGTA substrate were much cleaner and well defined. Generally, improved chelation capability of the ligand towards specific ion in precursor solution increases the energy barrier needed for nucleation; hence, those ligands having strong chelation capacity requires higher temperatures for crystallization[133]. DTPA being a stronger chelating agent, the processed films had a distinct glass-like underlying layer (FTO & PG, Fig. 4.2 h and i) which wasnot observed in the case of the other two chelating agents (Fig. 4.2 a-f).

On the other hand, irrespective of the chelating agent, when the film was deposited on ITO substrate, crystals were well faceted and discontinuous while the film coverage was poor (Fig. 4.2 a, d and g). This indicated the possible role of surface charge in controlling/accelerating crystal growth and morphology[13]. It is noteworthy that the upconverting particles grown over different substrates are micro-rod/ cylindrical, disc, flower-like shape by use of various chelating ligands. However, the upconverting particles formed by using EDTA ligands are cylindrical or micro-rod shaped. This can be correlated with the small molecular weight as well less complex structure of ligand as compared to EGTA and DTPA. Generally, ligand dynamics over the crystal surface have a strong tendency of controlling growth of $NaYF_4$: Yb^{3+}, Er^{3+} over substrate attached by coordination effect[134]. The DTPA ligand is an expanded version of EDTA, based on Diethylenetriamine backbone with five carboxy methyl group. Similarly, EGTA is an amino polycarboxylic acid as of EDTA but has an elongated structure due to additional R-O-R linkage. This makes EGTA and DTPA more complex and heavier moieties as compared to EDTA. Generally, smaller ligand has a greater tendency of leaving the crystal surface rapidly during hydrothermal synthesis, facilitating directional growth aligned along a certain crystallographic axis. This is clearly visible in the case of upconverting particles synthesized by EDTA over various substrates depicting nearly micro-rod/cylindrical morphology. Initially, there is a formation of flower like aggregation due to the faster leaving of the adsorbed ligand from a crystal surface, thus making its surface unstable. Subsequently, aggregated nuclei in combination with reactant media resulted in the full-grown crystal, which subsequently formed a flower-like structure as observed on the plain glass substrate. After a certain growth, extrusion leads to rod-like morphology. Whereas, in the case of DTPA and EGTA, due to large molecular structure, the tendency of leaving crystal surface during reaction stage is less; therefore, crystals grown along a lateral direction forming disc or plate-like hexagonal structure have small aspect ratio. However, due to nearly comparable molecular backbone, there is no distinct morphological difference between the films synthesized using EDTA, DTPA & EGTA chelating agent. Additionally, the unstable surface dynamics of crystals during their dissolution in the reaction media results in the formation of a small number of irregular morphologies. Furthermore, the size distribution analysis (Fig. 4.4) provided insight into the various factors controlling the upconverting particles growth on different substrates. The scanning electron microscopy results revealed micron-sized particles with varying morphology grown over conducting/non-conducting substrates, depending

upon the chelating ligand used. The EDTA and DTPA ligand produced large-sized particles as compared to EGTA assisted synthesis. Small-sized upconverting particles resultingfrom EGTA assisted synthesis may be correlated with the long-chain length of EGTA molecule which have a tendency of stabilizing small-sized nuclei formed during the initial phase of synthesis. These surface stabilized nuclei have a weaker tendency of dissolution in hydrothermal reaction mixture, thus inhibiting the growth of large-sized nuclei during subsequent crystallization. Notice that EDTA is relatively simple in structure and hence has a greater tendency of leaving crystal surface, with high surface dynamics. Similarly, bulkier DTPA facilitates aggregation of nuclei during the crystal growth process as small nuclei are not stable. Hence improved surface dynamics as well as large-sized nuclei helped in the formation of bigger sized upconverting particles.

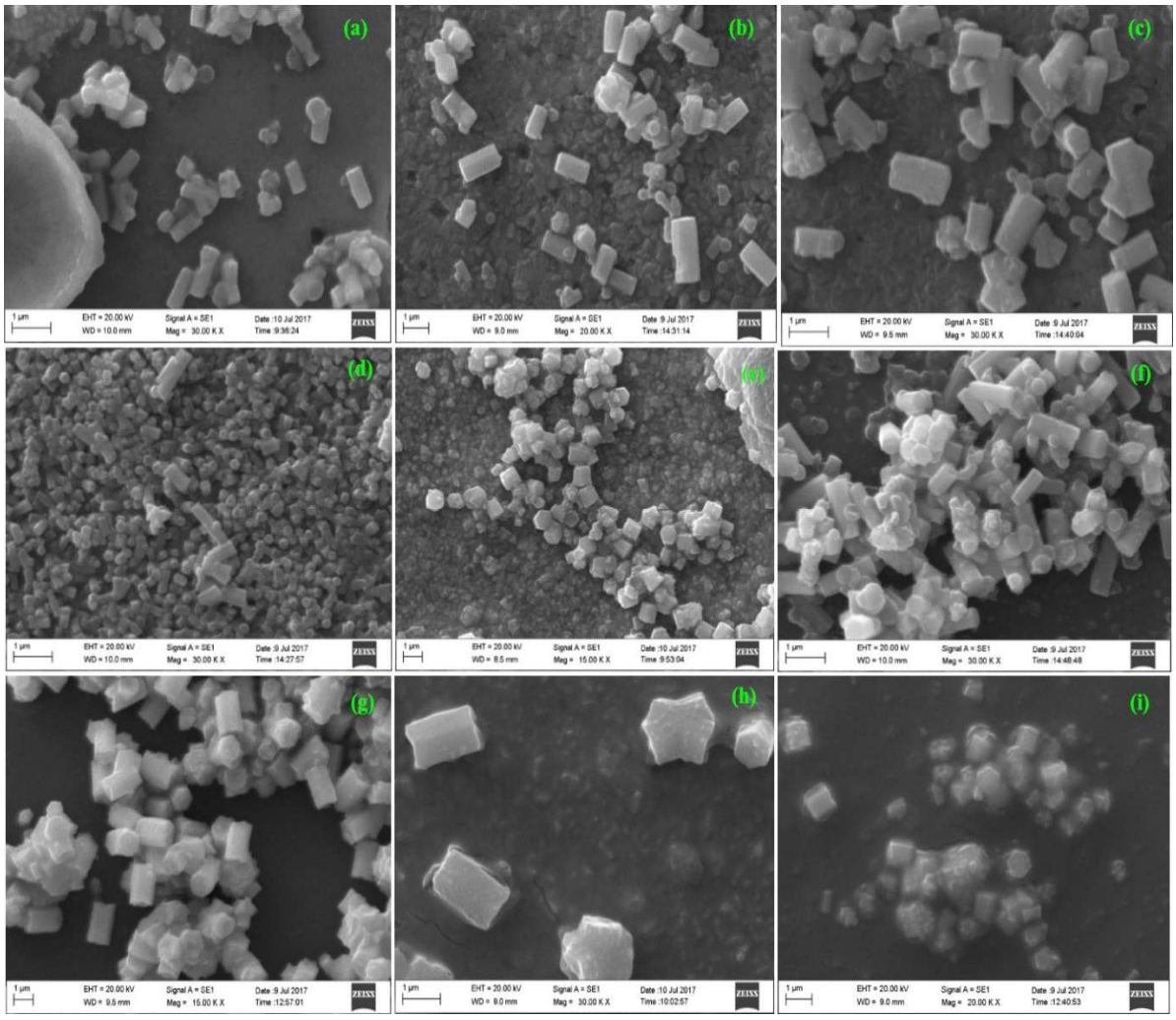

Fig 4.2.*Scanning electron micrographs of isolated upconverting particles over the film (UCF)*

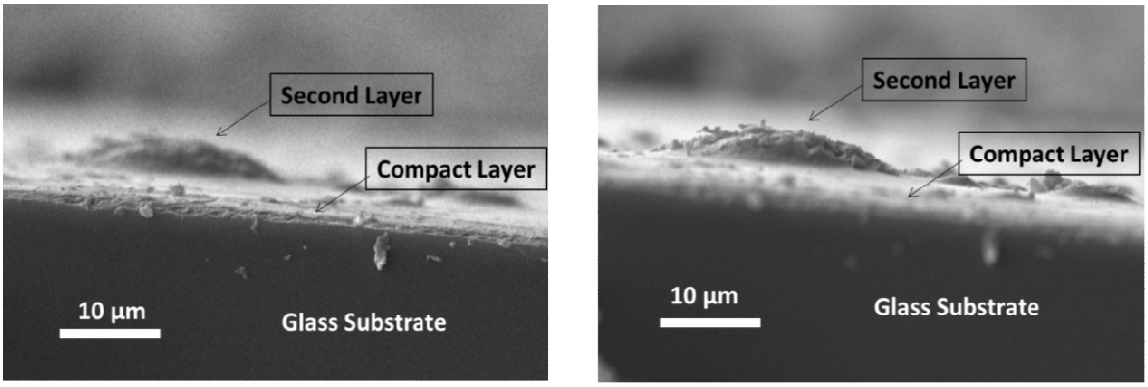

Fig. 4.3. *Cross sectional SEM image of the fractured surface of the prepared UCF*

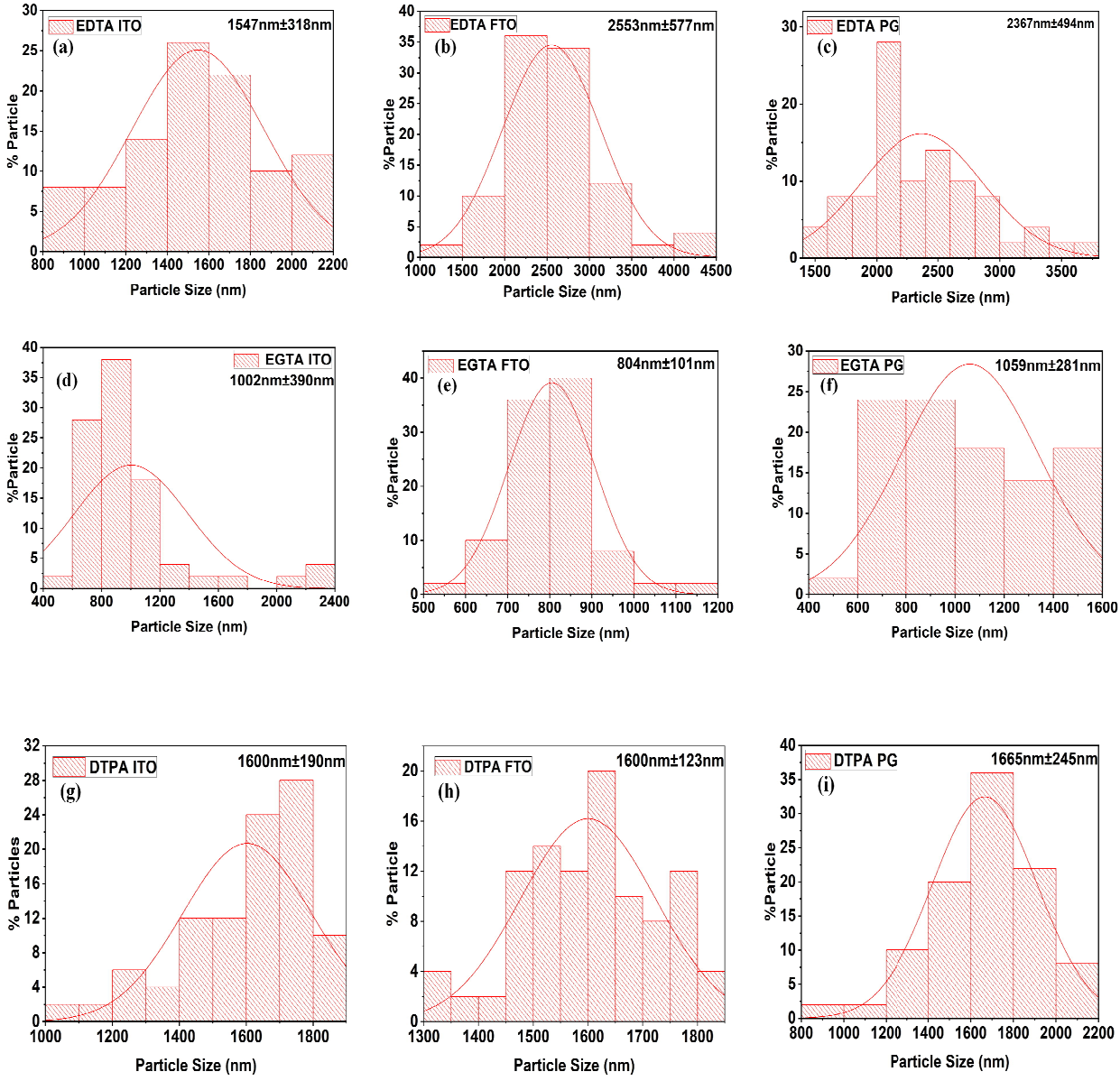

Fig. 4.4. *Size distribution analysis of upconverting particles synthesized over various substrates in combination with different chelating agents.*

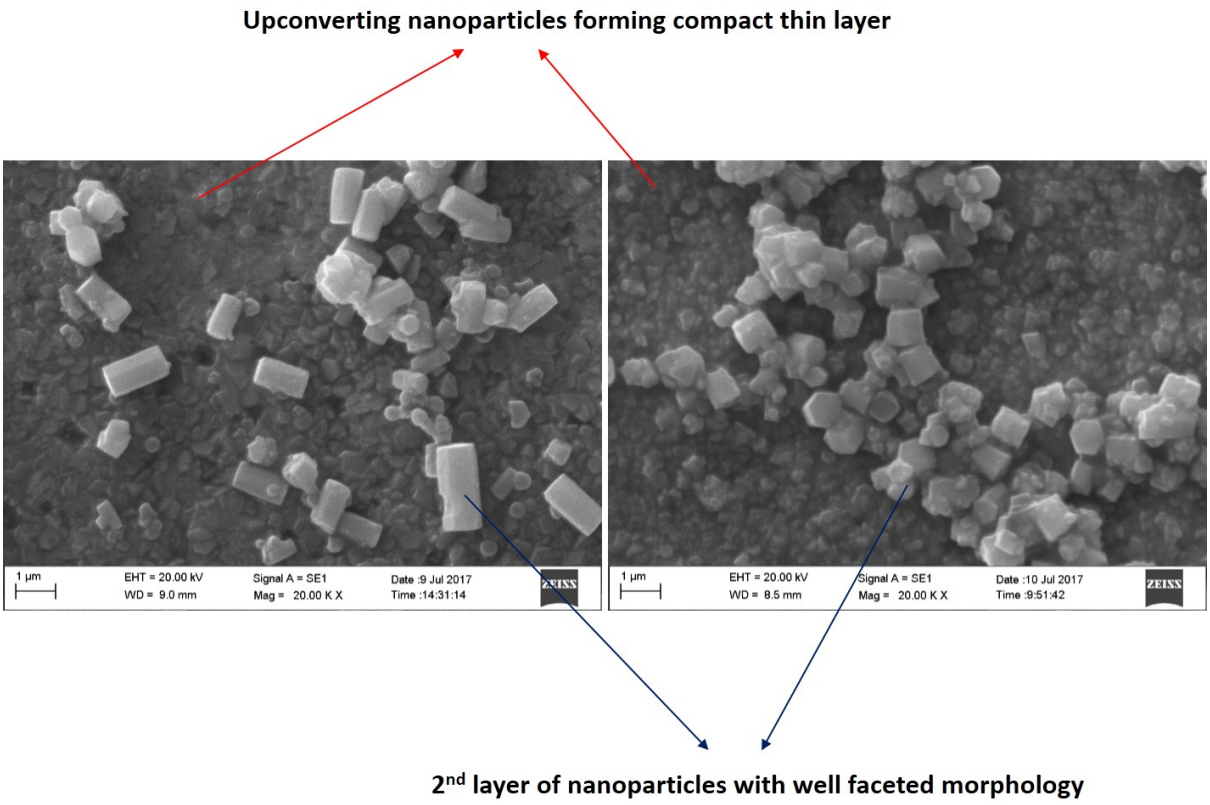

Fig. 4.5 *Magnified SEM image showing the formation of two layers of UCF over the substrate*

4.1.3.Atomic Force Microscopy (AFM) Analysis

The topography of the films was investigated using atomic force microscopy (AFM) in tapping mode. The maximum roughness of the film surface was found to be within 60 nm. For analysis, 10 µm × 10 µm area scans were obtained. The images were acquired by rastering 256 × 256 points. For the statistical analysis, 20 points (10 horizontal and 10 vertical) were considered. The average roughness (R_a), interface width, or root means square roughness (RMS) were statistically analyzed. Here, R_a indicates the absolute average distance of the surface point with respect to the mean plane. The RMS value indicates the standard deviation of the surface with reference to the mean plane[134]. The images in Fig. 4.6 show nine different UC films (UCF) with sample heights (from the mean plane) ranging from30 nm to 300 nm. Each figure panel was divided into central quadrant showing 3D UC film profile, and top left quadrant indicated surface topography and the top right quadrant displayed grain size. Further, the first row showed EDTA-assisted UCF, followed by EGTA and the third row of DTPA-assisted UCF deposited over ITO,

FTO and PG substrates respectively. The analyzed R_a and RMS values are summarized in Table 4.1. It is observed that an overall increase in RMS and average roughness of the films prepared by any chelating agent depends on the substrate used (Table 4.1). It is evident that while using EDTA and DTPA as chelating agents, minimum film roughness (RMS and average roughness) was observed from the UCF deposited onthe ITO substrate. At the same time, when EGTA was usedas a chelating agent, films deposited on PG substrate had minimum roughness. UCF over FTO (Fig. 4.6b) displayed a relatively broad surface roughness profile when compared to that of grown on ITO (Fig. 4.6a) and PG (Fig. 4.6c) substrates when EDTA was used as chelating ligand. Additionally, EGTA assisted UCF displayed sharper surface roughness profiles as observed in the case of PG substrate (Fig. 4f). Further, it is observed that the film grown on FTO (Fig. 4.6 h) and PG (Fig. 4.6 i) using DTPA as a chelating agent exhibited relatively broad peaks with substrate surface irregularities, but film deposited on ITO (Fig. 4.6g) displayed sharp peaks. All DTPA assisted UCFs resulted in greater root-mean-square roughness values. Further, statistical data suggests probably weak substrate effects on the morphology when compared with the effect of the chelating agents, as mentioned earlier. However, to study the effect of original substrate roughness on the surface textural property of prepared UCFs, an experiment was carried out by randomly examining AFM data of etched plain glass slide (Fig. 4.7). The Root mean square (RMS) and average (R_a) roughness of etched glass substrate (10 μm x10 μm) were found to be ~75 and ~51 nm, respectively. Moreover, the RMS and average roughness reduced for different UCFs deposited over a plain glass substrate (Table 4.1). This indicates the formation of a good upconverting layer over the substrate.

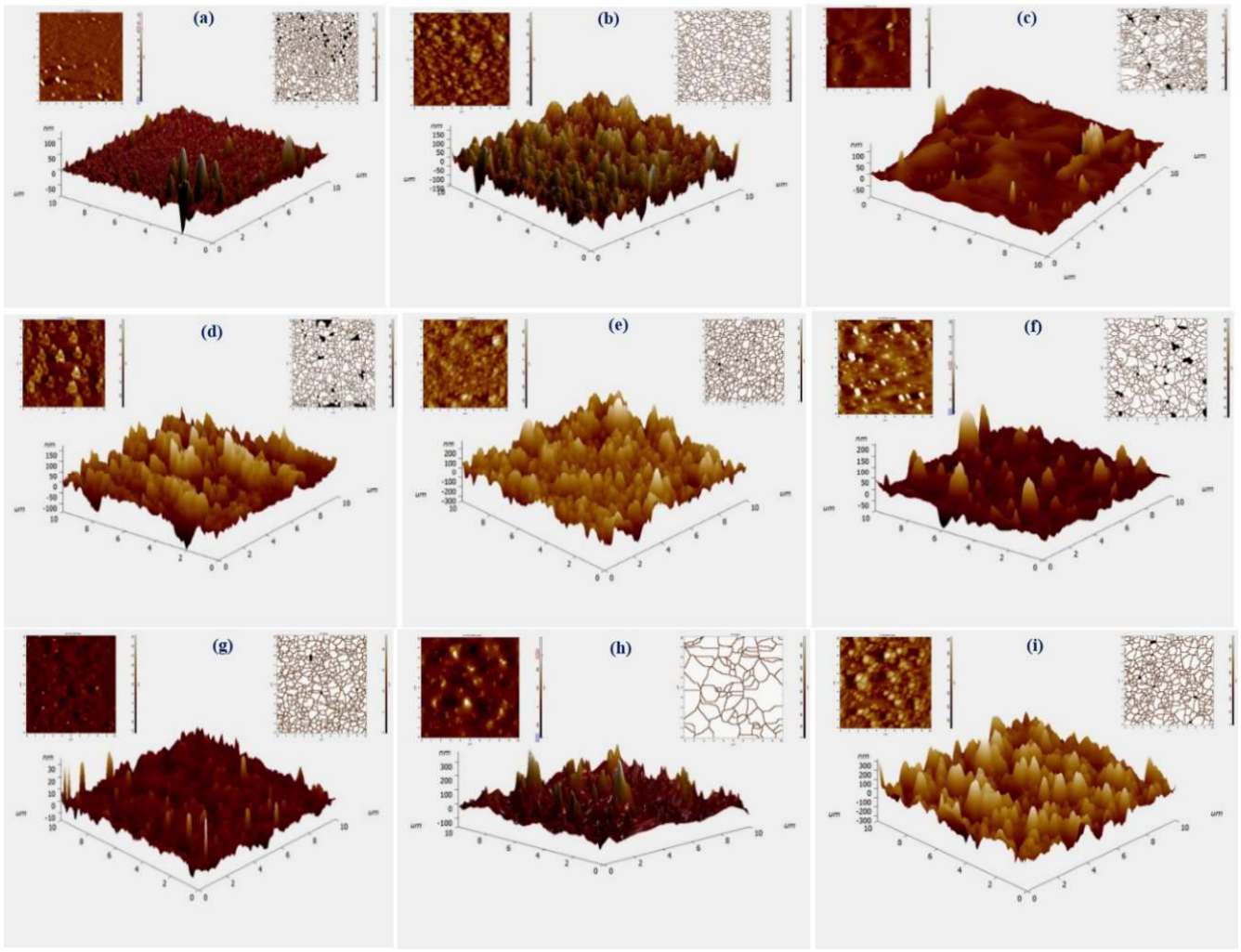

Fig. 4.6. *Atomic Force Micrographs of UCF along with surface topography*

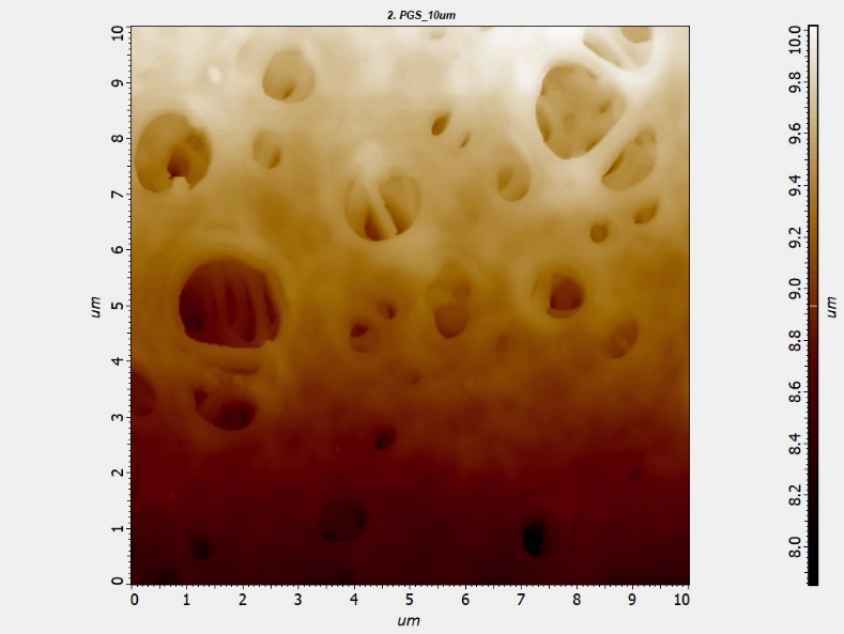

Fig. 4.7. *AFM image of etched plain glass slide before deposition of UCF*

Table 4.1. *The statistical parameters related to thin-film calculated based on AFM images*

Chelating Agent	**Substrate used**	**RMS Roughness R_q(nm)**	**Average Roughness R_a (nm)**
EDTA	ITO	5.83	4.34
	FTO	34.41	27.83
	PG	9.91	7.46
EGTA	ITO	34.88	27.46
	FTO	57.32	44.18
	PG	17.65	12.88
DTPA	ITO	3.05	2.39
	FTO	47.3	38.65
	PG	58.54	46.01

4.1.4. Photoluminescence Analysis

The thin-film deposited over conducting and non-conducting substrates were investigated for the photoluminescence upon excitation by 980 nm radiation using an inexpensive continuous-wave diode laser, resulting in four upconverted luminescence bands at wavelengths 390, 410, 525, 540and 650 nm (Fig. 4.8), which were attributed to $^4G_{11/2} \rightarrow {}^4I_{15/2}$, $^2H_{9/2} \rightarrow {}^4I_{15/2}$, $^2H_{11/2} \rightarrow {}^4I_{15/2}$, $^4S_{3/2} \rightarrow {}^4I_{15/2}$, $^4F_{9/2} \rightarrow {}^4I_{15/2}$ transition states respectively[96]. It is important to mention that Yb^{3+} acts as a sensitizer and is responsible for absorbing the NIR radiation. The absorbed energy is transferred to Er^{3+} due to close proximity between the two in the $NaYF_4$ lattice, resulting in characteristic upconversion emission (Fig. 4.8). This characteristic upconverted emission is strongly indicates the efficient incorporation of Yb^{3+} and Er^{3+} within the $NaYF_4$ structure and the successful formation of the upconverting film.

The qualitative comparison of characteristic luminescence intensity from different $NaYF_4$: Yb^{3+}, Er^{3+} substrates for the same chelating agent are summarized in Table 4.2. It is interesting to note that the highest luminescence intensity was observed in the case of films deposited on ITO substrates when DTPA and EDTA were used as chelating agents. On the other hand, when EGTA chelating agent was employed, the film deposited on the PG substrate showed the highest luminescence intensity. The effect of the cheating agent on different substrates is summarized in Table 4.3. EGTA chelating agent resulted in the highest luminescence intensity for films deposited on FTO and PG substrates, while the lowest luminescence intensity was observed for films deposited on ITO substrate. Results from Table 4.2 and 4.3 clearly demonstrate that both the chelating agent and substrate have a pronounced effect on the upconverting emission characteristic of the films.

One film characteristic which was observed to have a direct correlation in this study was the roughness of the deposited films. This is because of the fact that the film roughness can result in diffused scattering, reducing effective luminescence cross-section, thereby, suppressing luminescence intensity observed. Smoother films resulted in higher luminescence intensities, while the luminescence intensity decreased with increasing roughness. For instance, in the case of the films deposited using DTPA, a very smooth film having an RMS value of around 3 nm was obtained when deposited on ITO. On the other hand, using the same chelating agent films deposited on FTO and PG was way rougher, having RMS roughness values around 47 and 57

nm, respectively. Accordingly, the luminescence intensity (Fig. 4.8 c) obtained from UCF deposited on ITO was very high when compared to that obtained from the UCF deposited on FTO or PG substrate. Similarly, in the case of UCF deposited by using EDTA and EGTA as chelating agents, on ITO and PG substrate had thelowest RMS roughness values, which resulted in the highest luminescence intensity. However, generally, film roughness is difficult to control during solution-based processing. Nevertheless, the above study showed that film roughness depends both on the nature chelating agent and substrate used. Best luminescence intensity was observed from the films deposited on ITO substrate and DTPA as the chelating ligand.

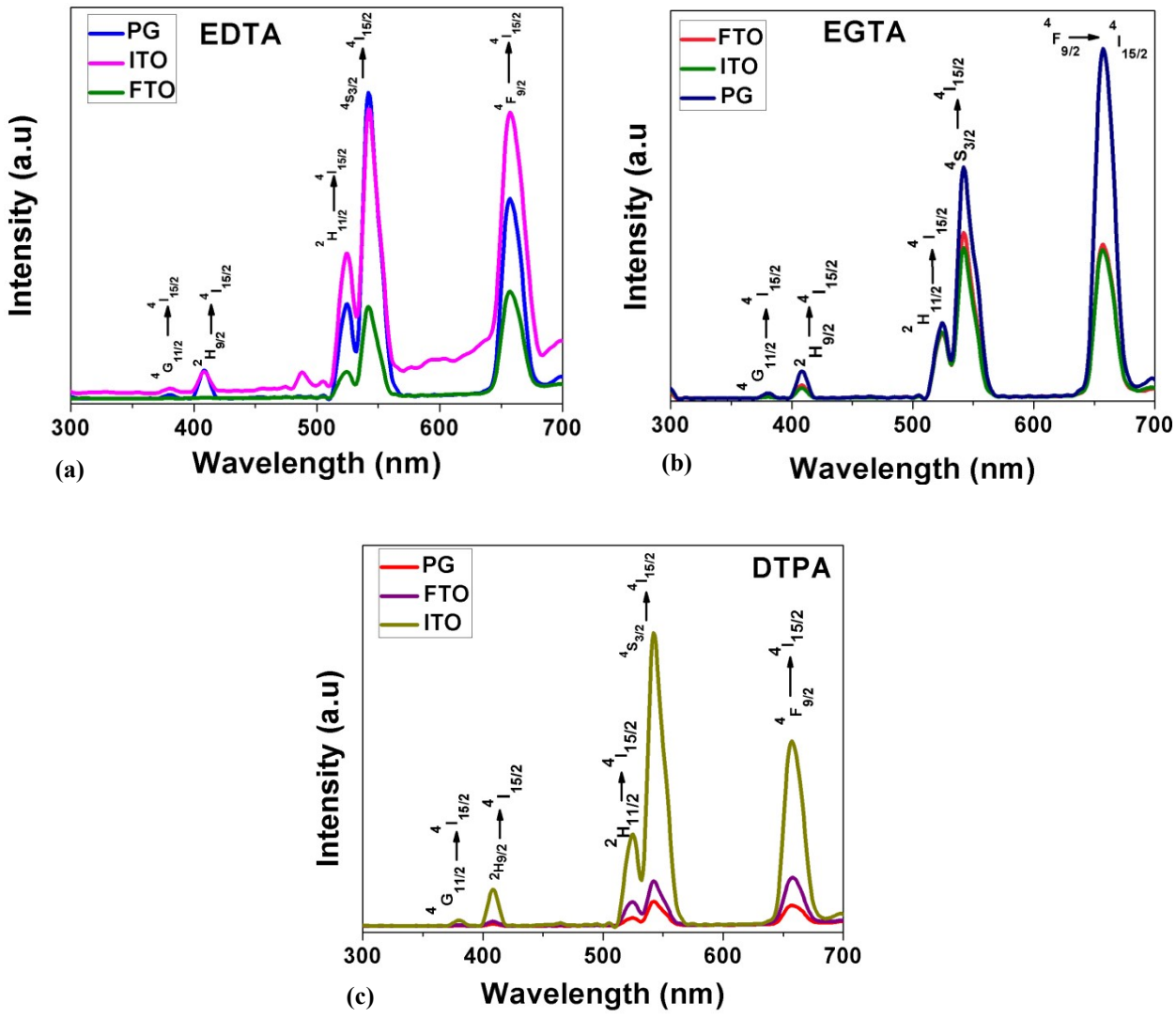

Fig. 4.8. *Luminescence spectra UCF were prepared using EDTA (a), EGTA (b) and DTPA (c) as chelating agents.*

As per early reports by Giedraityte et al.[86], the upconversion intensity is independent of film thickness. Hence the film thickness may not have a significant role in tuning upconversion emission intensity for the current study. However, it has been observed that film thickness varied slightly with a change in nature of the chelating agent used. On an average, films as thick as 3 μm were observed, as shown in (Fig. 4.9).

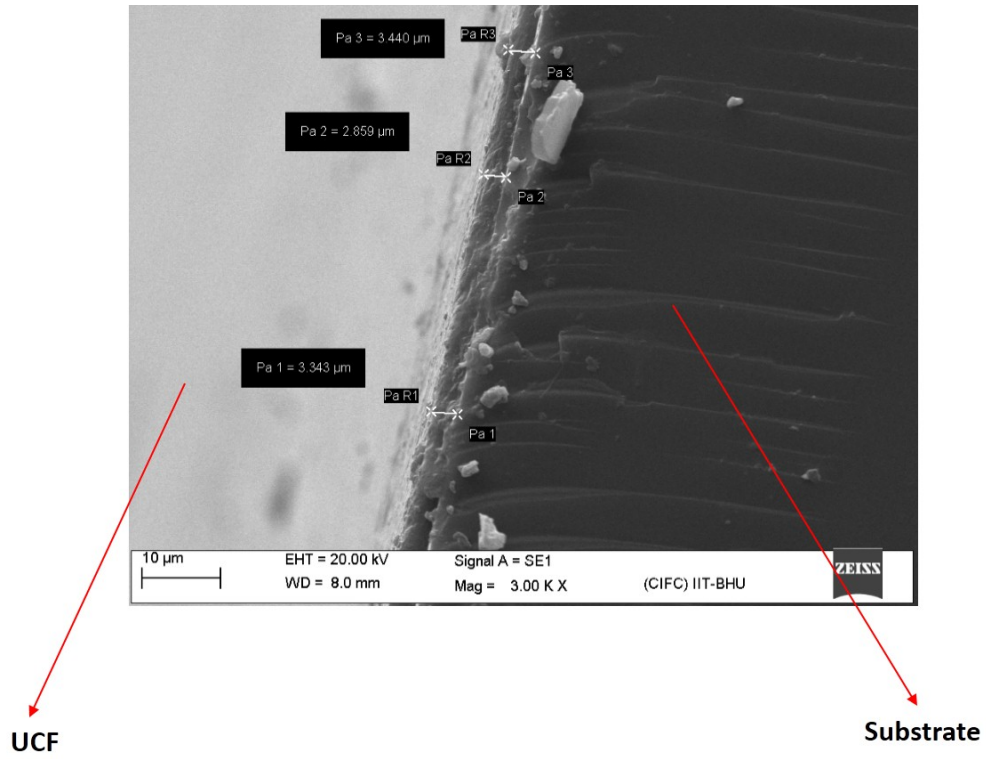

Fig. 4.9. *Scanning electron micrographs of cross-section of prepared UCF showing the formation of micron-sized film over the substrate.*

Table 4.2. *Effect of the chelating agent on characteristic luminescence intensity deposited on different substrates*

Chelating agent	Luminescence Intensity (Decreasing)
EDTA	**ITO>PG>FTO**
EGTA	**PG>FTO>ITO**
DTPA	**ITO>FTO>PG**

Table 4.3. *Effect of substrate on characteristic luminescence intensity from FTOs with different chelating agents*

Substrate	Luminescence Intensity (Decreasing)
ITO	DTPA>EDTA>EGTA
FTO	EGTA>DTPA>EDTA
PG	EGTA>EDTA>DTPO

4.2. Conclusions

In conclusion, $NaYF_4$:Yb^{3+},Er^{3+} upconverting films (UCFs) were deposited by low temperature, facile, one-step hydrothermal process.The film characteristics change interestingly when either substrate or the chelating agent is changed, showing that both substrate and chelating agent affect the film characteristics such as phase formation, roughness and luminescence intensity. The best emission intensities on the non-conducting substrate were achieved by using EGTA as a chelating agent. Further, in the case of conducting substrates, the combination of EGTA ligand with FTO substrate and DTPA ligand with ITO substrate produced upconverting films with improved luminescence intensities.

Chapter 5 – Development of Ultrasensitive As(III) Selective Upconverting ($NaYF_4$:$Yb^{3+}Er^{3+}$) Platform

5.1. Development of Ultrasensitive Platform for As(III) Detection

Our prior studies with different chealting agent and solid substrates (ITO, FTO and plain glass) indicated that using hydrothermal method thin-films can be formed, however the integrity of these films could still be improved. During further research with the plant it was observed that large molecules such as catechol and polyphenols are present that could act as good film binder, promoting film uniformity. Therefore a initial attempt was made to develop thin film of upconverting material using the film extract. Further, to demonstrate the use of these films in the detection of water pollutant such as As(III), plant with affinity to towards arsenic adsoption were used in a hope that the ligands present in the extract would participate in the As(III) sensing. Therefore, M.oliefera leaf extract were chosen as dispersion and reaction medium for the growth of the $NaYF_4$: Yb^{3+},Er^{3+} (upconverting material) film over the glass substrate. Therefore this section deals with investigation of leaf extract, development of $NaYF_4$: Yb^{3+}, Er^{3+} film, its optical homogeneity, and ability to detect As(III) optically and also display selectivity towards arsenic even in the presence of different analytes.

5.1.1. Design of As(III) sensitive upconverting platform

Earlier studies have demonstrated that the polyphenolic groups present in the leaf extracts chelate very well the arsenic ions. In a work, Iberhan et al.[135] demonstrated chelation of As(III) ions by polyphenol (e.g., catechol) under acidic condition. Incidentally, M.oleifera leaf extract used here contained catechol as evident from gas chromatography-mass spectrometry (GC-MS) analysis which is carried out with a Shimadzu GC-MS-QP2010 plus ultra-system (Fig. 5.1). It was envisaged that As(III) ions could possibly be detected with a suitable upconverting platform by invoking LRET modulation (i.e., varying the spectral overlap of acceptor and donor). The overlap between the absorbance band of catechol (acceptor) andemission spectra of the upconverting platform (donor) has been established (Fig.5.2).

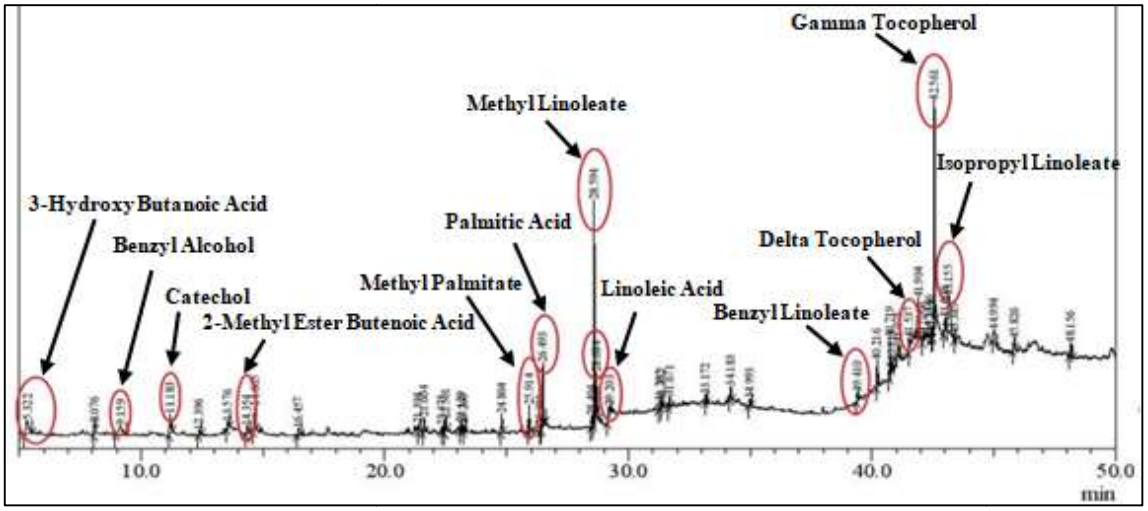

Fig. 5.1. *GCMS spectra of M.oleifera extract showing the presence of catechol alongside fatty acid ester compounds.*

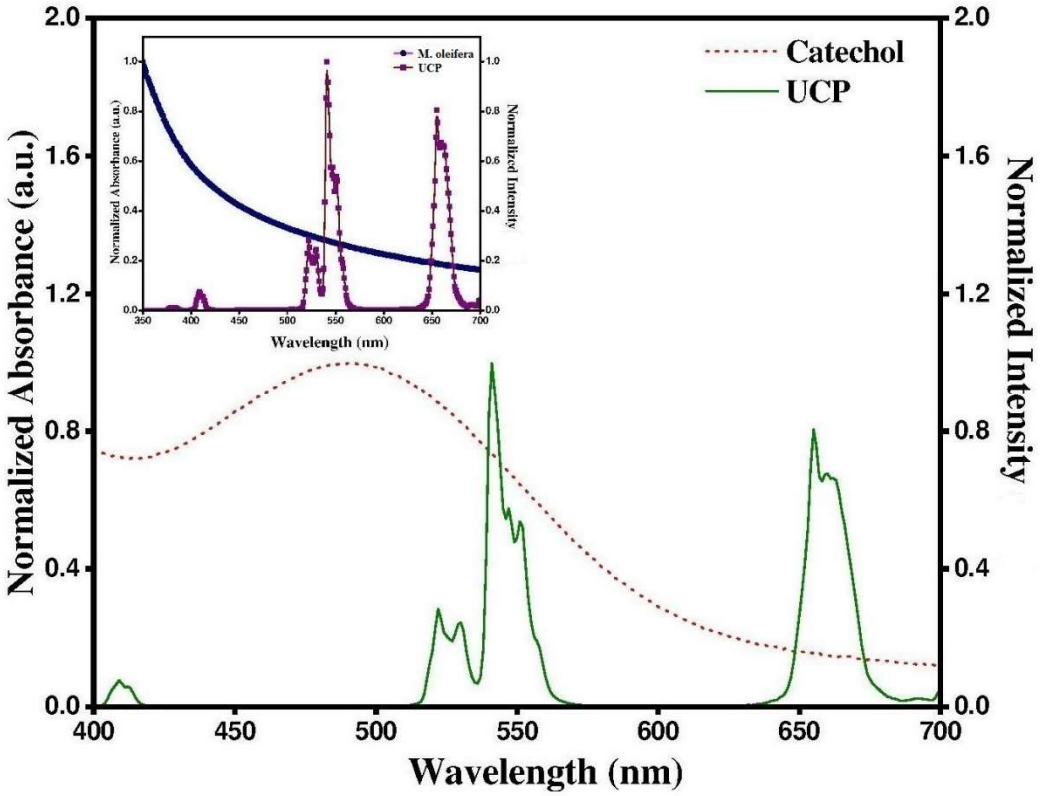

Fig. 5.2. *Optical absorption of catechol and emission spectra of UCP shows their overlapping. Inset figure shows the overlapping between UCP and M.oleifera on a similar pattern.*

It is important to note that the catechol (pure), absorbance band in visible range appeared due to the stacking of polyphenol monomers at the specified concentration. The changes in catechol absorbance with and without trivalent arsenic ions [As(III)] was also monitored. Accordingly, absorbance exhibits suppression of intensity in the presence of As(III) species (Fig. 5.3), indicating the potential of catechol for LRET modulation. The absorption spectra of M.oleifera with random addition of certain concentrations of As(III) ion within experimented region was also monitored (Fig. 5.4).

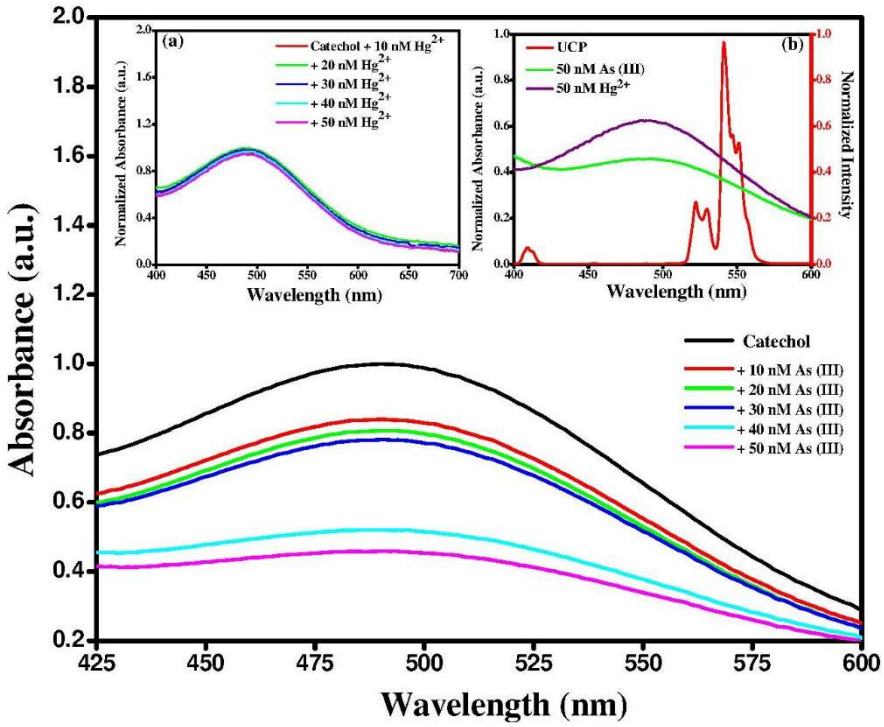

Fig. 5.3. *Change in catechol light absorption property on subsequent As(III) addition.*
Left Inset (a) showing nearly unaffected absorption of catechol on addition of mercury.
Right Inset (b) showing quenching in absorbance of catechol with respect to Hg^{2+} *addition whereas on same concentration of As(III) additions, spectra has more overlapping tendency towards upconverted emission*

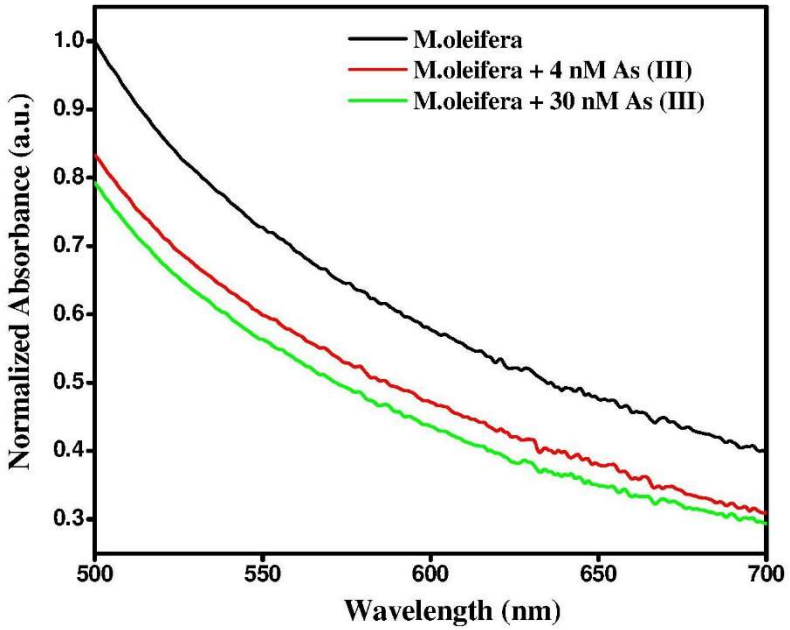

Fig. 5.4. *Absorption spectra of M.oleifera and alongwith the addition of As(III) 4nM and 30 nM solutions*

It is noteworthy that LRET is a very sensitive technique, especially when the acceptor (catechol) emission lies close to the donor (UCP) (within 10 nm). Accordingly, even a small amount of acceptor is sufficient enough to generate a signal in the presence of As(III) ions. Therefore, to examine the prospects of As(III) sensing, UCP at catechol and UCP at DW were also prepared. Upon 980 nm light excitation, UCP at catechol displayed a weak emission compared to that of UCP at DW (Fig.5.5inset), possibly due to LRET.

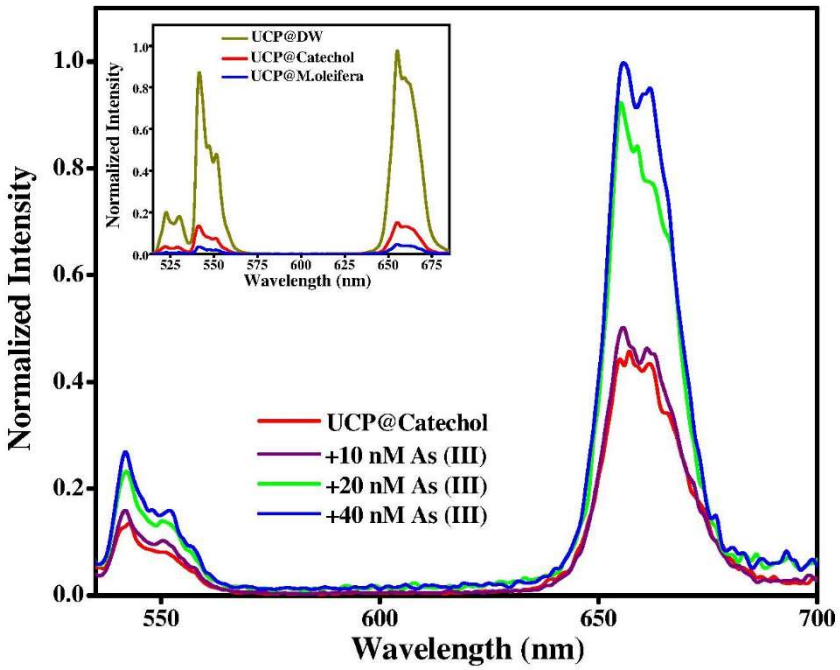

Fig. 5.5. *Emission reversal of UC platform produced with catechol and after exposure to As(III) 10, 20 and 40 nM solutions.*

Inset shows the emission spectra of luminescent material deposited on the glass slide using DI water.

It is important to note that the Beer–Lambert law presumes the non-existence of solute–solute interactions. However, catechol probably interacts with the As(III) ions in the present case and produces a non-linear signal. The absorbance response shown in (Fig. 5.3) is indeed not proportional to the As(III) contentin the solution (10–50 nM) and varies in steps. The other reason may be (i) catechol present in an equivalent quantity to that found in the plant extract and (ii) the presence of more As(III) ions than required for interaction with catechol. In the case of UCP at M.oleifera (Fig.5.6), the emission varied systematically with As(III) content in the entire solution range (0–50nM).

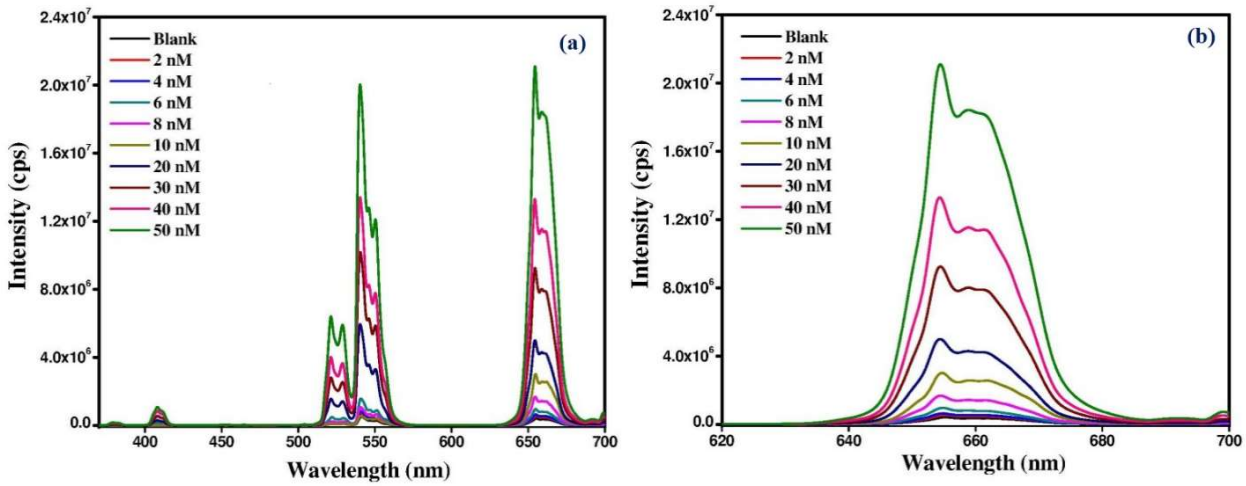

Fig.5.6.*(a) Spectral response of UCP at M.oleifera with addition of As(III) solutions in the concentration range of 0-50 nM and (b) Specific red emission ~ 655 nm showing systematic surge with As(III) content*

Moreover, the addition of As(III) (10, 20, or 40 nM) solution led to an increase in the intensity of the red and green bands, indicating the occurrence of emission reversal from UCP at catechol through LRET disruption (Fig.5.5). This fact formed the basis for the development of the As(III) selective platform. Obviously, the intensity improvement was insignificant in UCP at catechol (due to poor film stability perhaps), but may be considerable with the M.oleifera leaf extract. However, more work is needed to account for the observed emission variation in the case of catechol. Moreover, the M.oleifera leaf extract, enriched with long chain fatty acid esters (Fig. 5.1), can assist the nucleation and growth of the upconversion phosphor crystallites, giving stability to the developed platform on the substrate. Further, the other polyphenolic compounds such as rutin, quercetin, kaempferol, myriectin,and ishromentin present in M. oleifera[136,137] may also play important role in the detection of As(III).

5.1.2. Synthesis and Characterization of UCP at M.oleifera

The M.oleifera leaf extract (pH: 3–5) contains 3-hydroxy butanoic acid, linoleic acid, palmitic acid and gamma tocopherol, besides catechol. Their presence was confirmed by the signatures of the ligands in the GC-MS analysis (Fig. 5.1). The FTIR spectrum displays four infrared absorption peaks centered at around 2900, 1750, 1650, and 3500 cm^{-1} due to the C-H, C=O, C=C, and NH_2/OH bond stretching, respectively (Fig. 5.7). Two additional peaks at 750 and 900 cm^{-1}result presumably from the out-of-plane C–H bending in the substituted aromatic

compounds (mainly polyphenols)[138]. These findings confirm the presence of various fatty acid esters, polyphenols and amino acid compounds. The reaction of the ligands with the rare earth precursor solution led to the formation of the UC platform. Previously, Shan et al.[139] utilized long chain fatty acid esters such as oleic acid, stearic acid and lauric acid for the nucleation and growth of upconversion phosphors. It is believed that the long chain fatty acid ester undergoes chelation with rare earth (Re^{3+}) ions and forms a stable complex. Under hydrothermal conditions, they react with Na^{+} and F^{-} ions, leading to the nucleation and growth of stable upconversion crystals[140,141]. It is likely that linoleic acid or the analogous long chain fatty acid esters present in the leaf extract also play a similar role. Furthermore, the acidic nature (pH~ 4–6) of UCP at M.oleifera provides favorable conditions for As(III) chelation by the adhered polyphenolic groups, and hence improvement in selectivity. $NaYF_4:Yb^{3+},Er^{3+}$ powder was scraped from UCP at M.oleifera and suspended in DI water for ascertaining its acidic nature via pH measurement using astandard pH meter. The crystallinity, phase, surface coverage,and microstructure were evaluated using XRD and optical and electron microscopy.

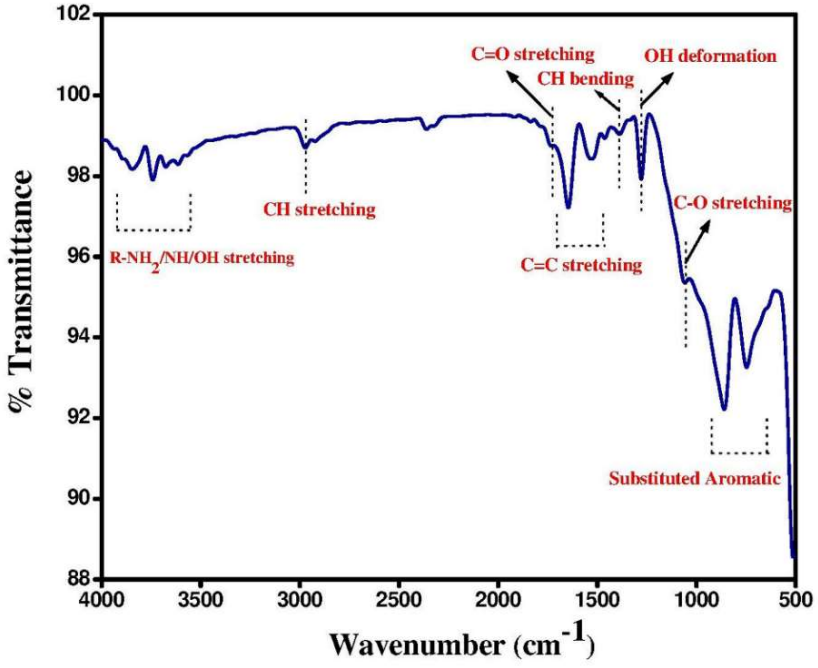

Fig. 5.7. *Attenuated total reflectance spectra of UCP synthesized using M.oleifera leaf extract*

The typical XRD pattern of UCP at M.oleifera depicted in (Fig. 5.8 a) corresponds to the well-known cubic phase of α-$NaYF_4$ (JCPDS-77-2042), confirming the formation of the crystalline platform. The typical scanning electron micrograph of UCP at M.oleifera revealed agglomerates

of faceted tubular rods of different dimensions (Fig. 5.8 b). An inverted fluorescence microscopic image revealed the formation of a nearly uniform phosphor layer over the glass substrate with some open patches and pinholes (Fig.5.9).

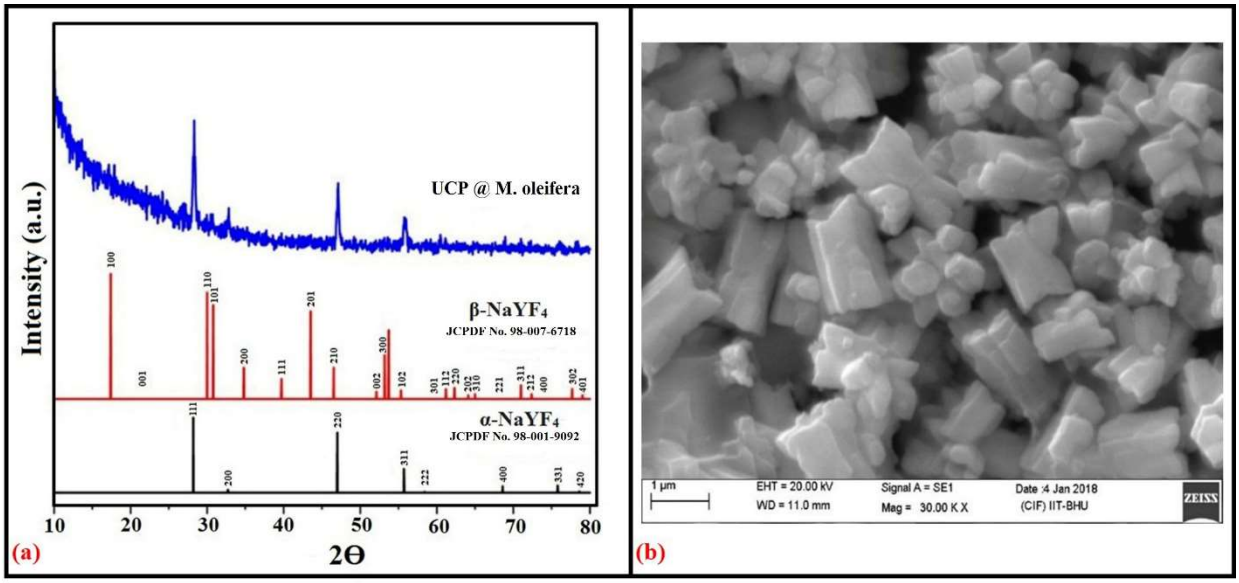

Fig. 5.8. *(a) X-ray diffraction pattern of UCP at M.oleifera and (b) a typical scanning electron micrograph of* $NaYF_4:Yb^{3+}, Er^{3+}$ *crystallites on the platform.*

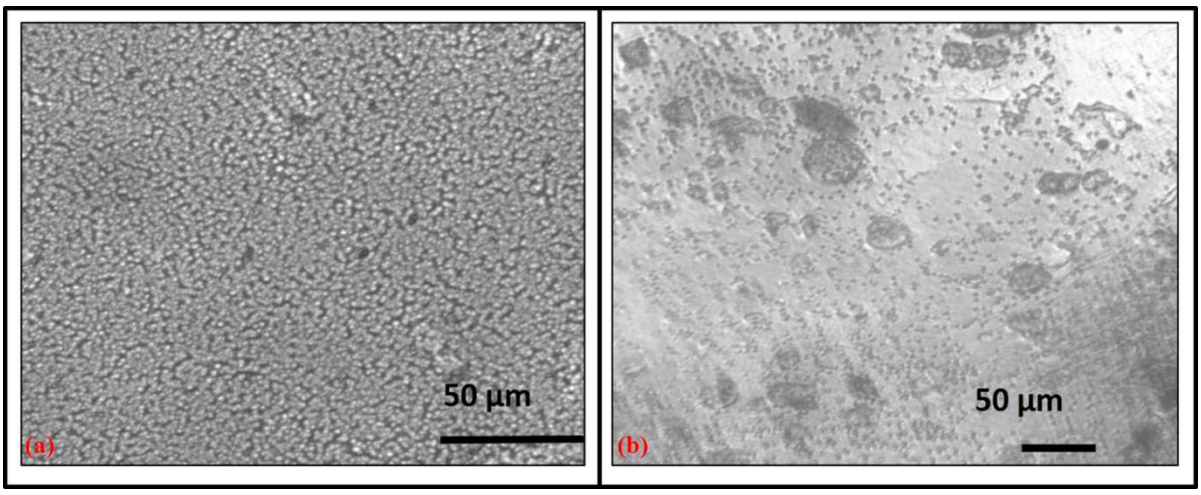

Fig. 5.9. *Inverted fluorescence microscopic images reveal fairly good coverage of upconverting nanostructures over large span of glass substrate (a) Bright-field images indicating upconverting platform integrity and consistency (b) Few empty patches and pin-holes over the entire surface of the substrate*

Upon excitation at 980 nm (power density 250 W cm^{-2}), UCP at M.oleifera produced an emission spectrum with bandsat 410 (violet), 520 (cyan) 540 (green) and 655 nm (red), corresponding to the Er^{3+} ion $^2H_{9/2} \rightarrow {}^4I1_{5/2}$, $^2H_{11/2} \rightarrow {}^4I_{15/}$, $^4S_{3/2} \rightarrow {}^4I_{15/2}$, and $^4F_{9/2} \rightarrow {}^4I_{15/2}$ transitions, respectively (Fig. 5.10), confirming the upconversion process.

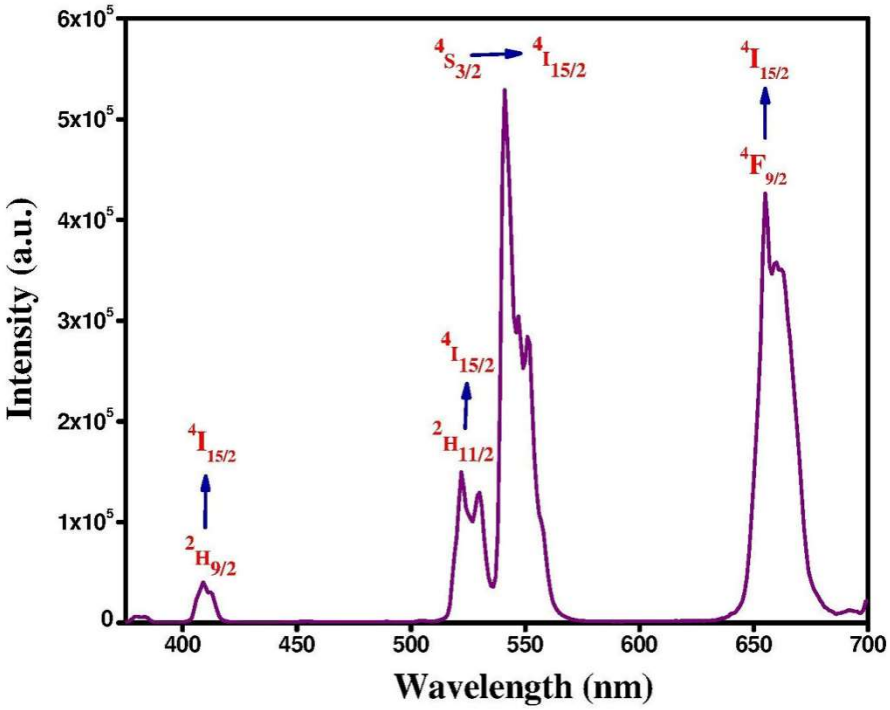

Fig. 5.10 *Luminescence output from the UCP synthesized using M.oleifera leaf extract.*

5.1.3. Detection by UCP at M.oleifera and its Selectivity

With As (III) addition, UCP at M.oleifera exhibits enhanced emission in green (525-575 nm) and red (625-700 nm) regimes (Fig.5.6 a). These are the characteristic spectra of Er^{3+} doped $NaYF_4$ upconverting system. A distinct and steady increase in red band (625-700 nm) is visible in (Fig.5.6b) with the use of [As(III)] 2-50 nM solution. Fig. 5.11 shows a steady increase in emission due to LRET disruption brought by the interaction of As (III) ions with UCP at M.oleifera (as discussed below).

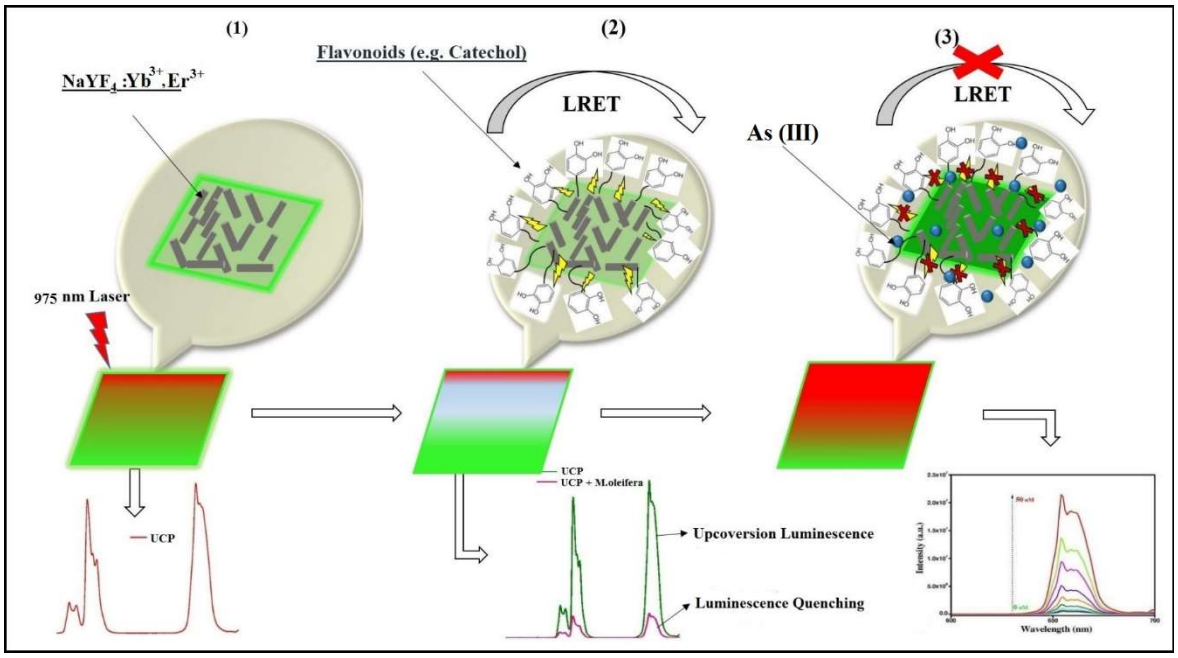

Fig. 5.11. *Schematic diagram showing mechanism of As(III) detection*

The resulting linear increase in red signal **(**Fig. 5.6 b**)**, covered a wide range of As (III) solution (2-50 nM), served as a calibration curve for quantitative detection of As(III) in water. In contrast, the intensity of green emission is also found to increase but only in As(III) solution of higher concentrations (20-50 nM) **(**Fig.5.6 a**)**.The probable explanation for this is based on the fluorescence resonance energy transfer efficiency (E_{ef}), which depends on emission lifetime[142] and can be expressed as:

$$E_{ef} = 1 - (\frac{\tau_{DA}}{\tau_D}) \quad (2)$$

where, τ_{DA} and τ_D represents the life time of the donor in the presence of an acceptor and without an acceptor, respectively. Previous studies have demonstrated a longer lifetime for the red in comparison to the green emission[143]. This implies extra energy transfer and hence relatively greater suppression of the red band (Fig.5.5 inset: comparison of emission spectra UCP at DW with UCP at Catechol and UCP at M.oleifera). Therefore, disruption of LRET became prominent in red emission upon the addition of As(III) even with a low concentration range (2-10 nM). For the green band, a larger concentration of As(III) was required to observe a similar effect.

Accordingly, red (instead of green) emission was preferred for analytical detection to cover a wide As(III) range, i.e., from low 2nM to high 50 nM concentration. However, it should be

emphasized that the inferences drawn from the red and green emissions are also consistent at a higher concentration range (20-50 nM). Utilizing the linear increase in the red band (655 nm), a linear calibration curve (least square method) was obtained by plotting I_{signal} versus [As(III)] as shown in (Fig. 5.12**)**.

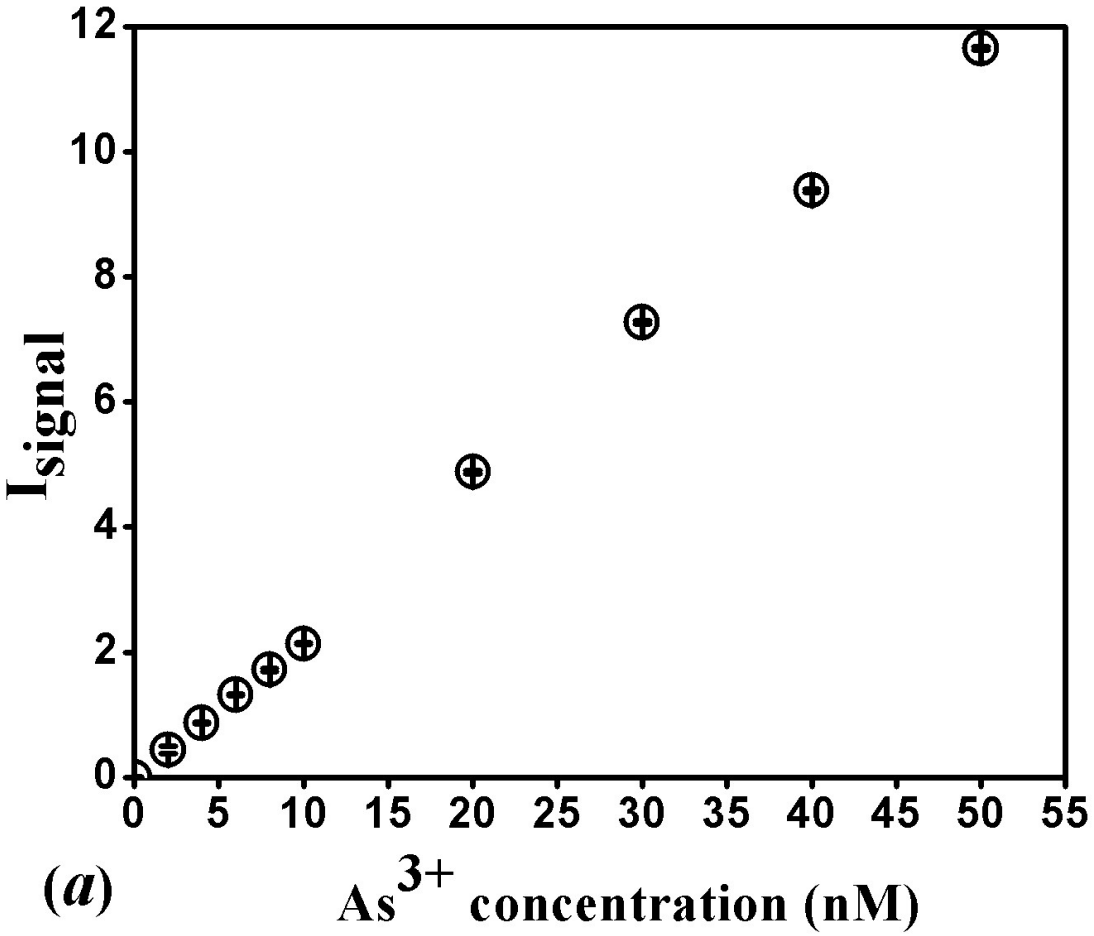

(b)

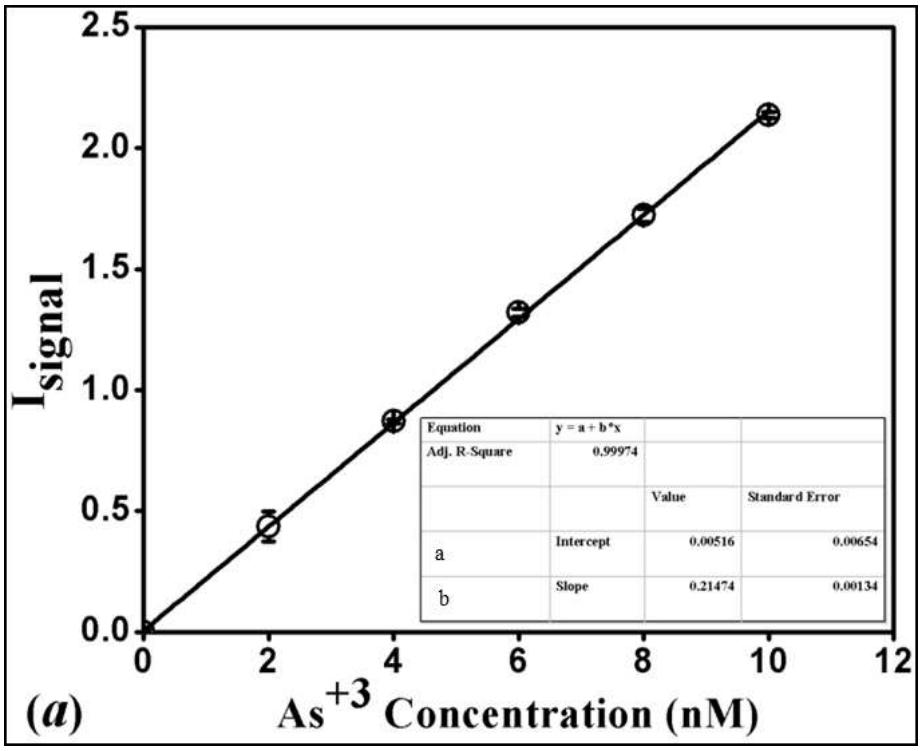

Fig. 5.12. *UCP at M.oleifera I_{signal} versus As(III) ion content plots in solution concentration ranges (a) 0-50 nM and (b) 2-10 nM showing linearity*

The overlap in the absorbance spectra of the acceptor (catechol) and upconverted emission of the donor (UCP at M.oleifera) was manifested as the luminescence resonance energy transfer (LRET) and resulted in a decrease in the Er^{3+} ion emission. The interaction between catechol and/or other polyphenols having a hydroxy group under acidic conditions results in the formation of a chelation complex with As(III) ion[135,144,145]. The formation of this complex may result in the rearrangement of the polyphenol molecular/electronic structure and a notable change in its light absorption property. The formation of the chelate and induced changes in the optical properties were monitored via UV-Vis and ESI-MS[144] (Fig.5.3 a) shows the effect of As(III) chelation on the optical absorption of catechol (a polyphenol). These changes caused a reduction in the efficiency of the energy transfer between the UCP and polyphenol, with relatively less emission occurring from UCP at catechol to revert/return. Thus, in the presence of As(III) species, the optical absorption was restricted, and donor emission remained intact (or recovered) and an

upsurge in the 655 nm band was observed. The mechanism of As(III) detection is schematically presented in (Fig. 5.11**)**.

The selectivity of UCP at M.oleifera towards twelve other ions (Hg^{2+}, Cd^{2+}, Pb^{2+}, Ca^{2+}, Mg^{2+}, Sn^{2+}, Cr^{6+}, $Fe^{2+,}$ Co^{2+}, $H_2PO_4^-$, Cl^-, F^-) was evaluated in a manner similar to that for the As(III) ion (Fig.5.13). In each case, I_{signal} was weak, signifying a strong LRET effect, i.e., efficient energy transfer between UCP and catechol.

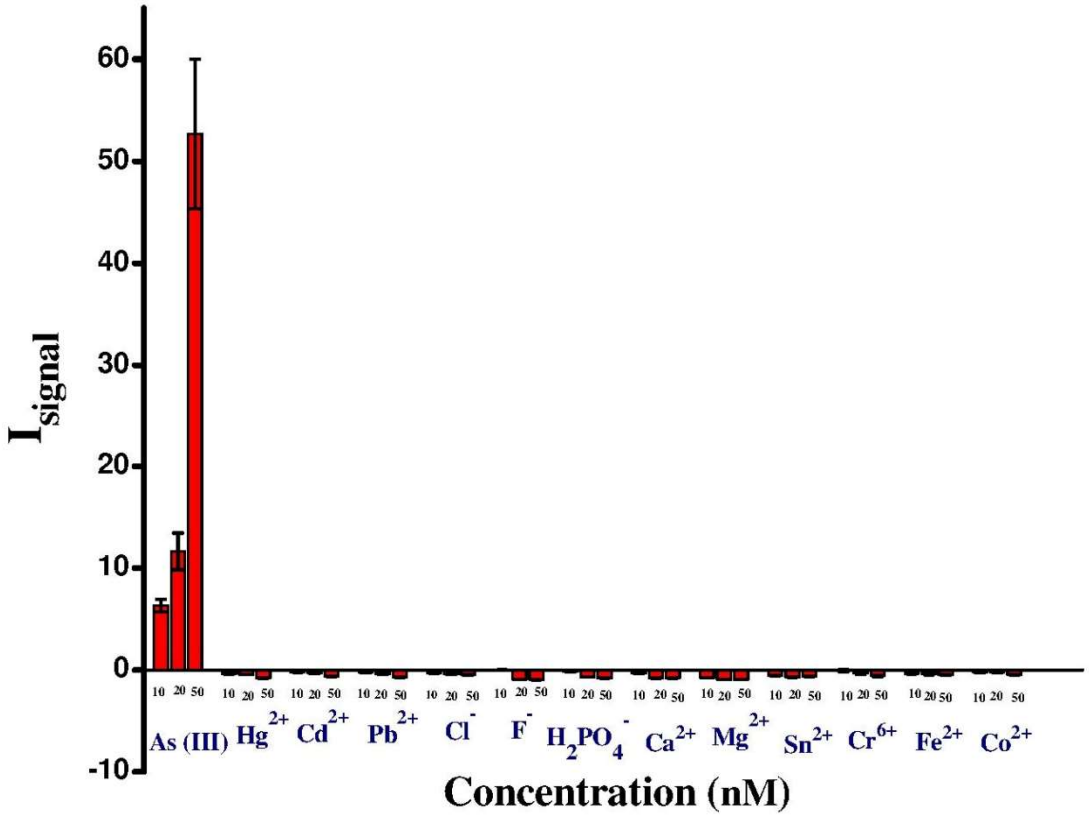

Fig. 5.13. *Response of UCP at M.oleifera in solutions containing various species.*

To establish this fact, the absorbance was measured by adding heavy metal species to the catechol solution. However, no visible suppression in the absorbance band compared to that of As(III) was observed **(**Fig 5.3 inset a**),** where I_{signal} always remained below I_{blank}. These results demonstrate the selectivity of UCP at M.oleifera towards As(III) ions.

The selectivity of UCP at M.oleifera towards As(III) species when other heavy ions (Cd^{2+} and Hg^{2+}) coexist in high concentrations was also investigated **(**Fig. 5.14**)**. For this, UCP at M.oleifera was drop casted with solutions containing 10 mM of Cd^{2+} and Hg^{2+} ions each, and the

emission was recorded before and after the addition of As(III) solution (1 nM). Since an emission enhancement was also observed, the platform selectivity appeared to remain intact for As(III) ions even in the presence of heavy ions in copious amounts. Obviously, the ligands present on UCP at M.oleifera interact with the As(III) ion selectively and cause changes in its emission also. Therefore, the developed platform is unique and allows the detection of As(III) with high sensitivity even in the presence of heavy metal ions such as Cd^{2+} and Hg^{2+}.

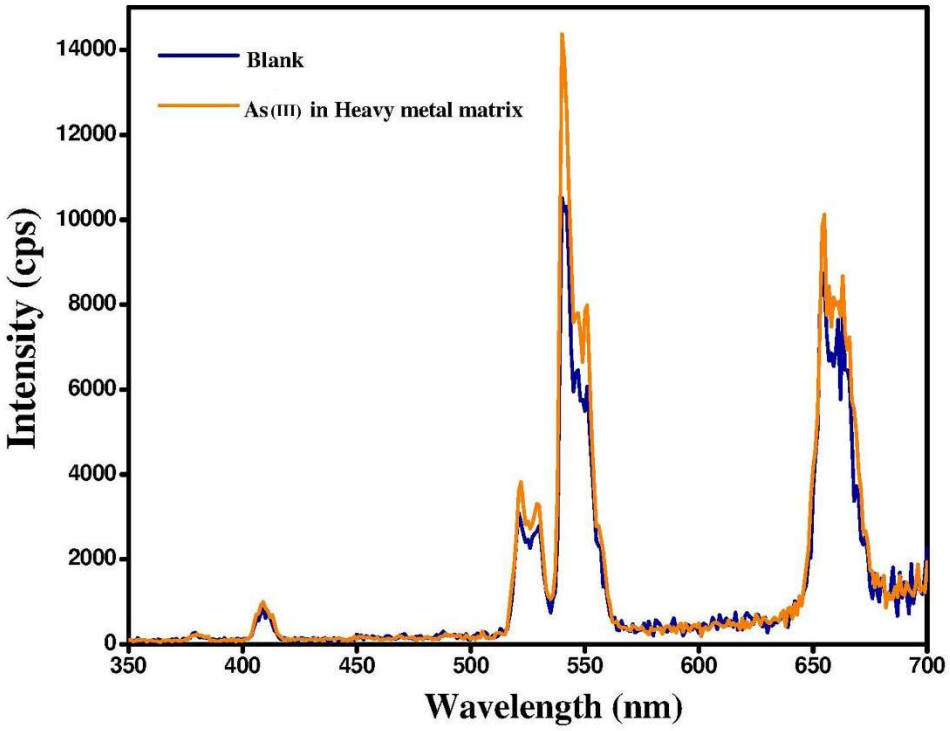

Fig. 5.14.*UCP at M.oleifera ability to distinguish As(III) even in the presence of other heavy metal ions (Hg^{2+}, Cd^{2+}): Blue color emission spectra is of the platform after exposure to mixture Hg^{2+} and Cd^{2+} ion solutions (each of 10 mM).*

During the development of UCP at M.oleifera, due care was taken to diminish the energy transfer by the radiative process. The transfer of energy usually occurs due to the emission and reabsorption of photons following the inner filter effect, the extent of which depends on the optical density, sample size, and path length. The radiative process seems to bear no effect in the present case. The UC platforms were sonicated for the removal of excess material. In each case, low absorbance (0.16-0.14) (Fig.5.15) and high transmittance (65-75%) (Fig.5.16) were maintained in the wavelength range of 400-700 nm to ensure uniformity in the thickness of the

luminescent layer. Thus, the decrease in emission caused by re-absorption is likely to be negligible and can be ignored.

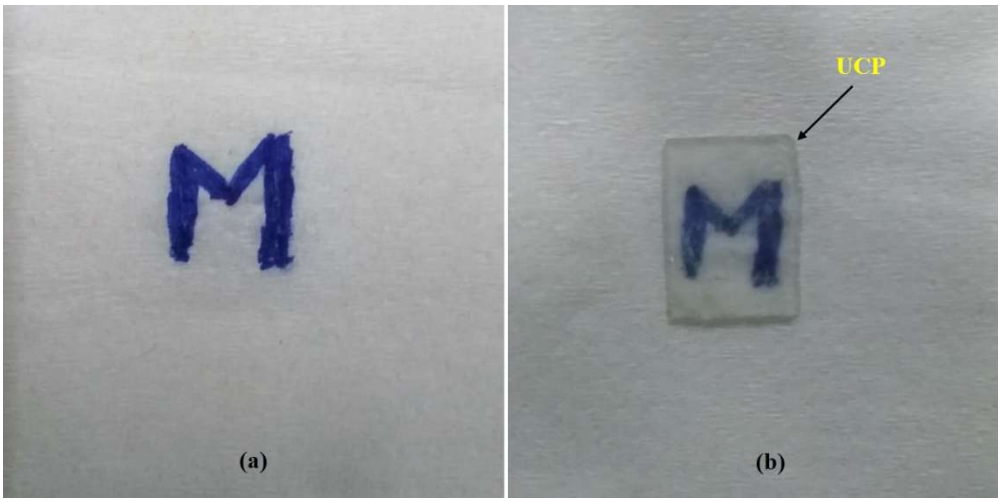

Fig. 5.15. *UCP at M.oleifera prepared over plain glass substrate showing its excellent transparency*

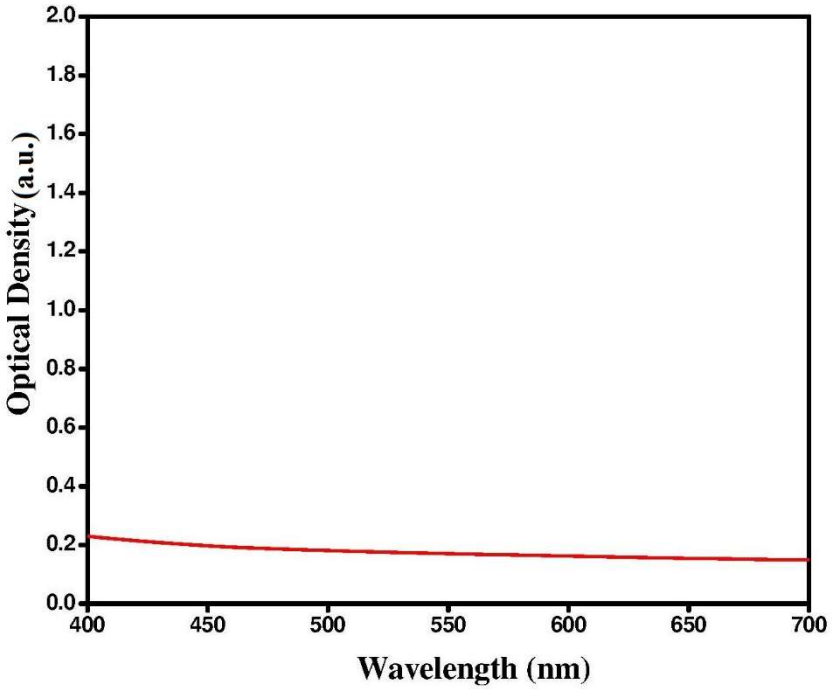

Fig. 5.16. *Optical density of prepared UCP at M.oleifera*

Secondly, all the selectivity tests were carried out on the same platform under similar conditions and parameters. Thus, any signal artifact due to radiative energy transfer in one experiment was being replicated in the other experiments. However, it was observed that the same platform produced an upsurge in I_{signal} in the presence of As(III) ions, which in the case of other interfering ions, showed I_{signal} close to the baseline (Fig.5.13). Hence, the signal variation due to re-absorption (if any) is expected to remain the same and not conflict with the detection process. Thus, the above facts confirm that the detection of As(III) is due to LRET and not radiative energy transfer.

5.1.4. UCP at M.oleifera Analytical Capability and Spike Recovery

The analytical parameters, i.e., the theoretical limit of detection (LOD) and limit of quantitation (LOQ= 10*LOD) of UCP at M. oleifera for As(III) ions were calculated (3σ) using the calibration chart (I_{signal} vs. As(III) concentration plot) to be 0.07 nM (5.7 ppt) and 0.7 nM (57 ppt), respectively. Interestingly, some fluorescent sensors such as silica NP aptasensor[106] and CdTe/ZnS QDs[111] were reported to possess similar detection limits. It is important to note that detection methods based on the fluorescence/luminescence techniques are known to be very sensitive. Besides, the near infrared excitability of the UCP at M.oleifera platforms resulted in an excellent signal to noise ratio, resulting in its low LOD. Furthermore, UCP at M.oleifera could practically detect As(III) ion as low as 1 nM (LOQ) (Fig.5.14). In this case $LOQ_{Actual} \approx LOQ_{Theoritical}$, which is very close to the theoretically calculated LOQ (0.7 nM). The LOD (3σ), fitting equations and calibration curve for UCP at M.oleifera were prepared in triplicate (Fig. 5.17 and 5.18) and provided in Table 5.1.

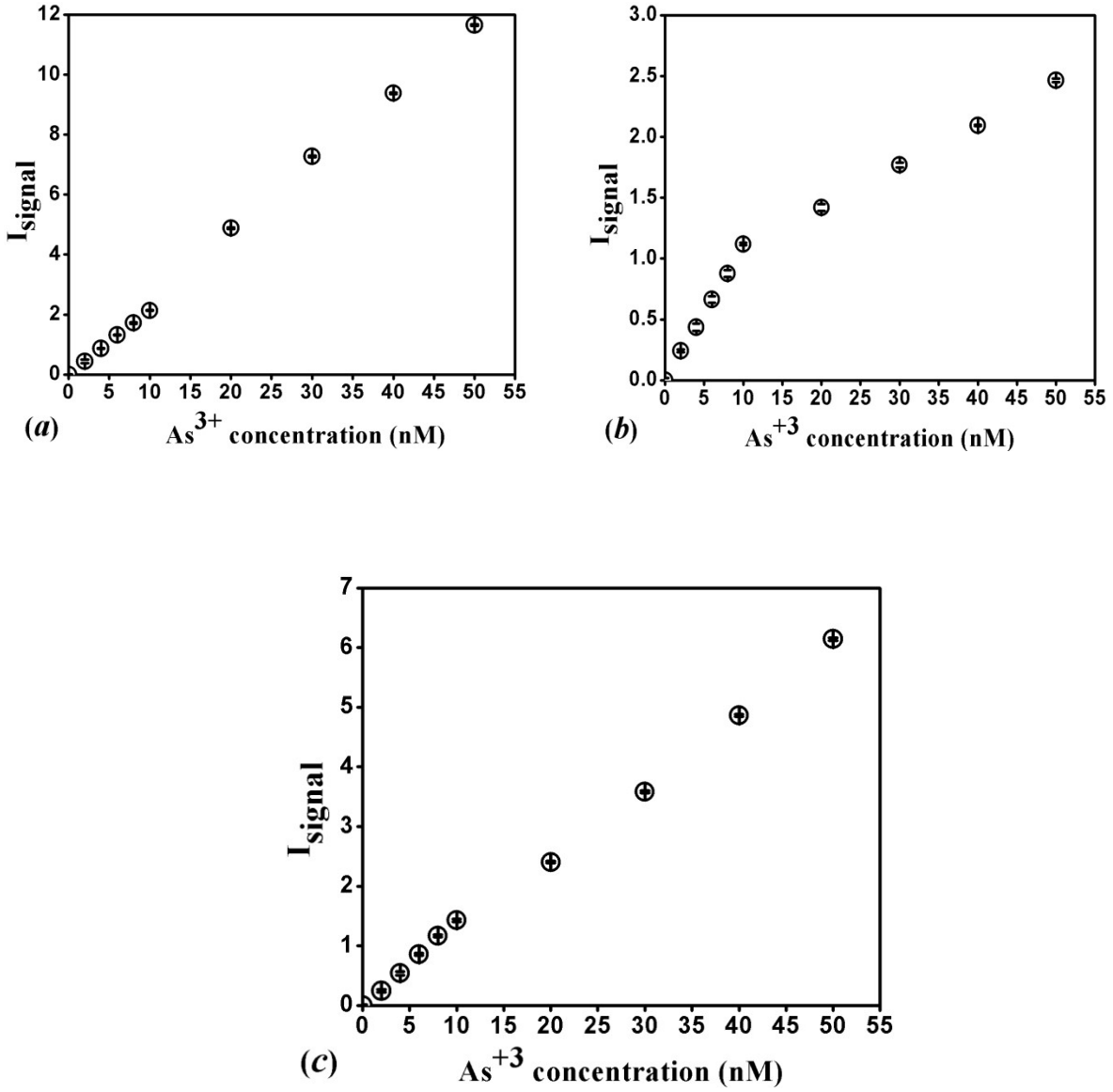

Fig. 5.17. *I_{signal} vs. Intensity plot for 3 UCP at M.oleifera in the entire detection range of As^{3+} (a) Platform 1 (b) Platform 2 (c) Platform 3*

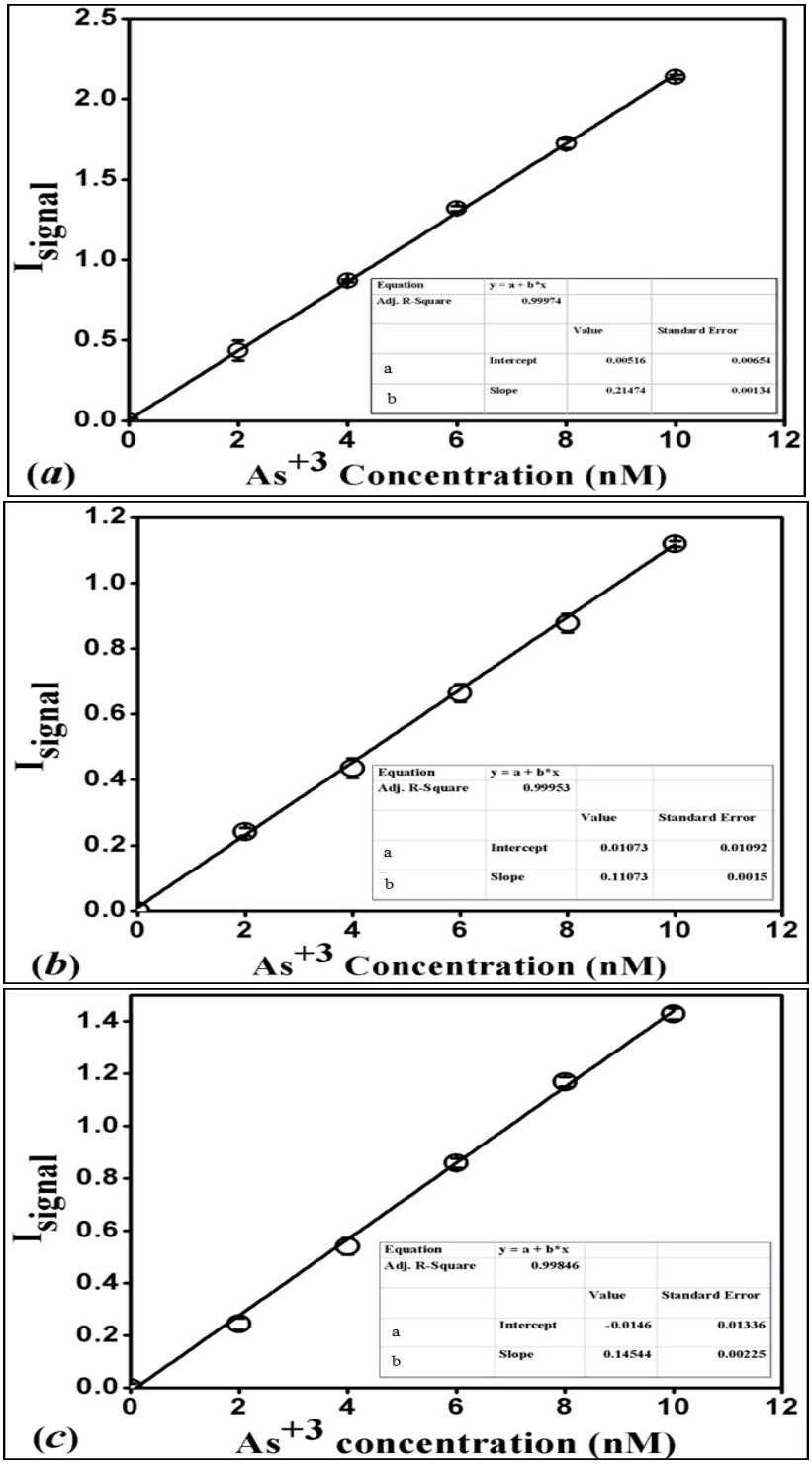

Fig. 5.18. *Linear fit of the calibration plot using least square method for 3 UCP @ M.oleifera (a) Platform 1 (b) Platform 2 (c) Platform 3*

Table 5.1. *As^{3+} Detection limit obtained from different UCP at M.oleifera*

UCF Platform no	Equation of Line	LOD (ppt)	LOQ (ppt)
1	0.21474x + 0.00516	5.72	57.2
2	0.11073x + 0.01073	28.48	284.8
3	0.14544x - 0.0146	32.20	322

There are two factors that determine the analytical sensitivity:(i) precision/reproducibility and (ii) variation in the slope of the calibration curve. Using the average standard deviation of measurements (in As(III) solution concentration range 2-10 nM), the precision/ reproducibility of the three platforms was found to be in the range of 0.021 and 0.025. Also, since the values display no significant variation, the reproducibility of results appears to be quite good. The slope of the calibration curve varied with the analyte concentration. Hence, due care was taken in introducing the solution precisely during calibration experiments. Accordingly, excellent linear fitting of the calibration curve in the As(III) concentration range of 2-10 nM was achieved **(**Fig.5.12b**)**. It should be mentioned that the platforms were synthesized and calibrated by two persons independently at different times for ensuring the reliability of the data. The results showed good reproducibility with detection variability of 30% and LOD (3σ) much lower than the prescribed maximum contamination limit (MCL) of 10 ppb by the US Environmental Protection Agency (US-EPA) and World Health Organization (WHO) for As (III) ions in safe drinking water. Obviously, the developed UCP at M.oleifera is quite suitable for the precise detection of As(III) contamination in water.

The performance of UCP at M.oleifera for the detection of As (III) ions in real water samples (containing no arsenic species) was undertaken using a spike recovery method. The investigated tap water sample reported to contain several ions including Cl^- (48.44 mg/l), SO_4^{2-} (40.65 mg/l), NO_3^- (27.89 mg/l), and F^- (0.13 mg/l)[146,147]. Thus, 1 nM of standard As(III) solution was poured into the water sample to serve as an impurity. Subsequently, spiking was realized by adding 3,6 and 9 nM of As(III) solution separately. The results revealed spike recovery of 104.1%, 97.9% and 100% for the 3, 6 and 9 nM solution, respectively (Table 5.2).

Table 5.2. *Spike recovery using UCPatM. oleifera in Tap water having a predetermined concentration of As(III) ion*

As(III) solution concentration (nM) used	**I_{signal}**	**As (III)solution concentration deduced (nM)**	**% Recovery**
3	1.02 ± 0.08	3.12	104.1
6	1.24 ± 0.10	5.87	97.9
9	1.49 ± 0.10	9.00	100.0

Thus, the prepared platform is capable of reproducing I_{signal} without interference from other ion impurities (mentioned above) and can be used reliably for the detection of As (III) in drinking water.

5.2. Conclusions

A solid-state α-$NaYF_4$:Yb^{3+}, Er^{3+} upconverting platform was developed using M.oleifera leaf extract and demonstrated to be capable of selectively detecting arsenic ion contamination in water. The catechol absorbance and $NaYF_4$:Yb^{3+}, Er^{3+} upconverting emission upon 975 nm excitation induced luminescence resonance energy transfer (LRET). This led to a reduction in the Er^{3+} red and green emissions, which were restored by the As(III) ions present in aqueous medium proportionately due to the disruption of the LRET process. This feature makes the selective detection of As(III) ions feasible with high sensitivity (3σ - LOD 5.7 ppt), i.e. the UCP at M.oleifera sensor can detect As(III) ion pollution in drinking water below the limit of 10 ppt as specified by the World Health Organization (WHO) and the US Environmental Protection Agency (US-EPA). Moreover, it can monitor arsenic contamination in actual samples containing heavy ions (Cd^{2+}, Hg^{2+}) without an effect on its signal reproducibility.

Chapter 6 – Conclusions and Scope for Future Work

6.1. Conclusions

In conclusion, we prepared a uniform luminescent $NaYF_4:Yb^{3+},Er^{3+}$ upconverting film using one-pot, hydrothermal facile method, exhibiting extraordinary selectivity and sensitivity in chemical sensing . These films were deposited overconducting (ITO and FTO) and non-conducting (plain) glass substrates using different chelating agents at low temperature. Upconverting films displayed high crystallinity, with changing film characteristics (phase, roughness and luminescence intensity) as a function of chelating agent. The best emission intensities on the non-conducting substrate were achieved by using EGTA as a chelating agent. Further, in the case of conducting substrates, combination of EGTA ligand with FTO substrate and DTPA ligand with ITO substrate produced upconverting films with improved luminescence intensities.

Inspired by the natural organic ligands present in the plant extract and their similarity with the chealting agents rare-earth doped $NaYF_4$ UC-films were deposited using plant extract. Current research demonstrates that use of the plant extract not only facilitated low temperature $\alpha \rightarrow \beta$ transition (~90 °C in 2h) but also promoted higher paramagnetic property to the film. These ligands are known to decompose at high temperatures, and therefore to obtain phase-pure hexagonal UC-films, high-temperature processing is undesirable. The hydrothermal synthesis route being a low-temperature process, easy to work with, and used in large-scale production, becomes a viable choice for the desired kind of application. Further, in only a few steps, UC-films can be formed using the hydrothermal route of synthesis. Further, current work incorporates a greener route in conjunction with the hydrothermal technique. Besides, this work demonstrated green route capability to form a stable film and perform selective arsenic detection below the prescribed limits. Further, current work also addressed the problem associated with solid-platform-based sensing systems like quenching and poor sensitivity. The overall objective of our current research work was to develop a cost-effective, easy-to-use, ultra sensitive, and selective sensor, to detect arsenic in different water samples, unlike popularly available expensive arsenic detection techniques that are available in the market which utilizes very toxic chemicals to do the same.

So, instead of going for expensive technologies, we experimented with the one-step process of synthesizing films i.e., the hydrothermal method, to see if we can grow stable, optically active and uniform film for the applications like sensing, specifically environmental friendly sensing. And for channelizing this aim, we primarily checked different substrates and different chelating agents through which we can grow an optically transparent film. As we aimed for pocket friendly sensing technique too, so, we chose naturally occurring chelating agent (plant extract) instead of commercially viable chelating agents. These chelating agents happen to mimic very closely to naturally occurring chelating agents available in the plant extract that acts as a great binder too. Also, using the greener technology, we have opened a new gate to develop various types of optical sensors using naturally occurring chelating agents.

6.2. Scope for Future Work

- Until, now UPCNs thin-film can't be grown on the transparent glass/conducting oxide coated glass. These developed thin films of UPCNs can be further cast to design a sensor on the basis of FRET, BRET principally.
- This approach can be developed further into a unique ready-to-use biosensing platform on metallic, cellulose (organic), polymer substrate, or on the transparent glass slide.
- This method could provide a simple alternative for coating upconverting nanoparticles directly on the substrates of different types.
- The developed platform could also provide a wide opportunity to generate sensing applications for energy-related devices such as solar cells.

References

1 P. Zhang, W. Steelant, M. Kumar and M. Scholfield, Versatile photosensitizers for photodynamic therapy at infrared excitation, *J. Am. Chem. Soc.*, 2007, **129**, 4526–4527.

2 X. Zhu, W. Feng, J. Chang, Y. W. Tan, J. Li, M. Chen, Y. Sun and F. Li, Temperature-feedback upconversion nanocomposite for accurate photothermal therapy at facile temperature, *Nat. Commun.*, DOI:10.1038/ncomms10437.

3 F. Vetrone, R. Naccache, A. Zamarrón, A. J. De La Fuente, F. Sanz-Rodríguez, L. M. Maestro, E. M. Rodriguez, D. Jaque, J. G. Sole and J. A. Capobianco, Temperature sensing using fluorescent nanothermometers, *ACS Nano*, 2010, **4**, 3254–3258.

4 M. Kumar and P. Zhang, Highly sensitive and selective label-free optical detection of mercuric ions using photon upconverting nanoparticles, *Biosens. Bioelectron.*, 2010, **25**, 2431–2435.

5 S. Wu, N. Duan, Z. Shi, C. Fang and Z. Wang, Simultaneous aptasensor for multiplex pathogenic bacteria detection based on multicolor upconversion nanoparticles labels, *Anal. Chem.*, 2014, **86**, 3100–3107.

6 H. P. Ho, W. W. Wong, S. Y. Wu and E. E. Y. Pun, Optical storage disc based on the frequency up-conversion effect from rare earth ions, *Proc. IEEE Hong Kong Electron Devices Meet.*, 2002, 117–120.

7 B. S. Richard and A. Shalav, The role of polymers in the luminescence conversion of sunlight for enhanced solar cell performance, *Synth. Met.*, 2005, **154**, 61–64.

8 S. Y. Lee, M. Lin, A. Lee and Y. Il Park, Lanthanide-doped nanoparticles for diagnostic sensing, *Nanomaterials*, 2017, **7**, 1–14.

9 S. Yang, W. H. Tse and J. Zhang, Deposition of Antibody Modified Upconversion Nanoparticles on Glass by a Laser-Assisted Method to Improve the Performance of Cell Culture, *Nanoscale Res. Lett.*, DOI:10.1186/s11671-019-2918-x.

10 W. J. Kim, M. Nyk and P. N. Prasad, Color-coded multilayer photopatterned microstructures using lanthanide (III) ion co-doped NaYF4 nanoparticles with upconversion luminescence for possible applications in security, *Nanotechnology*, , DOI:10.1088/0957-4484/20/18/185301.

11 S. Baruah and J. Dutta, Hydrothermal growth of ZnO nanostructures, *Sci. Technol. Adv. Mater.*, DOI:10.1088/1468-6996/10/1/013001.

12 S. Baruah, C. Thanachayanont and J. Dutta, Growth of ZnO nanowires on nonwoven polyethylene fibers, *Sci. Technol. Adv. Mater.*, DOI:10.1088/1468-6996/9/2/025009.

13 A. K. Dubey, H. Yamada and K. I. Kakimoto, Surface charge induced enhanced crystallization on the piezoelectric sodium potassium niobate substrate, *J. Cryst. Growth*, 2013, **382**, 7–14.

14 J. F. Suyver, A. Aebischer, D. Biner, P. Gerner, J. Grimm, S. Heer, K. W. Krämer, C. Reinhard and H. U. Güdel, Novel materials doped with trivalent lanthanides and transition metal ions showing near-infrared to visible photon upconversion, *Opt. Mater. (Amst).*, 2005, **27**, 1111–1130.

15 C. Chen, C. Li and Z. Shi, Current Advances in Lanthanide-Doped Upconversion Nanostructures for Detection and Bioapplication, *Adv. Sci.*, , DOI:10.1002/advs.201600029.

16 F. Auzel, Upconversion and Anti-Stokes Processes with f and d Ions in Solids, *Chem. Rev.*, 2004, **104**, 139–173.

17 G. Chen, H. Qiu, P. N. Prasad and X. Chen, Upconversion nanoparticles: Design, nanochemistry, and applications in Theranostics, *Chem. Rev.*, 2014, **114**, 5161–5214.

18 M. V. DaCosta, S. Doughan, Y. Han and U. J. Krull, Lanthanide upconversion nanoparticles and applications in bioassays and bioimaging: A review, *Anal. Chim. Acta*, 2014, **832**, 1–33.

19 M. Wang, G. Abbineni, A. Clevenger, C. Mao and S. Xu, Upconversion nanoparticles: Synthesis, surface modification and biological applications, *Nanomedicine Nanotechnology, Biol. Med.*, 2011, **7**, 710–729.

20 H. Dong, L. D. Sun and C. H. Yan, Basic understanding of the lanthanide related upconversion emissions, *Nanoscale*, 2013, **5**, 5703–5714.

21 R. T. Wegh, A. Meijerink, R. J. Lamminmäki and Jorma Hölsä, Extending Dieke's diagram, *J. Lumin.*, 2000, **87**, 1002–1004.

22 F. Wang, R. Deng, J. Wang, Q. Wang, Y. Han, H. Zhu, X. Chen and X. Liu, Tuning upconversion through energy migration in core–shell nanoparticles, *Nat. Mater.*, 2011, **10**, 968–973.

23 F. Vetrone, J. C. Boyer, J. A. Capobianco, A. Speghini and M. Bettinelli, Significance of Yb3+ concentration on the upconversion mechanisms in codoped Y2O3:Er3+, Yb 3+

nanocrystals, *J. Appl. Phys.*, 2004, **96**, 661–667.

24 G. S. Yi and G. M. Chow, Synthesis of hexagonal-phase NaYF4:Yb,Er and NaYF 4:Yb,Tm nanocrystals with efficient up-conversion fluorescence, *Adv. Funct. Mater.*, 2006, **16**, 2324–2329.

25 F. Wang and X. Liu, Recent advances in the chemistry of lanthanide-doped upconversion nanocrystals, *Chem. Soc. Rev.*, 2009, **38**, 976.

26 S. Ivanova, F. Pelle, A. Tkachuk, M. F. Joubert, Y. Guyot and V. P. Gapontzev, Upconversion luminescence dynamics of Er-doped fluoride crystals for optical converters, *J. Lumin.*, 2008, **128**, 914–917.

27 M. Haase and H. Schafer, Upconverting nanoparticles, *Angew. Chemie - Int. Ed.*, 2011, **50**, 5808–5829.

28 H. Dong, L. D. Sun and C. H. Yan, Energy transfer in lanthanide upconversion studies for extended optical applications, *Chem. Soc. Rev.*, 2015, **44**, 1608–1634.

29 G. Y. Chen, Y. Liu, Y. G. Zhang, G. Somesfalean, Z. G. Zhang, Q. Sun and F. P. Wang, Bright white upconversion luminescence in rare-earth-ion-doped Y2 O3 nanocrystals, *Appl. Phys. Lett.*, 2007, **91**, 1–4.

30 F. W. and X. Liu, Upconversion Multicolor Fine-Tuning: Visible to Near-Infrared Emission from Lanthanide-Doped NaYF4 Nanoparticles, *J. Am. Chem. Soc.*, **130**, 5642–5643.

31 G. Chen, H. Liu, G. Somesfalean, H. Liang and Z. Zhang, Upconversion emission tuning from green to red in Yb3+/Ho 3+-codoped NaYF4 nanocrystals by tridoping with Ce 3+ ions, *Nanotechnology*, , DOI:10.1088/0957-4484/20/38/385704.

32 N. Rakov, G. S. MacIel, M. L. Sundheimer, L. De, A. S. L. Gomes, Y. Messaddeq, F. C. Cassanjes, G. Poirier and S. J. L. Ribeiro, Blue upconversion enhancement by a factor of 200 in Tm 3+-doped tellurite glass by codoping with Nd 3+ ions, *J. Appl. Phys.*, 2002, **92**, 6337–6339.

33 C. Lin, M. T. Berry, R. Anderson, S. Smith and P. S. May, Highly luminescent NIR-to-visible upconversion thin films and monoliths requiring no high-temperature treatment, *Chem. Mater.*, 2009, **21**, 3406–3413.

34 S. Hogmark, S. Jacobson and M. Larsson, *Design and evaluation of tribological coatings*, 2000, vol. 246.

35 M. R. and P. H. Linz, Stephan J., Amorphous Thin Film Growth: Modelling and Pattern Formation, *Adv. Solid State Phys.*, 2001, **41**, 391–403.

36 K. L. Choy, Chemical vapour deposition of coatings, *Prog. Mater. Sci.*, 2003, **48**, 57–170.

37 E. Acosta, *Thin Films/Properties and Applications*, IntecOpen, London, 2021.

38 M. A. Mahmood, S. Jan, I. A. Shah and I. Khan, Growth Parameters for Films of Hydrothermally Synthesized One-Dimensional Nanocrystals of Zinc Oxide, *Int. J. Photoenergy*, , DOI:10.1155/2016/3153170.

39 G. Yang and S. J. Park, Conventional and microwave hydrothermal synthesis and application of functional materials: A review, *Materials (Basel).*, , DOI:10.3390/ma12071177.

40 M. Čekada, Properties and characterization of thin films, 1st edn., 2015.

41 A. A. and G. B. Gomez-Caminero, A, P Howe, M Hughes, E Kenyon, DR Lewis, Moore M. R, J Ng, *Environmental Health Criteria 224 Arsenic And Arsenic Compunds (Second Edition)*, 2001.

42 World Health Organization, *Air Quality Guidelines*, 2006.

43 M. Bissen and F. Frimmel, Arsenic – A Review. Part I: Occurrence, Toxicity, Speciation, Mobility, *Acta Hydrochim. Hydrobiol.*, 2003, **31**, 9–18.

44 G. Iervolino, V. Vaiano, L. Rizzo, G. Sarno, A. Farina and D. Sannino, Removal of arsenic from drinking water by photo-catalytic oxidation on MoOx/TiO2 and adsorption on γ-Al2O3, *J. Chem. Technol. Biotechnol.*, 2016, **91**, 88–95.

45 T. M. Clancy, K. F. Hayes and L. Raskin, Arsenic waste management: A critical review of testing and disposal of arsenic-bearing solid wastes generated during arsenic removal from drinking water, *Environ. Sci. Technol.*, 2013, **47**, 10799–10812.

46 N. Yogarajah and S. S. H. Tsai, *Environ. Sci. Water Res. Technol.*, 2015, 1, 426–447.

47 V. Hsiu-chuan Liao, *Development And Testing Of A Green Fluorescent Protein-Based Bacterial Biosensor For Measuring Bioavailable Arsenic In Contaminated Groundwater Samples*, 2005, vol. 24.

48 J. Saha, A. D. Roy, D. Dey, J. Nath, D. Bhattacharjee and S. A. Hussain, Development of arsenic(v) sensor based on Fluorescence Resonance Energy Transfer, *Sensors Actuators, B Chem.*, 2017, **241**, 1014–1023.

49 N. R. Nicomel, K. Leus, K. Folens, P. Van Der Voort and G. Du Laing, Technologies for

arsenic removal from water: Current status and future perspectives, *Int. J. Environ. Res. Public Health*, 2015, **13**, 1–24.

50 F. Faita, L. Cori, F. Bianchi and M. G. Andreassi, Arsenic-induced genotoxicity and genetic susceptibility to arsenic-related pathologies, *Int. J. Environ. Res. Public Health*, 2013, **10**, 1527–1546.

51 V. D. Martinez, D. D. Becker-Santos, E. A. Vucic, S. Lam and W. L. Lam, Induction of Human Squamous Cell-Type Carcinomas by Arsenic, *J. Skin Cancer*, 2011, **2011**, 1–9.

52 V. C. Ezeh and T. C. Harrop, A sensitive and selective fluorescence sensor for the detection of arsenic(III) in Organic Media, *Inorg. Chem.*, 2012, **51**, 1213–1215.

53 S. K. Pal, N. Akhtar and S. K. Ghosh, Determination of arsenic in water using fluorescent ZnO quantum dots, *Anal. Methods*, 2016, **8**, 445–452.

54 N. A. Yusof and K. Rashid, Development of optical test strip for rapid determination of trace arsenic using immobilized gallocyanine, *Asian J. Chem.*, 2009, **21**, 1747–1753.

55 Q. Wei, R. Nagi, K. Sadeghi, S. Feng, E. Yan, S. J. Ki, R. Caire, D. Tseng and A. Ozcan, Detection and spatial mapping of mercury contamination in water samples using a smart-phone, *ACS Nano*, 2014, **8**, 1121–1129.

56 Q. Liu, J. Peng, L. Sun and F. Li, High-efficiency upconversion luminescent sensing and bioimaging of Hg(II) by chromophoric ruthenium complex-assembled nanophosphors, *ACS Nano*, 2011, **5**, 8040–8048.

57 S. N. Iyer, N. Behary, V. Nierstrasz, J. Guan and G. Chen, Study of photoluminescence property on cellulosic fabric using multifunctional biomaterials riboflavin and its derivative Flavin mononucleotide, *Sci. Rep.*, 2019, **9**, 1–16.

58 L. Sen Qing, Y. Xue, Y. Zheng, J. Xiong, X. Liao, L. S. Ding, B. G. Li and Y. M. Liu, Ligand fishing from Dioscorea nipponica extract using human serum albumin functionalized magnetic nanoparticles, *J. Chromatogr. A*, 2010, **1217**, 4663–4668.

59 Y. Umezawa, An SPR-based screening method for agonist selectivity for insulin signaling pathways based on the binding of phosphotyrosine to its specific binding protein, *Anal. Chem.*, 2000, **72**, 6–11.

60 D. N. Gellner, Communications to the editor, *J. Asian Stud.*, 2004, **63**, 465–467.

61 P. Spessotto, K. Lacrima, P. A. Nicolosi, E. Pivetta, M. Scapolan and R. Perris, Fluorescence-based assays for in vitro analysis of cell adhesion and migration., *Methods*

Mol. Biol., 2009, **522**, 221–250.

62 S. H. J. Mei, Z. Liu, J. D. Brennan and Y. Li, An efficient RNA-cleaving DNA enzyme that synchronizes catalysis with fluorescence signaling, *J. Am. Chem. Soc.*, 2003, **125**, 412–420.

63 N. T. Kim Thanh and Z. Rosenzweig, Development of an aggregation-based immunoassay for anti-protein A using gold nanoparticles, *Anal. Chem.*, 2002, **74**, 1624–1628.

64 H. A. Ho and M. Leclerc, Optical Sensors Based on Hybrid Aptamer/Conjugated Polymer Complexes, *J. Am. Chem. Soc.*, 2004, **126**, 1384–1387.

65 R. Numann and P. A. Negulescu, High-throughput screening strategies for cardiac ion channels, *Trends Cardiovasc. Med.*, 2001, **11**, 54–59.

66 Å. Frostell-Karlsson, A. Remaeus, H. Roos, K. Andersson, P. Borg, M. Hämäläinen and R. Karlsson, Biosensor analysis of the interaction between immobilized human serum albumin and drug compounds for prediction of human serum albumin binding levels, *J. Med. Chem.*, 2000, **43**, 1986–1992.

67 M. A. Cooper, Optical biosensors in drug discovery, *Nat. Rev. Drug Discov.*, 2002, **1**, 515–528.

68 A.P.F. Turner, Biosensors- Sense and Sensitivity, Science's Compass, 2000, **290**, 3–5.

69 W. Feng, C. Han and F. Li, Upconversion-nanophosphor-based functional nanocomposites, *Adv. Mater.*, 2013, **25**, 5287–5303.

70 P. C. Ray, Z. Fan, R. A. Crouch, S. S. Sinha and A. Pramanik, Nanoscopic optical rulers beyond the FRET distance limit: Fundamentals and applications, *Chem. Soc. Rev.*, 2014, **43**, 6370–6404.

71 C. Zhang, L. Sun, Y. Zhang and C. Yan, Rare earth upconversion nanophosphors: Synthesis, functionalization and application as biolabels and energy transfer donors, *J. Rare Earths*, 2010, **28**, 807–819.

72 K. E. Sapsford, L. Berti and I. L. Medintz, Materials for fluorescence resonance energy transfer analysis: Beyond traditional donor-acceptor combinations, *Angew. Chemie - Int. Ed.*, 2006, **45**, 4562–4588.

73 B. Gu and Q. Zhang, Recent Advances on Functionalized Upconversion Nanoparticles for Detection of Small Molecules and Ions in Biosystems, *Adv. Sci.*, 2018, 5, 1700609-

170025.

74 S. Wen, J. Zhou, K. Zheng, A. Bednarkiewicz, X. Liu and D. Jin, Advances in highly doped upconversion nanoparticles, *Nat. Commun.*, , DOI:10.1038/s41467-018-04813-5.

75 Y. Bao, Q. A. N. Luu, C. Lin, J. M. Schloss, P. S. May and C. Jiang, Layer-by-layer assembly of freestanding thin films with homogeneously distributed upconversion nanocrystals, *J. Mater. Chem.*, 2010, **20**, 8356–8361.

76 W. Huang, C. Lu, C. Jiang, W. Wang, J. Song, Y. Ni and Z. Xu, Controlled synthesis of NaYF 4 nanoparticles and upconversion properties of NaYF 4: Yb, Er (Tm)/FC transparent nanocomposite thin films, *J. Colloid Interface Sci.*, 2012, **376**, 34–39.

77 C. Wang and X. Cheng, Synthesis of a NaYF4:Yb,Er upconversion film on a silicon substrate and its tribological behavior, *RSC Adv.*, 2015, **5**, 94980–94985.

78 Z. Jia, K. Zheng, D. Zhang, D. Zhao and W. Qin, Upconversion emission from Yb 3+ and Tm 3+ codoped NaYF 4 thin film prepared by thermal evaporation, *J. Nanosci. Nanotechnol.*, 2011, **11**, 9690–9692.

79 J. M. Chwalek and G. R. Paz-Pujalt, Upconverting Tm3+ doped Ba-Y-Yb-F thin film waveguides for visible and ultraviolet light sources, *Appl. Phys. Lett.*, 1995, 410.

80 S. Pawar, B. Vidyapeeth, H. Deshmukh, S. D. Vavale, S. G. Pawar, D. H. Deshmukh and H. P. Deshmukh, Hydrothermal method for Synthesis of different Nanostructure Metal Oxide thin film Physiochemical Investigations of Some Antiallergenic Indigenous Plants View project Physiochemical investigations of some antiallergenic indigenous plants View project Hydrothermal method for Synthesis of different Nanostructure Metal Oxide thin film, *Int. J. Innov. Knowl. Concepts*.

81 G. Qin, W. Qin, S. Huang, C. Wu, D. Zhao, B. Chen, S. Lu and E. Shulin, Infrared-to-violet upconversion from Yb3+ and Er3+ codoped amorphous fluoride film prepared by pulsed laser deposition, *J. Appl. Phys.*, 2002, **92**, 6936–6938.

82 G. Qin, W. Qin, C. Wu, S. Huang, J. Zhang, S. Lu, D. Zhao and H. Liu, Enhancement of ultraviolet upconversion in Yb3+ and Tm3+ codoped amorphous fluoride film prepared by pulsed laser deposition, *J. Appl. Phys.*, 2003, **93**, 4328–4330.

83 D. M. Bubb, D. Cohen and S. B. Qadri, Infrared-to-visible upconversion in thin films of LaEr(MoO 4) 3, *Appl. Phys. Lett.*, 2005, **87**, 1–3.

84 X. Liu, Y. Ni, C. Zhu, L. Fang, S. Hu, Z. Kang, C. Lu and Z. Xu, Near-Infrared

Upconversion Transparent Inorganic Nanofilm: Confined-Space Directed Oriented Crystal Growth and Distinctive Ultraviolet Emission, *Cryst. Growth Des.*, 2016, **16**, 5787–5797.

85 J. Xu, J. Liu, L. Yang, J. Liu and Y. Yang, Electroluminescent Y 3 Al 5 O 12 nanofilms fabricated by atomic layer deposition on silicon: using Yb as the luminescent dopant and crystallization impetus , *Opt. Express*, 2021, **29**, 37.

86 Z. Giedraityte, M. Tuomisto, M. Lastusaari and M. Karppinen, Three- and Two-Photon NIR-to-Vis (Yb,Er) Upconversion from ALD/MLD-Fabricated Molecular Hybrid Thin Films, *ACS Appl. Mater. Interfaces*, 2018, **10**, 8845–8852.

87 H. Jia, C. Xu, J. Wang, P. Chen, X. Liu and J. Qiu, Synthesis of NaYF4:Yb-Tm thin film with strong NIR photon up-conversion photoluminescence using electro-deposition method, *CrystEngComm*, 2014, **16**, 4023–4028.

88 H. Jia, Y. Zhou, X. Li, Y. Li, W. Zhang, H. Fu, J. Zhao, L. Pan, X. Liu and J. Qiu, Synthesis and phase transformation of NaGdF4:Yb-Er thin films using electro-deposition method at moderate temperatures, *CrystEngComm*, 2018, **20**, 6919–6924.

89 H. Park, G. Y. Yoo, M. S. Kim, K. Kim, C. Lee, S. Park and W. Kim, Thin film fabrication of upconversion lanthanide-doped NaYF4 by a sol-gel method and soft lithographical nanopatterning, *J. Alloys Compd.*, 2017, **728**, 927–935.

90 A. L. Pellegrino, M. R. Catalano, P. Cortelletti, G. Lucchini, A. Speghini and G. Malandrino, Novel sol-gel fabrication of Yb3+/Tm3+ co-doped β-NaYF4 thin films and investigation of their upconversion properties, *Photochem. Photobiol. Sci.*, 2018, **17**, 1239–1246.

91 A. L. Pellegrino, P. Cortelletti, M. Pedroni, A. Speghini and G. Malandrino, Nanostructured CaF2:Ln3+ (Ln3+ = Yb3+/Er3+, Yb3+/Tm3+) Thin Films: MOCVD Fabrication and Their Upconversion Properties, *Adv. Mater. Interfaces*, , DOI:10.1002/admi.201700245.

92 A. L. Pellegrino, S. La Manna, A. Bartasyte, P. Cortelletti, G. Lucchini, A. Speghini and G. Malandrino, Upconverting tri-doped calcium fluoride-based thin films: A comparison of the MOCVD and sol-gel preparation methods, *J. Mater. Chem. C*, 2020, **8**, 3865–3877.

93 X. Liu, C. Zhu, W. Liao, J. Jin, Y. Ni, C. Lu and Z. Xu, Spatial height directed microfluidic synthesis of transparent inorganic upconversion nano film, *Appl. Surf. Sci.*,

2017, **422**, 883–890.

94 T. T. Ghogare, R. B. Pujari, A. C. Lokhande and C. D. Lokhande, Hydrothermal synthesis of nanostructured β-LaS2 thin films, *Appl. Phys. A Mater. Sci. Process.*, , DOI:10.1007/s00339-018-1673-7.

95 X. Zhang, X. Qin and W. Zhang, NaYF4:Yb, Er with N-GQDs mixture: One-pot hydrothermal synthesis and its luminescent film, *Opt. Mater. (Amst).*, , DOI:10.1016/j.optmat.2021.110910.

96 W. Zhang, M. Tan, P. Zhang, L. Zhang, W. Dong, Q. Wang, J. Ma, E. Dong, S. Xu and G. Wang, One pot synthesis of Sb 2 S 3 nanocrystalline films through a PVP-assisted hydrothermal process, *Appl. Surf. Sci.*, 2018, **455**, 1063–1069.

97 F. Li, J. Li, L. Chen, Y. Huang, Y. Peng, Y. Luo, L. Zhang and J. Mu, Hydrothermal Synthesis and Upconversion Properties of About 19 nm Sc2O3: Er3+, Yb3+ Nanoparticles with Detailed Investigation of the Energy Transfer Mechanism, *Nanoscale Res. Lett.*, , DOI:10.1186/s11671-018-2794-9.

98 J. Mathew and E. I. Anila, Hydrothermal assisted chemical bath deposition of (Cd:Zn)S thin film with high photosensitivity and low dark current, *Sol. Energy*, 2018, **172**, 165–170.

99 M. Ishikawa, M. Kurosawa, N. Katsura and S. Takeuchi, *PZT Thick Films Deposited by Improved Hydrothermal Method for Thickness Mode Ultrasonic Transducer*, 2004.

100 K. Shimomura, T. Tsurumi, Y. Ohba and M. Daimon, Japanese Journal of Applied Physics, 1991, Vol. 30

101 T. Morita, Y. Wagatsuma, Y. Cho, H. Morioka, H. Funakubo and N. Setter, Ferroelectric properties of an epitaxial lead zirconate titanate thin film deposited by a hydrothermal method below the Curie temperature, *Appl. Phys. Lett.*, 2004, **84**, 5094–5096.

102 T. D. Dongale, S. S. Shinde, R. K. Kamat and K. Y. Rajpure, Nanostructured TiO2 thin film memristor using hydrothermal process, *J. Alloys Compd.*, 2014, **593**, 267–270.

103 S. Lohar, A. Sahana, A. Banerjee, A. Banik, S. K. Mukhopadhyay, J. Sanmartín Matalobos and D. Das, Antipyrine based arsenate selective fluorescent probe for living cell imaging, *Anal. Chem.*, 2013, **85**, 1778–1783.

104 M. Dolai, R. Alam, A. Katarkar, K. Chaudhuri and M. Ali, Oxime based selective flourescent sensor for Arsenate ion in a greener way with bio-imaging application, *Anal.*

Sci., 2016, **32**, 1295-1300.

105 A. Sahana, A. Banerjee, S. Lohar, S. Panja, S. K. Mukhopadhyay, J. Sanmartín Matalobos and D. Das, Fluorescence sensing of arsenate at nanomolar level in a greener way: Naphthalene based probe for living cell imaging, *Chem. Commun.*, 2013, **49**, 7231–7233.

106 S. M. Taghdisi, N. M. Danesh, M. Ramezani, A. Sarreshtehdar Emrani and K. Abnous, A simple and rapid fluorescent aptasensor for ultrasensitive detection of arsenic based on target-induced conformational change of complementary strand of aptamer and silica nanoparticles, *Sensors Actuators, B Chem.*, 2018, **256**, 472–478.

107 A. Ravikumar, P. Panneerselvam, K. Radhakrishnan, A. A. B. Christus and S. Sivanesan, MoS 2 nanosheets as an effective fluorescent quencher for successive detection of arsenic ions in aqueous system, *Appl. Surf. Sci.*, 2018, **449**, 31–38.

108 R. N. Moussawi and D. Patra, Modification of nanostructured ZnO surfaces with curcumin: Fluorescence-based sensing for arsenic and improving arsenic removal by ZnO, *RSC Adv.*, 2016, **6**, 17256–17268.

109 S. Roy, G. Palui and A. Banerjee, The as-prepared gold cluster-based fluorescent sensor for the selective detection of As III ions in aqueous solution, *Nanoscale*, 2012, **4**, 2734–2740.

110 S. K. Vaishanav, J. Korram, P. Pradhan, K. Chandraker, R. Nagwanshi, K. K. Ghosh and M. L. Satnami, Green Luminescent CdTe Quantum Dot Based Fluorescence Nano-Sensor for Sensitive Detection of Arsenic (III), *J. Fluoresc.*, 2017, **27**, 781–789.

111 A. A. Ensafi, N. Kazemifard and B. Rezaei, A simple and sensitive fluorimetric aptasensor for the ultrasensitive detection of arsenic(III) based on cysteamine stabilized CdTe/ZnS quantum dots aggregation, *Biosens. Bioelectron.*, 2016, **77**, 499–504.

112 L. Zhang, X. Z. Cheng, L. Kuang, A. Z. Xu, R. P. Liang and J. D. Qiu, Simple and highly selective detection of arsenite based on the assembly-induced fluorescence enhancement of DNA quantum dots, *Biosens. Bioelectron.*, 2017, **94**, 701–706.

113 D. Pooja, S. Saini, A. Thakur, B. Kumar, S. Tyagi and M. K. Nayak, A "Turn-On" thiol functionalized fluorescent carbon quantum dot based chemosensory system for arsenite detection, *J. Hazard. Mater.*, 2017, **328**, 117–126.

114 X. Wang, Y. Lv and X. Hou, A potential visual fluorescence probe for ultratrace arsenic (III) detection by using glutathione-capped CdTe quantum dots, *Talanta*, 2011, **84**, 382–

386.

115 C. A. De Villiers, M. C. Lapsley and E. A. H. Hall, A step towards mobile arsenic measurement for surface waters, *Analyst*, 2015, **140**, 2644–2655.

116 N. Butwong, T. Noipa, R. Burakham, S. Srijaranai and W. Ngeontae, Determination of arsenic based on quenching of CdS quantum dots fluorescence using the gas-diffusion flow injection method, *Talanta*, 2011, **85**, 1063–1069.

117 Z. Liu, G. Li, T. Xia and X. Su, Ultrasensitive fluorescent nanosensor for arsenate assay and removal using oligonucleotide-functionalized CuInS2 quantum dot@magnetic Fe3O4 nanoparticles composite, *Sensors Actuators, B Chem.*, 2015, **220**, 1205–1211.

118 G. Tang, J. Wang, Y. Li and X. Su, Determination of arsenic(iii) based on the fluorescence resonance energy transfer between CdTe QDs and Rhodamine 6G, *RSC Adv.*, 2015, **5**, 17519–17525.

119 R. Deng, X. Xie, M. Vendrell, Y.-T. Chang and X. Liu, Intracellular glutathione detection using MnO2-nanosheet- modified upconversion nanoparticles, *J. Am. Chem. Soc.*, 2011, **133**, 20168–20171.

120 L. Yao, J. Zhou, J. Liu, W. Feng and F. Li, Iridium-complex-modified upconversion nanophosphors for effective LRET detection of cyanide anions in pure water, *Adv. Funct. Mater.*, 2012, **22**, 2667–2672.

121 Y. Liu, M. Chen, T. Cao, Y. Sun, C. Li, Q. Liu, T. Yang, L. Yao, W. Feng and F. Li, A cyanine-modified nanosystem for in vivo upconversion luminescence bioimaging of methylmercury, *J. Am. Chem. Soc.*, 2013, **135**, 9869–9876.

122 X. Liu, N. Ding, J. Wang, H. Chen, X. Chen, Z. Wang and X. Peng, Rhodamine B derivative-modified up-conversion nanoparticle probes based on fluorescence resonance energy transfer (FRET) for the solid-based detection of copper ions, *RSC Adv.*, 2019, **9**, 30917–30924.

123 F. Zhou, M. O. Noor and U. J. Krull, Luminescence Resonance Energy Transfer-Based Nucleic Acid Hybridization Assay on Cellulose Paper with Upconverting Phosphor as Donors, *Anal. Chem.*, 2014, **86**, 2719–2726.

124 R. S. Niedbala, H. Feindt, K. Kardos, T. Vail, J. Burton, B. Bielska, S. Li, D. Milunic, P. Bourdelle and R. Vallejo, Detection of analytes by immunoassay using Up-Converting Phosphor Technology, *Anal. Biochem.*, 2001, **293**, 22–30.

125 M. Ylihärsilä, T. Valta, M. Karp, L. Hattara, E. Harju, J. Hölsä, P. Saviranta, M. Waris and T. Soukka, Oligonucleotide array-in-well platform for detection and genotyping human adenoviruses by utilizing upconverting phosphor label technology, *Anal. Chem.*, 2011, **83**, 1456–1461.

126 F. Auzel, D. Pecile and D. Morin, Rare Earth Doped Vitroceramics: New, Efficient, Blue and Green Emitting Materials for Infrared Up-Conversion, *J. Electrochem. Soc.*, 1975, **122**, 101–107.

127 G. Yi, H. Lu, S. Zhao, Y. Ge, W. Yang, D. Chen and L. H. Guo, Synthesis, characterization, and biological application of size-controlled nanocrystalline NaYF4:Yb,Er infrared-to-visible up-conversion phosphors, *Nano Lett.*, 2004, **4**, 2191–2196.

128 J. H. Zeng, J. Su, Z. H. Li, R. X. Yan and Y. D. Li, Synthesis and upconversion luminescence of hexagonal-phase NaYF 4:Yb, Er3+ phosphors of controlled size and morphology, *Adv. Mater.*, 2005, **17**, 2119–2123.

129 S. Wu, Y. Liu, J. Chang and S. Zhang, Ligand dynamic effect on phase and morphology control of hexagonal NaYF4, *CrystEngComm*, 2014, **16**, 4472–4477.

130 S. Liu, G. De, Y. Xu, X. Wang, Y. Liu, C. Cheng and J. Wang, Size, phase-controlled synthesis, the nucleation and growth mechanisms of NaYF4:Yb/Er nanocrystals, *J. Rare Earths*, 2018, **36**, 1060–1066.

131 C. Liu, H. Wang, X. Li and D. Chen, Monodisperse, size-tunable and highly efficient β-NaYF 4:Yb,Er(Tm) up-conversion luminescent nanospheres: Controllable synthesis and their surface modifications, *J. Mater. Chem.*, 2009, **19**, 3546–3553.

132 M. Ding, C. Lu, L. Cao, Y. Ni and Z. Xu, Controllable synthesis, formation mechanism and upconversion luminescence of β-NaYF4:Yb3+/Er3+ microcrystals by hydrothermal process, *CrystEngComm*, 2013, **15**, 8366–8373.

133 S. H. Yoon, D. Liu, D. Shen, M. Park and D. J. Kim, Effect of chelating agents on the preferred orientation of ZnO films by sol-gel process, *J. Mater. Sci.*, 2008, **43**, 6177–6181.

134 J. D. Miller, S. Veeramasuneni, J. Drelich, M. R. Yalamanchili and G. Yamauchi, Effect of roughness as determined by atomic force microscopy on the wetting properties of PTFE thin films, *Polym. Eng. Sci.*, 1996, **36**, 1849–1855.

135 L. Iberhan and M. Wiśniewski, Removal of arsenic(III) and arsenic(V) from sulfuric acid

solution by liquid-liquid extraction, *J. Chem. Technol. Biotechnol.*, 2003, **78**, 659–665.

136 R. Mallya, P. K. Chatterjee, N. A. Vinodini, P. Chatterjee and P. Mithra, Moringa oleifera leaf extract: Beneficial effects on cadmium induced toxicities - A review, *J. Clin. Diagnostic Res.*, 2017, **11**, CE01–CE04.

137 P. M. Aja, N. Nwachukwu, U. A. Ibiam, I. O. Igwenyi, C. E. Offor and U. O. Orji, Chemical constituents of Moringa oleifera leaves and seeds from Abakaliki, Nigeria, *Am J Phytomedicine Clin Ther*, 2014, **2**, 310–321.

138 K. G. S. and V. J. A. Pavia D. L, Lampman G. M, *Introduction to spectroscopy, Cengage Learning, 2008*, Cengage Learning, 5th edn., 2008.

139 J. Shan, N. Yao and Y. Ju, Ligand effects and synthesis of NaYF4 Based up and downconversion colloidal nanophosphors, *ACS Symp. Ser.*, 2011, **1064**, 71–85.

140 T. Jiang, W. Qin and J. Zhou, Citric acid-assisted phase controlled synthesis of NaYF4:Yb 3+,Tm3+ crystals and their intense ultraviolet upconversion emissions, *J. Fluor. Chem.*, 2013, **156**, 177–182.

141 T. Jiang, W. Qin, W. Di, R. Yang, D. Liu, X. Zhai and G. Qin, Citric acid-assisted hydrothermal synthesis of α-NaYF 4:Yb 3+,Tm 3+ nanocrystals and their enhanced ultraviolet upconversion emissions, *CrystEngComm*, 2012, **14**, 2302–2307.

142 L. J.R., Ed., *Principles of Fluorescence Spectroscopy*, Springer, Boston, MA., 2006.

143 S. Radunz, A. Schavkan, S. Wahl, C. Würth, H. R. Tschiche, M. Krumrey and U. Resch-Genger, Evolution of Size and Optical Properties of Upconverting Nanoparticles during High-Temperature Synthesis, *J. Phys. Chem. C*, 2018, **122**, 28958–28967.

144 P. G. Sutariya, H. Soni, S. A. Gandhi and A. Pandya, Single-step fluorescence recognition of As3+, Nd3+ and Br− using pyrene-linked calix[4]arene: application to real samples, computational modelling and paper-based device, *New J. Chem.*, 2019, **43**, 737–747.

145 A. Simple, L. Detection, A. Ligand, J. Park, G. Yeom, D. Hong, E. Jo, C. Park and M. Kim, sensors.

146 K. Mohan, A. Srivastava and P. K. Rai, Ground Water in the City of Varanasi, India: Present status and prospects, *Quaest. Geogr.*, 2011, **30**, 47–60.

147 M. D. Jhariya G, Singh R.M, No TitleSeasonal Assessment of Groundwater Quality in Bhagwanpur, Varanasi, *Curr World Env.*, , DOI:10.12944/CWE.13.3.21.

LIST OF PUBLICATIONS

Publications:

A. In Peer-reviewed (SCI) journals

1. **Suman Duhan,** Kedar Sahoo, Md. Imteyaz Ahmad, Sudhir Kumar Singh, Manoj Kumar, "Chelating agent and substrate effect on hydrothermal growth of Yb^{3+}/Er^{3+} doped $NaYF_4$ film" *Processing and Application of Ceramics* (2021), 15(1), 69–78. (Impact Factor: **1.804**).
2. **Suman Duhan**, Kedar Sahoo, Sudhir Kumar Singh and Manoj Kumar, "Development of ultrasensitive and As(III)-selective upconverting ($NaYF_4$:Yb^{3+},Er^{3+}) platform" *Analyst*, 2020, 145, 6378-6387 (Impact Factor: **4.616**).

B. In conference

1. **Suman Duhan,** Sudhir Ranjan, Manoj Kumar, **"**Thin-film Deposition of Upconverting Materials on solid substrates Using Low Temperature, Simple, Inexpensive Facile Hydrothermal Method for Biosensing Application**"** Fourth International Conference on Nanomedicine and Tissue Engineering (ICNT 2016) 12-14 August 2016, Kottayam, Kerala, Hosted by: Mahatma Gandhi University, Kottayam, Kerala, India-686560**.**

REPRINTS OF PUBLISHED ARTICLES

Analyst

ROYAL SOCIETY OF CHEMISTRY

PAPER

View Article Online
View Journal | View Issue

Cite this: *Analyst*, 2020, **145**, 6378

Development of ultrasensitive and As(III)-selective upconverting ($NaYF_4$:Yb^{3+},Er^{3+}) platform†

Suman Duhan,[a] Kedar Sahoo,[b] Sudhir Kumar Singh[a] and Manoj Kumar *[b]

Received 10th April 2020,
Accepted 17th July 2020

DOI: 10.1039/d0an00717j

rsc.li/analyst

The development of a sensitive α-$NaYF_4$:Yb^{3+},Er^{3+} solid-phase upconverting platform (UCP) was realized using *Moringa oleifera* leaf extract for selective detection of the trivalent arsenic ion [As(III)] contamination in drinking water. The presence of polyphenols in the leaf extract were shown to induce luminescence resonance transfer (LRET), thereby diminishing the Er^{3+} emission (red and green band) when activated by 980 nm excitation. However, the addition of As(III) species interrupted the LRET process and restored the emissions proportionately. This feature allowed the platform to selectively detect arsenic pollution in water below the safe limit of 10 ppt. The uniqueness of UCP lies in monitoring the As(III) contamination in samples containing heavy ions (Cd^{2+} and Hg^{2+}) also, without an apparent effect on the signal reproducibility. The UCP was also found to be insensitive to other interfering ions including Pb^{2+}, $H_2PO_4^-$, F^-, Cl^-, Ca^{2+}, Mg^{2+}, Sn^{2+}, Cr^{6+}, Fe^{2+} and Co^{2+}, if present.

1. Introduction

Arsenic is a known human carcinogen,[1] with 144 million people exposed to it.[2] Its trivalent (+3) oxidations state[3] is known to be the most toxic and causes serious health problems.[4] Accordingly, the US Environmental Protection Agency (US-EPA) and the World Health Organization (WHO) lowered the maximum arsenic contamination level (MCL) in drinking water from 50 to 10 parts per billion (ppb).[5] However, arsenic can only be reliably detected using an inductively coupled plasma-mass spectrometer (ICP-MS), atomic absorption spectrometer (AAS), stripping cyclic voltammetry (CV), and other sophisticated instruments.[5,6] These facilities are bulky, difficult to transport, incur a high capital cost, and require specialized manpower, besides, complex and time-consuming sample preparation.[7] Thus, these limitations constrain the detection of arsenic in the resource-limited areas. Therefore, there is an urgent demand to develop inexpensive, lightweight, luminescence-based, arsenic sensitive, and selective sensors, amenable to the conventional spectrofluorometer or cell-phone-based system, for example, the colorimetric sensor developed by Wei *et al.*[8] to detect mercuric ions (LOD = 3.5 ppb). This sensor measured changes in the solution absorbance using a cell-phone camera attached to a cuvette holder. Detection was carried out using nanosensors suspended in the sample solution. Additionally, a few more solution-based fluorescent arsenic [(As(III)/As(V)] sensors have been reported, as presented in Table 1.

These sensors are either organic (APSAL, NAPSAL, acriflavine, and oxime-based) or inorganic (quantum dots, gold nanoclusters, silica nanoparticles, ZnO/curcumin and MoS_2-based) in nature.

These solution-based fluorescent sensors possess numerous advantages, such as multicolor emission, large dynamic range, low standard deviation and high quantum yield (~0.9). However, they are known to suffer from poor colloidal stability, quenching, pH sensitivity, solvent-dependent emission, and overlapping broad excitation and emission spectra. Due to the spectral overlap, inherent noise is carried in the signal, resulting in a poor signal to noise ratio and hence low sensitivity. Meanwhile, inorganic fluorescent sensors such as ZnO/curcumin/MoS_2, silica or gold-based nanosystems, quantum dots (QDs), and carbon dots (CDs), display poor reliability due to their OFF-type signaling, employ expensive nucleotides, complex chemistry, show heavy metal toxicity and false-positive signals. The false-positive signal occurs due to inability of the sensor in differentiating between the analyte and the interfering ions present in the vicinity of sensor.

Consequently, robust solid-phase, luminescent sensors with stable emission (no quenching), facile synthesis, long shelf-life, and capability to detect arsenic with high sensitivity and selectivity are urgently required. The upconverting

[a]*Department of Chemical Engineering, Thapar Institute of Engineering and Technology, Patiala, India*
[b]*Department of Chemical Engineering and Technology, IIT (BHU), Varanasi-221005, India. E-mail: manojk.che@iitbhu.ac.in; Tel: +918283839972*

†Electronic supplementary information (ESI) available: The details of UCP@*M. oleifera* sensor, *viz.* GC-MS spectra of *M. oleifera* leaf extract, *M. oleifera* absorbance variation with the addition of As(III) ions, ATR spectroscopy, microscopic analysis, luminescence spectra, platform transparency, calibration curves, and LOD & LOQ values. See DOI: 10.1039/d0an00717j

Processing and Application of Ceramics 15 [1] (2021) 69–78
https://doi.org/10.2298/PAC2101069D

Chelating agent and substrate effect on hydrothermal growth of Yb^{3+}/Er^{3+} doped $NaYF_4$ film

Suman Duhan[1], Kedar Sahoo[2], Md. Imteyaz Ahmad[3], Sudhir Kumar Singh[1], Manoj Kumar[2,*]

[1]*Department of Chemical Engineering, Thapar Institute of Engineering and Technology, Patiala, Punjab, India*
[2]*Department of Chemical Engineering and Technology, Indian Institute of Technology, Banaras Hindu University, Varanasi-221005, India*
[3]*Department of Ceramic Engineering, Indian Institute of Technology, Banaras Hindu University, Varanasi-221005, India*

Received 4 September 2020; Received in revised form 29 December 2020; Aaccepted 10 February 2021

Abstract

We report simultaneous crystal growth and deposition of upconverting Yb^{3+}/Er^{3+} doped $NaYF_4$ film (UCF) on conducting and non-conducting substrates by one-step hydrothermal method. The characteristics such as film topography, morphology, crystallographic phase and upconverting luminescence intensity were found to depend both on the chelating agent and nature of the substrate. The characteristics of the prepared films varied interestingly when either the chelating agent or the substrate was changed. The upconversion emission intensities were found to increase with decreasing film roughness. Further, current investigation demonstrated that the $NaYF_4$ films deposited using EDTA or DTPA chelating agents on ITO substrate and EGTA chelating agent on PG substrate were more uniform and resulted in greater upconverted emission intensities. We envision plausible use of current technology in the development of affordable optical platforms for several optoelectronic applications.

Keywords: *upconverting films, doped $NaYF_4$, hydrothermal synthesis, effect of substrate and chelating agent*

I. Introduction

Upconverting (UC) materials absorb multiple low-energy photons (wavelength in the order of 980 nm) to emit a high energy photon (400–700 nm). It finds extensive applications in the areas of photothermal and photodynamic therapy [1,2], nanothermometers [3], imaging labels [4], heavy metal detection [5] and multiplex biosensing [6]. Additionally, UC materials are being projected as a promising material for applications in the areas of multilayer optical storage disks [7], photoluminescent display screen [8], photovoltaic cells [9,10], diagnostics platform [11], improved cell culture analysis devices [12], optical security systems [13] and optical waveguides [14] requiring development of novel upconverting films (UCF) on the desired substrates.

Several processing methods for growing rare-earth doped upconverting platforms have been reported using thin-film deposition techniques, such as layer by layer deposition (LBL) [15], dip-coating [16], pulsed laser deposition (PLD) [17–19], spin coating [20], thermal evaporation [21] electron-beam vaporization [14], etc. However, these technologies start with an already synthesized upconverting base material, which are subsequently processed to make films. Further, LBL, PLD, electron-beam vaporization require high capital cost, sophisticated instrumentation and dedicated workforce. Additionally, rare-earth doped $NaYF_4$ upconverting films are difficult to synthesize by these conventional techniques due to the presence of fluorine and difficulty in formation of hexagonal phase at low temperature [22]. Applications requiring the development of affordable platforms can not utilize these cost-intensive techniques. In such cases, affordable synthetic methods such as hydrothermal processing would be a more viable choice for preparation of the phase pure upconvert-

*Corresponding author: tel: +918283839972,
e-mail: *manojk.che@iitbhu.ac.in*